Enhanced terahertz emission from thin film semiconductor/metal interfaces

Proefschrift

ter verkrijging van de graad van doctor
aan de Technische Universiteit Delft,
op gezag van de Rector Magnificus prof. ir. K. C. A. M. Luyben,
voorzitter van het College voor Promoties,
in het openbaar te verdedigen op woensdag 19 december 2012 om 12:30 uur

door
Gopakumar RAMAKRISHNAN

Master of Technology in Applied Optics
Indian Institute of Technology, Delhi, India
geboren te Nemmara, India.

Dit proefschrift is goedgekeurd door de promotor:

Prof. dr. P. C. M. Planken

Samenstelling promotiecommissie:

Rector Magnificus,	voorzitter
Prof. dr. P. C. M. Planken,	Technische Universiteit Delft, promotor
Prof. dr. H. P. Urbach,	Technische Universiteit Delft
Prof. dr. A. Neto,	Technische Universiteit Delft
Prof. dr. H. J. Bakker,	FOM-Instituut voor Atoom- en Molecuulfysica
Prof. dr. J. Gómez Rivas,	FOM-Instituut voor Atoom- en Molecuulfysica
Dr. A. J. L. Adam,	Technische Universiteit Delft
Prof. dr. ir. L. J. van Vliet,	Technische Universiteit Delft, reservelid

This work was funded by the Nederlandse Organisatie voor Wetenschappelijk Onderzoek (NWO) and the Stichting voor Technische Wetenschappen (STW).

ISBN: 978-94-6191-564-1

Printed in the Netherlands by Ipskamp Drukkers, Enschede.

A free electronic version of this thesis can be downloaded from:
http://www.library.tudelft.nl/dissertations

Author email: G.Ramakrishnan@tudelft.nl

Contents

1 Introduction **1**

1.1 Terahertz radiation 1
1.2 Terahertz time-domain spectroscopy 2
1.3 Experimental setup 3
1.4 Electro-optic detection 4
1.5 Terahertz generation mechanisms 5
1.6 Optical rectification 5
1.6.1 THz generation from gallium phosphide 6
1.7 Third-order optical rectification 7
1.8 Auston switch 7
1.9 THz generation from indium arsenide and gallium arsenide surfaces . 8
1.9.1 Transient current surge in surface space-charge layer 9
1.9.2 Photo-Dember field 10
1.10 Thin films 12
1.11 Thesis context and overview 12

2 Terahertz emission from graphite **15**

2.1 Introduction 15
2.1.1 Structure of graphite 16
2.1.2 Highly-oriented pyrolytic graphite 16
2.2 Optical rectification by graphite 17
2.3 Experimental 17
2.4 Terahertz emission 18
2.4.1 Basal-plane surface illumination 18
2.4.2 Magnetic-field enhancement 20
2.4.3 Edge-plane surface illumination 21
2.5 THz generation from pencil-lead 23
2.6 Discussion 23
2.6.1 Subsequent works 24

2.7 Conclusion 25

3 Terahertz emission from cuprous oxide/metal interfaces 27
3.1 Introduction 27
3.2 Oxides of copper 28
3.2.1 Cuprous oxide 28
3.2.2 Cupric oxide 28
3.3 Preparation of cuprous oxide thin films 29
3.3.1 Low temperature oxidation of thin films of copper 29
3.3.2 Chemical deposition of cuprous oxide 30
3.4 Experimental setup 31
3.5 THz emission from partially oxidized Cu foils 32
3.6 THz emission from Cu_2O/Au interface 35
3.7 THz generation mechanism 37
3.7.1 Photocurrent surge in the Schottky field 38
3.7.2 Internal photoemission 39
3.7.3 Depletion field-induced optical rectification 40
3.8 Above bandgap excitation of Cu_2O with 400 nm light 41
3.9 THz generation from nonplanar surfaces 42
3.10 Conclusion 43

4 Terahertz emission from semiconductor thin-films 45
4.1 Terahertz emission from semiconductors 45
4.1.1 Transient photocurrent 45
4.1.2 Schottky interface 46
4.1.3 Germanium and silicon 48
4.2 Experimental 49
4.2.1 Sample preparation 49
4.3 Terahertz emission from Cu_2O 50
4.4 Terahertz emission from sputtered Ge 53
4.4.1 Photocurrent in the Schottky field 58
4.5 Terahertz generation from sputtered Si 59
4.6 Conclusion 61

5 Plasmonics for enhanced terahertz emission 63
5.1 Terahertz emission from metal surfaces 63
5.1.1 Percolating gold films 64
5.2 Excitation of surface plasmons 65
5.3 Experimental 67
5.3.1 Setup for exciting the percolating Au film 67
5.3.2 Excitation using Kretschmann geometry 67

5.4 Sample preparation 68
5.4.1 Ultrathin Au films 68
5.4.2 Thin films of Au on prisms 68
5.4.3 Cu_2O thin films 69
5.4.4 Hemicyanine self-assembled monolayer 69
5.5 Percolation-enhanced THz emission 70
5.5.1 Surface plasmon-enhanced optical rectification 72
5.6 THz emission from Cu_2O/Au interfaces 73
5.7 Excitation using ATR geometry 77
5.8 Results and discussion 78
5.8.1 THz emission from a thin continuous Au layer 78
5.8.2 THz emission from a self-assembled monolayer of hemicyanine 79
5.8.3 Cu_2O/Au interface 81
5.9 Second-order and higher-order optical rectification 82
5.10 Conclusion 83

6 Conclusion **85**
6.1 Discussion 85
6.2 Future work 86

Bibliography **87**

Summary **101**

Samenvatting **105**

Acknowledgements **109**

Biography **111**

Chapter 1

Introduction

1.1 Terahertz radiation

In the electromagnetic spectrum, 'terahertz light' occupies the region between the high-frequency edge of the microwave band, 300 GHz (0.3×10^{12} Hz), and the low frequency edge of the infrared band, 10000 GHz (10×10^{12} Hz) as shown in Figure 1.1. In terms of wavelength, this range corresponds to 0.03 mm (or 30 μm) to 1.0 mm. The terahertz (THz) band encompasses the region where electronics and optics meet. These days, in the scientific literature, the term 'terahertz' has almost become synonymous with light waves with frequencies in the THz range, *i.e.,* 10^{12} Hz. Such is the increase in popularity this band of electromagnetic radiation has attained over the past two decades. Today, the applications of THz technology are widespread in several areas such as the semiconductor industry, biological and medical sciences, homeland security, quality control of food and agricultural products, global environmental monitoring, ultrafast computing etc [1, 2]. A significant number of scientific reports from areas related to THz light appear regularly in every major journal published in the field of optics.

There are specific advantages of using THz radiation which make it very suitable for industrial applications. For example, THz waves can pass through many packaging materials like cardboard, plastic or wood, revealing what is inside the package. Compared to X-rays, which are generally used for such purposes, THz waves or T-rays, as they are sometimes called, are non-ionizing and do not cause any detectable damage to biological specimens or cause any health problems. This makes THz radiation safe to use in security applications. The recent remarkable advances in the field of THz time-domain spectroscopy (THz-TDS), have made it possible also to identify materials inside packages using their THz spectral absorption signatures [3, 4].

It is not very surprising that the advancements in both imaging and spectroscopic capabilities lead to the concept of a THz microscope, or a THz nanoscope [5, 6]. This takes THz imaging technology to an unprecedented level where micro-spectroscopy

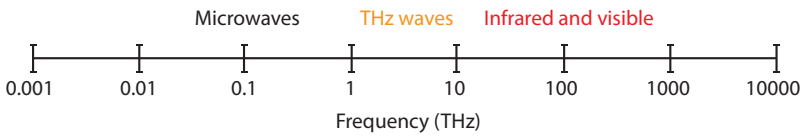

Figure 1.1: Electromagnetic spectrum showing the THz region.

of biological cells, and the inspection of very large scale integrated circuit (VLSIC) elements may become possible. For the realization of a THz microscope, one major initial hurdle is to overcome the Rayleigh diffraction limit, as the THz waves have much longer wavelengths than the sizes of the typical specimens under study [7]. Beating the diffraction limit has been demonstrated by several groups, using adaptations of different techniques used to overcome the diffraction-limit in visible light microscopy [7–9]. Both aperture and apertureless near-field imaging solutions were demonstrated [10–13]. Making use of field enhancement by a copper tip, and selective electro-optic (EO) detection of THz polarizations, in the early 2000's, van der Valk *et al.* demonstrated that a resolution of $\lambda/110$ can be achieved at THz frequencies [13]. In this way, THz light can be used for a myriad of applications. Biological molecules such as amino acids, proteins, and de-oxyribonucleic acid (DNA) have intermolecular and intramolecular modes oscillating at THz frequencies. Label-free sensing of DNA by THz spectroscopy has been reported [14]. The THz spectra of biological specimens are sensitive to changes such as hydration, binding, conformational change, and temperature [4].

1.2 Terahertz time-domain spectroscopy

The advent of ultrafast lasers facilitated the development of optical techniques to generate and detect pulses of broadband electromagnetic radiation in the THz range. As the electric field of these waves oscillate at a relatively low frequency (10^{12} Hz) compared to visible light, it is possible to detect the electric field of the radiation as a function of time instead of detecting the oscillation-period-averaged power. Both the amplitude and the phase of the light can be obtained from which both the absorption coefficient and the refractive-index of a sample at different frequencies can be calculated. The complex valued permittivity of the sample can thus be directly obtained without using the Kramers-Kronig analysis [4, 15].

In a typical THz-TDS setup, broadband THz pulses are generated by optical rectification (OR) of ultrafast laser pulses with a duration typically between 10 and 100 fs. These THz pulses are then focused onto the sample under study. After transmission through (or reflection from) the sample, the amplitude of the electric field of the radiation is directly detected as a function of time using EO detection (see section 1.4). Fourier transforming the electric field pulse provides the amplitude and phase spectra of the sample in the THz range.

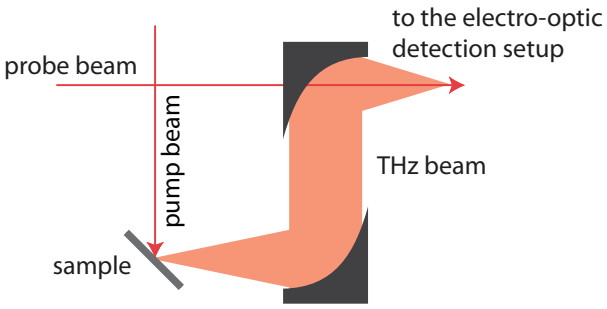

Figure 1.2: Schematic of the experimental setup for the generation and detection of THz light using ultrafast laser pulses.

In semiconductors, THz-TDS can be very useful in understanding the dynamics of the mobile charge carriers created by photo-excitation or doping. The scattering rates of electrons and holes in semiconductors are often on the order of 10^{12} - 10^{14} s^{-1} [1]. This results in a characteristic response in the THz frequency range. In addition to measuring the dynamics of electrons and holes, THz light is also sensitive to low energy excitations and quasi-particles, including excitons, polarons, and phonons [16–18].

THz emission spectroscopy (TES) is another branch of THz-TDS and can be carried out in certain materials. [4,19] In this case, femtosecond laser pulses are focused onto the samples of interest, and the emitted THz waveforms are detected and analyzed. Many different ultrafast photo-induced processes can lead to the generation of THz dipoles in different materials. The emitted THz pulses carry information on the nonlinear optical properties, local symmetry, ultrafast carrier dynamics, etc. of the material under study. In Chapter 2, we show the results of femtosecond laser excitation of graphite and the resulting THz emission from it. It is seen that graphite can emit THz pulses when excited using femtosecond laser pulses. Analysis of the emitted pulse reveals new and interesting information on the photogenerated currents [20]. TES can be effectively used to study semiconductor ICs, as most of the semiconductor materials are capable of emitting THz pulses when they are excited with femtosecond laser pulses. It is to be noted that in the case of TES, the spatial resolution of the system depends not on the wavelength of the THz light, but on the wavelength of the near-infrared pump light.

1.3 Experimental setup

A typical THz generation and detection setup is shown in Figure 1.2 [20]. This is a reflection-type setup, where we collect the THz light in the specular reflection direction of the pump beam. In all the experiments described in this thesis, the

optical excitation is done using a Ti:Sapphire oscillator (Scientific XL, Femtolasers) generating p-polarized light pulses of 50 fs duration, centered at a wavelength of 800 nm with a repetition rate of 11 MHz. The average output power from this oscillator is 800 mW which is split into two arms by an 80/20 beam-splitter. The 80% part is used as the pump beam, and the 20% part as the sampling beam. The pump beam is focused onto the sample surface. The generated THz beam is collected using off-axis paraboloidal mirrors and focused onto an EO detection setup as described below.

1.4 Electro-optic detection

The time-gated detection system is the most important part of any THz-TDS setup. It is in this part of the setup where the electric-field of the THz radiation is directly detected. A very common method of time-gated detection of the electric field is by using a second-order optical nonlinear processes in EO crystals [21]. We used a (110) oriented 500 μm thick zinc telluride (ZnTe) crystal and a (110) oriented 300 μm thick gallium phosphide (GaP) crystal for the various experiments described in this thesis. The THz beam and the polarized sampling laser beam are focused onto the same spot on the detection crystal. The induced birefringence by the THz electric-field incident on the EO crystal elliptically polarizes the probe beam to an extent proportional to the instantaneous THz electric-field value [22]. The probe beam then propagates towards a differential detection setup consisting of a quarter-wave plate, a Wollaston prism and a differential optical detector as shown in Figure 1.3. The quarter-wave plate is used to balance the two orthogonal components of the polarization ellipse of the probe beam which are separated by the Wollaston prism. In the absence of a THz electric field, the linearly polarized probe beam after the EO crystal is circularly polarized by the quarter-wave plate. This is split into linearly polarized orthogonal components of equal intensity by the Wollaston prism. These are measured by the differential detector diodes D1 and D2 as shown in the figure. When an electric field is present, the differential signal is nonzero and is directly proportional to the instantaneous THz electric-field [23].

When the THz light and the probe light are polarized either in the same direction or orthogonally, the measured THz electric field can be expressed as [22, 24],

$$E_{THz} \propto \frac{c\Delta I}{I_{probe}} \left(\frac{1}{\omega n^3 r_{41} L} \right), \tag{1.1}$$

where $\Delta I = I_1 - I_2$ is the difference in the intensities falling on the two photodiodes, $I_{probe} = I_1 + I_2$ is the total intensity of the probe light, n is the refractive index, c is the velocity of light in vacuum, ω is the angular frequency of the probe light, r_{41} is the EO coefficient, and L is the thickness of the EO crystal.

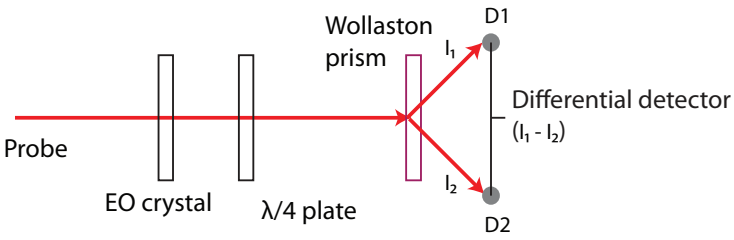

Figure 1.3: Schematic of the THz detection setup. The difference in the intensities of the two beams after the Wollaston prism is measured with a differential detector which, apart from the electronics, consists of two photodiodes D1 and D2.

1.5 Terahertz generation mechanisms

Until the early 1990s, the lack of suitable, easy-to-use sources led to the designation of the THz frequency range as the THz gap [25]. 'Bridging the THz gap' can be done in different ways, with sources ranging from incandescent lamps to quantum cascade lasers (QCL). In this thesis, however, we restrict ourselves to the THz sources based on the ultrafast laser excitation of semiconductors and nonlinear optical materials. Ultrafast laser excitation of these materials leads to the generation of a picosecond transient dipole, which can emit THz pulses into the far-field. The detected subpicosecond THz pulse is suitable for broadband imaging and THz-TDS. This technique grew from the work done in the 1980s at AT&T Bell Labs and IBM Thomas J. Watson Research Center in the United States of America (USA). Soon afterwards, EO detection was also demonstrated. As we discussed earlier in section 1.2, time-gated detection makes the THz-TDS unique. For this reason, the method of generating THz radiation using ultrafast lasers is widely in use.

A wide range of materials can emit THz pulses when excited with femtosecond laser pulses. In a general sense, such THz emission from materials can be broadly termed *optical rectification*, as the process rectifies the incident femtosecond optical pulses to produce subpicosecond THz pulses. This process can happen in multiple ways which can be classified roughly into two cases. In one case, the laser excitation of the material is non-resonant, *i.e.,* no real charge carriers are excited in the material and only a displacement current is created. In the other case, the generation of electron-hole pairs takes place by resonant photo-excitation [26].

1.6 Optical rectification

OR refers to the creation of a static polarization in a material which is illuminated with an intense light beam. This is a second-order nonlinear optical process, similar to second harmonic generation (SHG). OR can be described as difference-frequency generation, and when the two frequencies involved are the same, this results in a

static (DC) polarization. The first report on OR was by Bass *et al.* in 1962 [27]. They observed a DC polarization that developed in potassium dihydrogen phosphate (KDP) and potassium dideuterium phosphate (KD_dP) crystals, upon the passage of an intense ruby laser beam through them. A qualitative description of the phenomenon was given by them as follows. Consider a crystal lacking inversion symmetry so that the polarization induced by an applied electric field need not reverse exactly when the field is reversed. If the applied electric field varies sinusoidally with time, then a net, time-averaged DC polarization will develop, in analogy with the DC currents in ordinary electronic rectifiers. A few subsequent works also were reported after the publication of this phenomenon [28–31]. However, OR gained more popularity when it was shown that THz pulses can be generated by rectifying femstosecond laser pulses. Femtosecond laser excitation of nonlinear crystals having a non-vanishing second-order susceptibility, $\chi^{(2)}$, creates an ultrashort, quasi-static *time-dependent* polarization,

$$P(t) \propto I_{opt}(t), \tag{1.2}$$

where $I_{opt}(t)$ is the intensity of the pump light. This transient polarization $P(t)$ emits a THz pulse that, in the far-field, can be expressed as as,

$$E_{THz} \propto \partial^2 P(t)/\partial t^2. \tag{1.3}$$

In 1971 Yang *et al.* reported the generation of far-infrared pulses from $LiNbO_3$ crystals upon excitation with picosecond laser pulses [32, 33]. Later, the generation of free-space THz-frequency radiation with a bandwidth of 1 THz by OR of femtosecond dye laser pulses in $LiNbO_3$ was reported by Hu *et al.* in 1990 [34]. Today, OR is widely used as a source of THz radiation in different THz imaging and spectroscopy applications.

The emitted THz pulse can also be used to probe the second-order nonlinear optical properties of the material. OR can only occur in materials without a centre of inversion symmetry. Note that this also includes the interfaces between different materials, and materials in which the inversion symmetry is broken by an applied electric or magnetic field. Crystals of gallium phosphide (GaP), zinc telluride (ZnTe), lithium niobate $LiNbO_3$, gallium arsenide (GaAs) etc. are widely used as sources of THz radiation, these days. Certain organic materials also have a large second-order nonlinear susceptibility, which results in strong THz emission. In 1992, Zhang *et al.* reported OR and subsequent generation of THz radiation from a nonlinear organic crystalline salt; 4-dimethylamino-N-methyl-4-stilbazolium tosylate (DAST) [35].

1.6.1 THz generation from gallium phosphide

GaP is a compound semiconductor material with an indirect bandgap of 2.26 eV [36]. It has a zincblende crystal structure similar to ZnTe. OR of femtosecond laser pulses by zincblende crystals is commonly used for the generation of broadband THz radiation [31]. GaP has a smaller EO coefficient (1 pm/V) compared to ZnTe (4 pm/V) [37]. However, the phonon resonance of GaP is at 11 THz which makes it

a better choice compared to ZnTe, for broadband THz generation [38]. In the case of ZnTe, the bandwidth is limited by a strong transverse-optical (TO)-phonon line at 5.3 THz. This, together with two weak lower-frequency phonon lines at 1.6 and 3.7 THz, absorbs frequencies mostly in the range of $\sim$ 3.5 - 6 THz [39]. Non-resonant excitation of GaP crystals with femtosecond light pulses centered at a wavelength of 800 nm leads to the emission of THz pulses along the transmission direction of the pump laser light. This process is dependent on the crystal orientation of GaP. It has to be noted that for (100) oriented zincblende crystals, no THz emission is detected when the pump beam is incident normal to the surface. The THz polarization is developed along the <100> axis. For applications in which normal incidence of the pump beam is required, a (110) or a (111) oriented crystal is used. Broadband generation and detection of THz pulses of bandwidth up to 9 THz have been reported using GaP (110) crystals [38, 40].

1.7 Third-order optical rectification

The polarization giving rise to OR need not necessarily be second-order in the pump light electric field. It can be shown that higher-order nonlinear polarizations can also lead to rectification when suitable combinations of frequencies are used [41]. As mentioned earlier, second-order OR is not possible from a material which possesses a centre of inversion symmetry. However, a quasi-static polarization can still be created in materials with a large third-order nonlinear susceptibility, $\chi^{(3)}$, if a two-color excitation is done such that

$$2\omega_1 - \omega_2 = 0 \tag{1.4}$$

where ω_1 and ω_2 represent the fundamental and the second harmonic central frequencies of the light pulses respectively [24]. In this case, the rectification process is through a third-order nonlinear optical process,

$$E_{THz} \propto \chi^{(3)} E^2(\omega) E^*(2\omega), \tag{1.5}$$

where $E(\omega)$ and $E(2\omega)$ are the complex electric fields of fundamental and second harmonic light respectively. In principle, a third-order process is possible from almost all materials [42]. THz emission through a third-order process by a single central wavelength femtosecond laser excitation is also possible. In this case, one of the electric fields involved in the expression for the third-order polarization is a static field. This is called field-induced THz generation. Such cases are shown to arise at the surfaces and interfaces of semiconductors where a depletion field is present, or when an external electric field is applied [43].

1.8 Auston switch

THz pulse generation by resonant OR, also called ultrafast photo-conductive (PC) switching, was pioneered by Auston and Lee in the 1970s [44, 45]. In their exper-

iments, optical pulses from a mode-locked Nd:glass laser were used to excite high resistivity silicon (Si), or chromium (Cr)-doped semi-insulating gallium arsenide (SI-GaAs). The resulting charge carriers accelerate in an applied static electric field, and emit a coherent, quasi-single cycle THz pulse. This device has become known as the Auston switch. The same principle is also applied to various photoconductive materials other than Si and GaAs [2]. In general, femtosecond laser excitation of a biased semi-insulating semiconductor can lead to the emission of relatively strong THz pulses. The laser pulse generates electron-hole pairs in the semiconductor which drift in the applied bias. The picosecond time variation in the photocurrent $J(r,t)$ will result in the emission of a THz pulse E_{THz}, according to

$$E_{THz} \propto \partial J(r,t)/\partial t. \tag{1.6}$$

Here the variables r and t represent position and time respectively. THz emission by PC antennas is also widely used in THz imaging and for spectroscopic applications. It is also possible to generate a transient current at the surfaces and interfaces of semiconductors where a built-in electric field is present, as we will discuss in the next section [46]. There too, an ultrafast, transient photocurrent can lead to the emission of a THz pulse. In the case of certain semiconductors, like indium arsenide (InAs), gallium arsenide (GaAs) etc., the intrinsic $\chi^{(2)}$ also contributes to the THz emission [47, 48].

1.9 THz generation from indium arsenide and gallium arsenide surfaces

In many semiconductors, THz emission after the excitation with a femtosecond laser pulse occurs from a thin layer close to the surface. There are different ultrafast processes taking place near the semiconductor surface (or in the bulk) which can give rise to the emission of THz pulses. In order to illustrate this, in this section, a general overview of the THz emission from two commonly used semiconductors, InAs and GaAs, is given.

Femtosecond laser excitation of semiconductors like InAs and GaAs leads to the emission of relativly strong THz pulses. A comparison of the THz electric field emitted from the surface of undoped InAs (100) and semi-insulating (SI) GaAs (100) is shown in Figure 1.4. In terms of the electric field amplitude, InAs emits about 15 times stronger THz pulses compared to GaAs in our experimental setup. The THz electric field pulses consist of a nearly single-cycle subpicosecond oscillation, followed by a rapidly oscillating tail. In the EO detection crystal, the phase velocity of the THz pulse should match the group velocity of the probe pulse for correct phase-matching [22, 38]. For a broadband pulse, phase-matching does not occur for all frequency components simultaneously. This results in distortion of the measured field which can manifest itself as oscillations in the trailing part of the THz pulse. The absorption and the re-emission of the THz light by the water vapor molecules in the atmosphere, also leads to quasi-periodic oscillations in the time trace of the pulse.

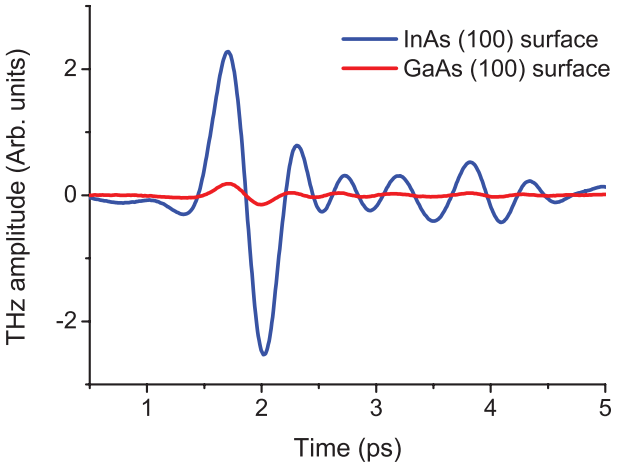

Figure 1.4: Measured THz electric field as a function of time, emitted from an InAs (100) surface and a GaAs (100) surface.

In the case of unbiased GaAs (100), the main THz generation mechanism is reported to be the creation of transient photocurrents in the surface depletion field [46]. In the case of unbiased InAs (100) the main contribution to the THz emission is from the photo-Dember effect [49]. These two processes are discussed below.

1.9.1 Transient current surge in surface space-charge layer

We already saw that THz emission is possible from femtosecond laser excitation of the surfaces of semiconductors. Surface states and bulk states of the electrons will be different in a semiconductor, as a surface represents a discontinuity. Fermi level pinning by the surface states leads to energy band bending for air-exposed or chemically prepared semiconductor surfaces. In the region near the surface where this occurs, the semiconductor becomes depleted of free carriers which are intentionally or non-intentionally present due to impurities or doping, and this region is therefore known as the surface depletion region [50–52]. Since there is a redistribution of charge carriers near the surface of the semiconductor, a built-in electric field $E^{(depl)}(z)$ is present which has the functional form (for an extrinsic semiconductor),

$$E^{(depl)}(z) = \frac{qN_d}{\epsilon}(W - z) \tag{1.7}$$

where z is along the surface normal, q is the absolute value of the electronic charge (1.602×10^{-19} C), N_d is the total donor atom concentration, W is the space-charge layer width and ϵ is the permittivity [50,53]. z-axis is pointed as shown in Figure 1.5.

When charge carriers are generated in the depletion region by photoexcitation, these charges will start to drift under the influence of the depletion field, constituting

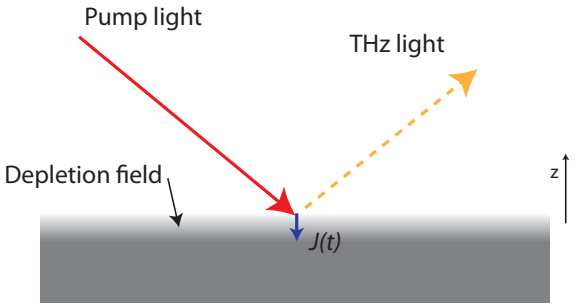

Figure 1.5: Cartoon representation of photocurrent generation in the surface depletion field.

a photocurrent. This is very similar to the photoexcitation of a p-n junction or a Schottky junction diode, or a PCA emitter biased externally. When the excitation is done using femtosecond laser pulses, the resultant transient current emits THz pulses. A cartoon representation of the THz emission is shown in Figure 1.5.

The strength of the depletion field depends on the extent of the bending of the valence and conduction bands of the semiconductor near the surface. Stronger depletion fields result in stronger acceleration of the charge carriers, and thus stronger THz emission. The build-up of the photocurrent and the subsequent decay depend on the properties of the semiconductor, such as mobility, recombination time, etc. For an ideal case, the repetition rate of the femtosecond laser should be such that the optical pulse hits the sample only after the photo-excited charge carriers by the previous pulse have all recombined, and the semiconductor is thus back in its original unperturbed state. For the generation of the photocurrent it should also be noted that the photoexcitation should preferably be above the bandgap of the semiconductor in terms of the photon energy, to excite a sufficient number of charge carriers. Laser light with a wavelength of 800 nm (corresponding to a photon energy of 1.55 eV) can resonantly excite electron-hole pairs in GaAs. GaAs has a bandgap of 1.55 eV. Transient photocurrents are thus the dominant mechanism for the generation of THz radiation from the surface of GaAs.

1.9.2 Photo-Dember field

When the photogeneration of electron-hole pairs takes place near a semiconductor surface, these charge carriers diffuse away into the bulk. If the mobilities of the two are different, one type of charge carrier, most often the electrons, moves faster than the other, resulting in a spatial separation of charges as shown in Figure 1.6. This is knows as the photo-Dember effect, and the electric-field thus developed is known as the photo-Dember field [54]. The effective current of each carrier type is the sum of diffusive motion and drift motion under a local electric field. A simplified model of the ultrafast photo-Dember effect is provided by Kono *et al.* [55]. A cartoon

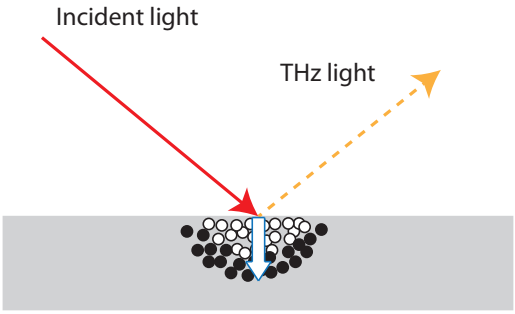

Figure 1.6: Cartoon representation of the photo-Dember effect. The incident pump beam generates electron (dark dots) and hole (white dots) pairs at the surface of the semiconductor. When these charge carriers diffuse away, electrons move faster than holes (in general) to build up a transient polarization near the surface.

representation of the THz emission by photo-Dember effect is shown in Figure 1.6. The diffusive currents of electrons (J_n) and holes (J_p) can be expressed as,

$$J_n \propto eD_e \frac{d\Delta n}{dx} \tag{1.8}$$

and

$$J_p \propto eD_h \frac{d\Delta p}{dx}, \tag{1.9}$$

where e is the electron-charge, $\frac{d\Delta n}{dx}$ and $\frac{d\Delta p}{dx}$ are the density gradients of the photo-generated electrons and holes respectively. The diffusion coefficient D of electrons and holes $D = D_e$ and $D = D_h$ are defined as,

$$D = k_B T\mu/e, \tag{1.10}$$

where $\mu = \mu_e$ and $\mu = \mu_h$ are the mobilities of electrons and holes respectively, k_B is the Boltzmann constant and T is the temperature of the corresponding carrier distribution. The photo Dember current, $J_D = J_n + J_p$, is thus seen to be proportional to the carrier mobilities. Because the effective mass of electrons is typically much smaller than that of holes, most of the excess energy of photo-excitation will be transferred to the electrons. The large mobility and large kinetic energy of electrons result in a large diffusive current. The contribution from holes can thus be neglected [55]. The emitted THz field can be expressed as,

$$E_{THz} \propto \frac{\partial J_n}{\partial t} \propto \mu(T) \frac{d\Delta n}{dx}. \tag{1.11}$$

When the surface depletion field of the semiconductor is significantly strong, this also contributes to the THz emission together with the photo-Dember effect. In semiconductors with smaller bandgap, the surface depletion field is usually weaker, and

the photo-Dember effect can be the dominant THz generation mechanism. This generation mechanism has been reported from semiconductors like InAs, indium antimonide (InSb), germanium (Ge), silicon (Si) etc [55–57]. For *n*- and *p*- type semiconductors, the direction of the surface depletion field will be different, but the photo-Dember effect will be more or less the same for both types of semiconductors. This makes it possible to separate the contributions to the THz emission by the photo-Dember effect from the current surge in the surface depletion region. For example, the THz electric fields emitted through the photo-Dember effect in *n*-type InSb, and *p*-type InSb were shown to be of the same polarity. The photo-Dember field formed by optical excitation only depends on the difference in the mobilities of electrons and holes in this case, and is in the same direction, irrespective of the doping type [2].

1.10 Thin films

Ultrafast excitation of semiconductor materials is a commonly used technique to generate broadband THz pulses for imaging and spectroscopy applications. In general, the semiconductors are used either in bulk or as thin films of about ~ 1 μm thickness [58–60]. Thin layers of thickness ~ 100 nm or less are typically not used. One of the main reasons for this might be the fact that as the thickness of the film decreases the interaction length of the pump light with the semiconductor decreases. However, it has recently been demonstrated that the interaction of coherent laser light with thin film semiconductors can lead to counter-intuitive strong absorption [61]. Thin layers of materials are of profound importance in both optical and semiconductor technologies. In optics, thin layers of materials of thicknesses on the order of the wavelength of light are used as anti-reflection coatings, high precision wavelength filters etc. Electronic devices made of thin films of semiconductors are widely used, for example in solar cells. There are various methods which are used for preparing thin films of a few nanometer thickness with high precision, namely thermal evaporation, plasma sputtering, chemical vapor deposition, electro-deposition etc. As we will show in this thesis, femtosecond laser excitation of ultrathin semiconductor layers deposited on metals can lead to surprisingly strong emission of THz pulses.

1.11 Thesis context and overview

In this thesis, we largely focus on the ultrafast optical generation of THz radiation from thin films of semiconductors with thicknesses ranging from a few nanometers to a few hundreds of nanometers. We show that the THz amplitude emitted from thin layers can be much larger compared to that emitted from bulk samples of the same material. Thin films of semiconductors or nonlinear materials also facilitate plasmonic enhancement of the THz generation process. Surface-plasmon enhancement of OR of nanosecond laser pulses in thin films of nonlinear materials has been reported recently [62]. There have been a few reports on the role of surface plas-

mons in enhancing the ultrafast optical generation of terahertz radiation. Most of these works were concentrated on surface plasmon assisted multi-photon excitation of metallic nanostructures. In contrast to these works, we show surface-plasmon enhanced terahertz emission by *second-order* OR from different thin film systems.

In Chapter 2, we discuss the emission of THz pulses from graphite surfaces excited with femtosecond laser pulses. The emission is found to be mainly the result of the generation of an ultrafast photocurrent. Interesting results are obtained when different faces of a highly-oriented graphite crystal are used in the experiments. THz generation from thin films of cuprous oxide (Cu_2O)is discussed in detail in Chapter 3. Easy to prepare, and very versatile, Cu_2O/metal interfaces can be very promising THz sources for THz-TDS or THz imaging applications. In the same way, very thin films of semiconductors like germanium (Ge) and silicon (Si) deposited on metal substrates are also shown to be strong THz emitters compared to thick layers or bulk materials. This is discussed in detail in Chapter 4. Light manipulation and nanoscale concentration of light using plasmonics can be very promising also for THz generation. In Chapter 5, the role of surface plasmons in enhancing THz emission is dicussed. Surface plasmon excitation on metal surfaces enhances the THz emission through enhanced OR from both bare Au surfaces as well as Au surfaces covered with thin layers of nonlinear optical materials or semiconductors. Using this technique, we show that even a 1.2 nm thick monomolecular layer of hemicyanine can emit significant amount of THz radiation.

Chapter 2

Terahertz emission from graphite

Emission of pulses of electromagnetic radiation in the terahertz range is observed when graphite surfaces are illuminated with femtosecond laser pulses. The nonlinear optical generation of terahertz pulses from graphite is unexpected since, in principle, the material possesses a center of inversion symmetry. Experiments with highly-oriented pyrolytic graphite crystals suggest that the terahertz radiation is generated by a transient photocurrent in a direction normal to the graphene planes, along the c-axis of the crystal. This is supported by magnetic-field induced changes in the direction of the terahertz electric-field polarization, and consequently, the direction of the photocurrent.

2.1 Introduction

Graphite is one of the different forms in which the element carbon can exist in nature. It is an allotrope of carbon. The properties of graphite are such that it can be classified as a semimetal. Another very popular allotrope of carbon is diamond. While diamond is a hard material and an electrical insulator, graphite is soft and a relatively good conductor. Allotropes of the same element can have such strikingly different physical properties because of the difference in the arrangement of atoms in them. Graphite has many applications in industries, for example in arc-lamp electrodes. It is soft and flaky in nature, and also finds an application in everyday life as pencil-lead. In pencil-lead, graphite is mixed with a binding clay. Marks can be made on a sheet of paper or on other surfaces by pencils by physical abrasion which leaves behind traces of graphite. There has been increased interest recently in graphite and certain other allotropes of carbon, such as graphene and carbon nanotubes, because of their potential application in carbon-based electronics [63]. Graphene and graphite are known to be capable of sustaining high current densities.

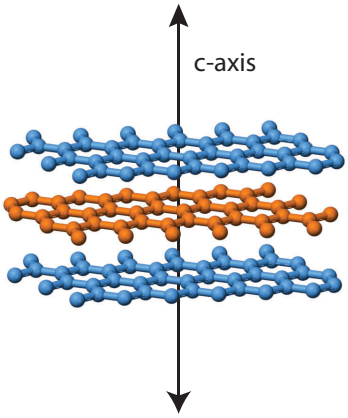

Figure 2.1: A simple representation of the structure of graphite. The c-axis is defined in a direction perpendicular to the graphene planes.

2.1.1 Structure of graphite

Structurally, graphite crystals consist of stacks of identical atomic planes of carbon, as shown in Figure 2.1. Within each single plane, carbon atoms interact much more strongly than with those from the adjacent planes, and form covalent bonds in a honeycomb structure possessing hexagonal symmetry. Such a two dimensional single-atom thick plane is known as graphene. Different graphene planes in graphite are attached to each other by weak van der Waals forces. The direction perpendicular to the graphene layers is the c-axis, as shown in Figure 2.1. The thermal, electrical and optical properties of graphite in a direction parallel or perpendicular to these graphene layers are known to be different [64, 65]. This peculiar structure gives graphite unique qualities which are widely made use of in its different applications [66, 67]. Time and again, the structure of graphite has attracted the attention of various physicists because of its unique electronic and lattice properties. To this end, extensive studies have been carried out on the transport properties and ultrafast carrier dynamics in graphite, in both theory and in experiments [68, 69].

2.1.2 Highly-oriented pyrolytic graphite

The graphite in pencil-lead, or the graphite found in nature, does not necessarily consist of uniformly aligned stacks of graphene planes. Such samples can therefore not be used in the experiments where the structure of graphite plays an important role. Highly-oriented pyrolytic graphite (HOPG) is a form of graphite where the quality of the alignment of graphene layers is well defined. However, HOPG itself does not consist of extended graphene layers neatly stacked on top of each other. HOPG consists of a collection of micro-crystallites of graphite, with their c-axes all

aligned more or less in a specific direction. The quality of HOPG crystals is usually expressed in terms of the consistency in the alignment of the micro-crystallites in them. The angular spread in the orientation of the c-axes of the micro-crystallites is called the *mosaic spread* [70]. HOPG crystals usually have a *mosaic spread* of $< 1^{\circ}$. For this reason, HOPG crystals are generally used for the study of various physical properties of graphite.

2.2 Optical rectification by graphite

In 2004, Mikheev *et al.* reported the observation of second-order nonlinear optical rectification of nanosecond laser pulses by nano-graphite films, proposing that magnetic dipoles or electric quadrupoles are responsible for the emission of a transient pulse [71]. This suggests the possibility of using graphite surfaces and related materials as sources of electromagnetic radiation in the terahertz (THz) region, by the rectification of femtosecond laser pulses. In principle, graphite is a system with a center of inversion symmetry, which does not allow electric dipole second-order nonlinear processes from the bulk of the crystal, as the $\chi^{(2)}$ of such a system vanishes [42]. Another report by Newson *et al.* in 2008, showed the generation of photocurrents in carbon nanotubes and graphite using a third-order nonlinear optical process. In that experiment, laser pulses with a central wavelength of 1400 nm and its second-harmonic are focused onto a graphite surface to create a picosecond transient photocurrent. The magnitude and sign of the photocurrent are determined by the phase difference between the two optical beams. This transient photocurrent is detected via the emitted THz radiation [72]. In principle, third-order nonlinear processes are allowed in all media, whether they possess inversion symmetry or not.

Excitation of graphite with short light pulses, and the subsequent carrier dynamics is a topic of detailed study in the literature [68]. The dynamics of elementary excitations in graphite and graphene occur on ultrafast time scales, governed by the interaction among carriers and their coupling to the lattice. As shown in the subsequent part of this chapter, femtosecond laser excitation of graphite can also lead to the emission of THz pulses. The study of the emitted THz electric field provides information on the movement of photogenerated charge carriers in HOPG crystals.

2.3 Experimental

A schematic of the experimental setup is shown in Figure 2.2. For the laser source, we used a Ti: Sapphire oscillator (Scientific XL, Femtolasers) generating p-polarized light pulses of 50 fs duration, centered at a wavelength of 800 nm with a repetition rate of 11 MHz. The average power output from this oscillator is 800 mW which is split into two by an 80/20 beam splitter. The 80% part is used as the pump beam, and the 20% part as the sampling beam. The pump beam is focused onto the sample by an $f = 150$ mm lens. A tight focus was avoided to prevent any photo-induced

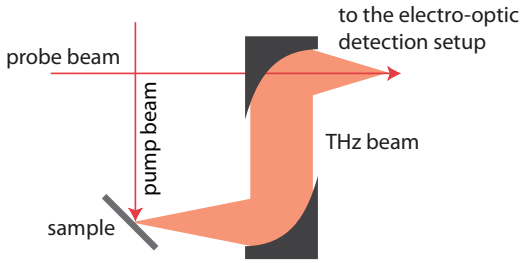

Figure 2.2: Schematic of the experimental setup. The pump beam is focused onto the sample surface at a 45° angle of incidence.

damage. The generated THz beam was collected using off-axis paraboloidal mirrors and focused onto an electro-optic detection crystal (500 μm thick ZnTe (110)) [22]. The synchronized, co-propagating, sampling pulse is also focused onto the detection crystal. The THz electric-field elliptically polarizes the probe beam to an extent proportional to the instantaneous THz electric-field value. The probe beam then propagates toward a differential detection setup consisting of a quarter wave plate, a Wollaston prism and a differential detector. This setup measures the ellipticity of the beam and thus the instantaneous THz electric-field strength. [23]

HOPG crystals used in the experiment were purchased from Optigraph GmbH, Berlin,[1] and were used in the experiments with freshly cleaved surfaces, mostly without any further processing. In our experiments we used crystals of mosaic spread 0.8° as well as 0.4°. The face of the crystal which ideally ends with a graphene plane with the c-axis normal to the surface, is called the basal plane surface and the crystal faces perpendicular to it are called the edge plane surfaces. Both the basal plane surfaces and the edge plane surfaces of the crystal were used in our experiments for the generation of THz radiation.

2.4 Terahertz emission

2.4.1 Basal-plane surface illumination

Figure 2.3(a) shows the temporal waveform of the electric-field generated from the basal plane surface of an HOPG crystal, electro-optically detected in a nitrogen purged environment using a 500 μm thick ZnTe (110) crystal. The angle of incidence of the pump beam was 45°. The waveform consists of a nearly single-cycle pulse followed by a rapidly oscillating decaying tail. The rapidly oscillating tail is due to the phase-mismatching in the detection crystal. For proper phase matching, the phase velocity of the THz radiation should match the group velocity of the probe

[1] http://www.optigraph.eu/index.html

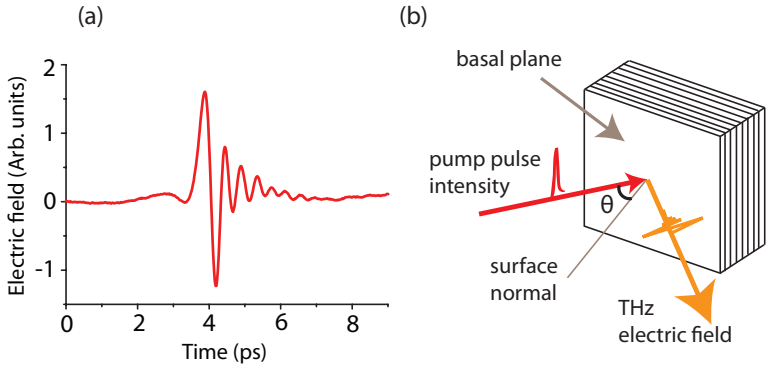

Figure 2.3: a) A typical THz electric field emitted from HOPG basal-plane, plotted vs. time, b) Scheme of illuminating the basal-plane of HOPG.

pulse. A phase-mismatch causes additional oscillations to appear in the trailing part of the THz pulse [73]. The polarization of the emitted THz pulse was checked with a wire-grid polarizer and was found to be in the plane of incidence, irrespective of the polarization of the pump beam. A schematic of the basal-plane excitation is depicted in Figure 2.3(b). Little or no horizontally or vertically polarized THz electric-field is detected in the back-reflection direction, when the angle of incidence of the pump beam is 0°. All of this indicates that the THz emission is mainly due to a possible transient charge movement along the surface normal when the basal-plane is illuminated.

The emitted THz electric field from the basal-plane (at 45° illumination) does not change when the HOPG crystal is rotated about the surface normal. In other words, the THz emission does not depend on the azimuthal angle orientation of the crystal. This suggests the absence of any preferential direction of charge movement within the basal-plane. In principle, there are three equivalent directions in the basal plane owing to the symmetry of arrangement of carbon atoms [66]. However, we do not observe any effect of this in the azimuthal angle dependence.

Scotch tape was used to remove layers of graphite from the basal-plane and fresh surfaces were tested for their ability to generate THz pulses during illumination with femtosecond laser pulses. The THz pulses generated from different freshly cleaved surfaces all look similar in shape, and amplitude. The polarity of the generated THz electric-field is also the same for the two opposite faces of the crystal. Generation of THz radiation at the basal-plane of the crystal is thus likely a surface phenomenon, which is identical for all the HOPG basal-plane surfaces tested, even surfaces that previously were connected (before cleaving).

The amplitude of the generated electric field is about 5% of that generated from an unbiased semi-insulating GaAs (100) surface at pump intensities below about 3 W/cm^2, and is opposite in polarity. This increases to about 11% at higher pump

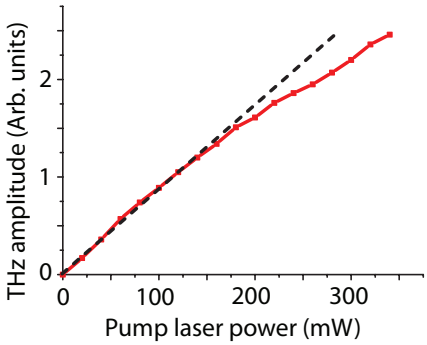

Figure 2.4: The THz amplitude from HOPG basal-plane is plotted as a function of the incident laser power. The dashed line is a linear fit to the data at low pump power.

powers, presumably due to the difference in pump-power saturation between the two materials. The generated THz electric field as a function of increasing pump power, is shown in Figure 2.4. At low pump powers the dependence is linear, which is indicative of a second-order nonlinear process. At higher powers, the THz generation increases sub-linearly, indicating the onset of saturation. Graphite, in principle, is a material which possesses a centre of inversion symmetry, which prohibits $\chi^{(2)}$ processes from the bulk of the crystal [71]. Based on the fact that graphite is more or less opaque to the pump beam, the generation of THz radiation near the surface must be localized to a thin layer consisting of multiple graphene planes within the penetration depth of the pump beam.

2.4.2 Magnetic-field enhancement

Application of a magnetic field of about 1 T across the HOPG basal-plane surface was found to affect the generated THz electric field amplitude and polarity. At 0° pump beam incidence, little or no THz emission is observed in the back-reflection direction. When the magnetic-field is applied, in the plane parallel to the optical table and perpendicular to the c-axis of the crystal as shown in Figure 2.5(a), we see a vertically polarized component of the emitted THz electric-field. Ideally, in this configuration, the THz electric-field is detected only in the presence of the magnetic-field. When the magnetic-field is reversed, the polarity of the THz pulse reverses too (Figure 2.5(b)). This strongly suggests that the illumination of the surface with femtosecond laser pulses initially causes a transient current along the c-axis, perpendicular to the surface. The application of the magnetic-field $\vec{B}$ creates a Lorentz force $\vec{F_L}$ as defined by Equation 2.1 acting on the charge q moving with a velocity $\vec{v}$, which adds a vertical component to the current, parallel to the basal-plane, and thus creates a vertically polarized THz electric-field component similar to what has been observed

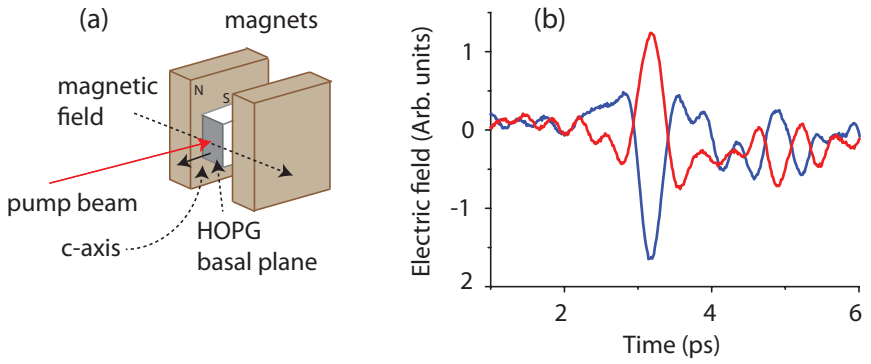

Figure 2.5: (a) Schematic of the magnetic field enhancement setup. The basal-plane of graphite is placed between two powerful magnets. The direction of the magnetic field is as shown, (b) Comparison of the THz waveform for opposite directions of the applied magnetic field.

in semiconductors such as indium arsenide (InAs) [74–77].

$$\vec{F_L} = q(\vec{v} \times \vec{B}) \tag{2.1}$$

Reversal of the direction of the magnetic field thus reverses the direction of the force on the photocurrent, flipping the sign of the THz pulse. This provides a strong indication that the photo-induced currents are, indeed, perpendicular to the basal plane.

2.4.3 Edge-plane surface illumination

The edge-plane surface contains the c-axis of the crystal. When the edge-plane surface is illuminated, therefore, two configurations are possible; one with the c-axis in the plane of incidence and the other with the c-axis perpendicular to the plane of incidence. Emission of THz pulses is observed from the edge-plane surface for both 0° and 45° illuminations, and the THz electric fields emitted are fairly strong and comparable in amplitude with the THz electric field generated from the basal-plane surface at 45° illumination. A schematic of the edge-plane illumination is shown in Figure 2.6(a).

When we rotate the crystal about the surface normal, the polarization of the emitted THz radiation rotates with it, always remaining in a plane perpendicular to the surface containing the c-axis. In order to further illustrate this, two THz pulses emitted from the crystal oriented at azimuthal orientations; ϕ =90° and ϕ = 270° are shown in Figure 2.6(b). The angle of illumination of the pump beam in this case is 0°. The emitted THz amplitude from the edge-plane surface of the crystal illuminated at 0° angle of incidence, is plotted against the azimuthal angle ϕ in Figure 2.6(c). Note that the electro-optic detection system is polarization sensitive, and only one polarization component of the generated THz is detected at a time [22]. The THz

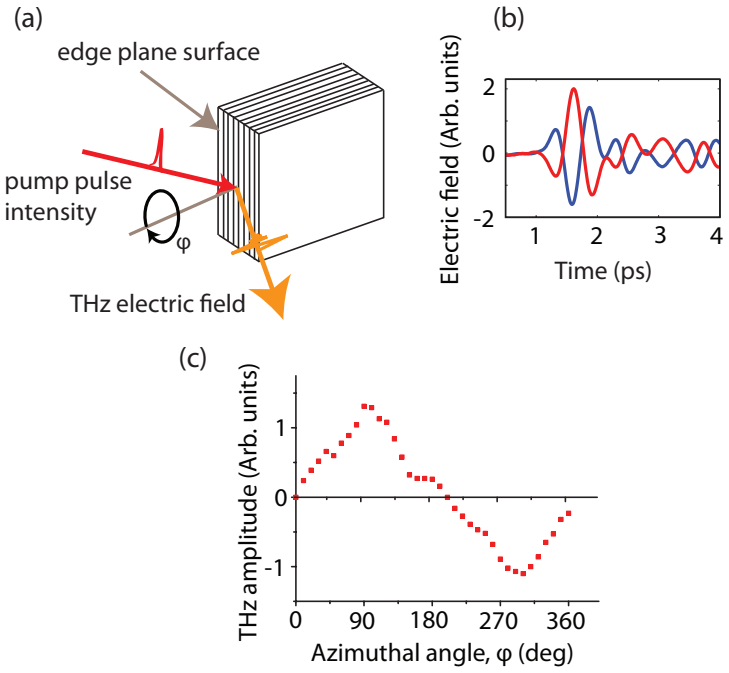

Figure 2.6: (a) Scheme for illuminating the edge-plane of HOPG. The emission from the edge-plane could be observed at both 0° angle of pump beam illumination, as well as 45°, (b) Comparison of two THz electric field pulses emitted from the edge-plane surface of HOPG for $\phi = 90°$ (blue) and $\phi = 270°$ (red). The illumination in this case was done at 0° angle of incidence, (c) The amplitude of the THz electric field emitted from the edge-plane surface of HOPG, as a function of the angle ϕ, with the angle of pump illumination 0°.

amplitude shows a single-cycle sinusoidal behavior over a 360° azimuthal rotation of the crystal, which is an indication of an in-plane THz dipole. Magnetic-field enhancement measurements could not be performed in this case. It was impossible to prepare very thin edge-plane samples owing to the flaky nature of HOPG. However, the azimuthal angle dependence shown in Figure 2.6(a) already strongly indicates that the transient charge movement at the edge-plane takes place mainly parallel to the sample surface and parallel to the c-axis, which conforms with our observations with the basal-plane illumination discussed in section 2.4.1. This means that we expect an in-plane magnetic-field perpendicular to the transient currents, would lead to a decrease in the emitted THz amplitude whereas no effect would be observed when the two are parallel.

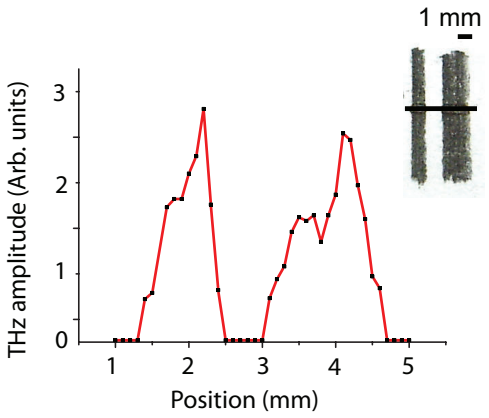

Figure 2.7: THz amplitude emitted from two lines drawn on paper (inset) using a graphite pencil, plotted as a function of position on the paper.

2.5 THz generation from pencil-lead

Interestingly, we find that other forms of graphite are also capable of emitting THz pulses, when illuminated with femtosecond laser pulses. In fact, even the graphite present in pencil-lead emits THz pulses when illuminated with femtosecond pulses. In Figure 2.7 we show the THz electric-field amplitude measured as a function of position along a line across a pencil drawing on paper, consisting of two stripes, as shown in the inset. For this experiment, the laser beam was focused to a 1 mm spot-size on the paper. From the figure it is clear that only the graphite emits THz radiation and not the paper. Pencil-lead contains graphite as a major component along with clay and other substances which define its hardness. We note here that, recently, Abraham *et al.* reported the imaging of graphite pencil drawings on paper using THz transmission imaging [78]. Using THz time-domain spectroscopy (THz-TDS), they measured the transmission of THz pulses of bandwidth up to 2 THz through papers containing pencil drawings, and assessed the gradual absorption dependence on the graphite proportion for different pencils, from hard to soft graphite leads. Our work shows that the pencil drawings on paper are also capable of *emitting* measurable THz pulses when excited using femtosecond laser pulses.

2.6 Discussion

Combining the observations from both 0° and 45° angle of incidence illumination, we see that the generated THz dipole at the HOPG surface is always oriented along the c-axis of the crystal. As mentioned earlier, a possible underlying mechanism for the generation of THz radiation is a transient charge movement along the c-

axis of the crystal. The conductivity of graphite along the c-axis is known to be at least three orders of magnitude smaller than the conductivity along the graphene planes [64–67]. A preferred charge movement along the c-axis, following an ultrafast excitation of graphite, has not been reported in the literature to our knowledge.

The THz electric-field generated from any basal-plane surface, always has the same polarity. Even when new basal-plane surfaces are created by repeatedly cleaving the sample, the surfaces from both new samples that are formed give rise to the emission of THz radiation with the same polarity. There are at least two possible generation mechanisms involving charge movement that can give rise to THz emission. Graphite basal-plane surfaces are reported to have a space charge layer of a few nanometers thickness [79, 80]. The femtosecond laser-created charge carriers, accelerated in this space charge layer, can emit pulses of THz radiation.

Another possible mechanism is the photo-Dember effect [54]. The strong optical absorption of the laser pulses by graphite leads to the formation of a carrier concentration gradient perpendicular to the surface. If the electron and hole mobilities along the HOPG c-axis are different, this can give rise to the development of a time-dependent dipole along the c-axis, which emits a THz electric-field pulse. These mechanisms are similar to that reported earlier for semiconductor surfaces, such as GaAs [81].

The azimuthal-angle dependence of the THz electric-field generated from the edge-plane surface, resembles that of an in-plane biased semiconductor surface where the photo-generated charge carriers move preferentially in one direction along the surface and which therefore reverses direction when the sample is rotated by 180°. However, here, no external bias is applied to the HOPG sample. The above proposed mechanisms for the emission of THz radiation when the basal-plane surface is illuminated, namely, carrier acceleration in a space-charge layer and the photo-Dember effect, cannot completely explain this. Although HOPG is the best available well-oriented system of graphite, it does not constitute a perfect crystal. HOPG is known to contain stacking faults [82]. Graphite mainly exists in hexagonal form, but the rhombohedral form can also exist together with the hexagonal structure. Stacking faults in the crystal can act as breaks in the conduction paths along the c-axis direction, which can lead to accumulation of charges [83, 84]. These accumulated charges can lead to built-in electric potentials in the crystal. Along the c-axis, graphite is known to behave electrically like a semiconductor [66]. Perhaps these built-in potentials in the crystal can give rise to charge acceleration in a preferred direction leading to the emission of THz pulses when the edge plane surface is irradiated with femtosecond laser pulses [85]. This implies that weaker THz electric-field would be emitted from the edge-planes of a sample with fewer stacking faults.

2.6.1 Subsequent works

Recently, another theoretical explanation for the THz emission from graphite was given by Carbonne. They suggested c-axis compression and expansion soon after the femtosecond laser excitation of graphite, which can be responsible for the charge

movement along the c-axis that was observed in our experiments. In their work, they calculated the *ab initio* charge density of graphite, and studied its evolution during the photo-induced structural distortions [86]. Nagel *et al.* in 2010 reported the results of their near-field study of THz surface waves emitted from graphite flakes, excited with femtosecond laser pulses. A radially symmetric transport of the photo-excited charges at the pump location was held responsible for the THz emission in their study [87], partially contradicting our results.

2.7 Conclusion

In conclusion, the emission of transient subpicosecond pulses of electromagnetic radiation in the THz region, is observed when graphite surfaces are illuminated with femtosecond laser pulses. The emitted THz radiation is mainly polarized along the c-axis of the crystal [20]. The THz pulses emerging from the basal-plane surface are most likely created by a transient charge movement along the c-axis, either because of the charge acceleration in the thin surface-space-charge layer of graphite, or because of the photo-Dember effect. Involvement of the charge carrier movement is confirmed by magnetic-field induced changes in the emitted THz electric-field. The polarity changes in the emitted THz electric field showed that there is a charge movement along the c-axis direction. The emission of the THz pulses from the edge plane surfaces is tentatively ascribed to built-in potentials created by stacking faults in the material.

Chapter 3

Terahertz emission from cuprous oxide/metal interfaces

Cuprous oxide/metal interfaces are found to emit surprisingly strong terahertz pulses when illuminated with femtosecond laser pulses. The emission is surprising because the illumination is done at a wavelength of 800 nm, which corresponds to a photon-energy much smaller than the bandgap energy of cuprous oxide. Our experimental results suggest that the terahertz emission mainly originates from the creation of charge carriers in the Schottky field near the cuprous oxide/metal interface.

3.1 Introduction

Optical rectification (OR) of femtosecond laser pulses is widely used as a mechanism for generating broadband pulses in the terahertz (THz) frequency range [2]. The emitted THz pulse is also often used to probe the ultrafast dynamics taking place in the material following the photoexcitation process [88, 89]. It has already been shown that THz pulses can be generated by exciting the surfaces and interfaces of various semiconducting materials. Presently, gallium phosphide (GaP), zinc telluride (ZnTe), indium arsenide (InAs), and gallium arsenide (GaAs) etc. are most often used as sources of THz radiation [2, 90]. As we discussed in Chapter 1, this helps to bridge the THz gap to some extent. A suitable, low cost, easy to prepare THz source, though, still remains desirable.

In this chapter, we discuss the generation of THz pulses from oxidized copper (Cu) surfaces or, in general, from the interfaces of cuprous oxide and some metals, when they are illuminated with femtosecond near-infrared laser pulses. We show that the emission from this interface is comparable in strength to the conventionally used THz emitting materials like GaP (110) crystals. Such a strong THz emission from Cu_2O is unexpected, because the bulk Cu_2O possesses a centre of inversion symmetry

and is supposed to absorb only weakly at the wavelength of 800 nm. Conventional second-order nonlinear processes like OR are not possible in materials which possess a centre of inversion symmetry [42].

3.2 Oxides of copper

Under atmospheric conditions, Cu can form two types of oxides. These are copper (I) oxide, called cuprous oxide (Cu_2O) and copper (II) oxide, called cupric oxide (CuO) [91]. These two oxides of Cu are known to be semiconductors. Historically, Cu_2O was one of the first known semiconductors. A Schottky interface of Cu and Cu_2O constituted the first semiconductor diode [89]. The mechanism of oxidation of Cu has been the subject of detailed studies in the literature [92, 93]. Because of their potential use in solar cells, photovoltaic research on the oxides of Cu remains very active.

3.2.1 Cuprous oxide

Cu_2O is readily formed when fresh Cu surfaces are exposed to ambient air at room temperature. It gives unprotected Cu a reddish tint whereas an unoxidized clean Cu surface has a pink appearance. Bare, unprotected Cu gets oxidized by interacting with atmospheric oxygen (O_2),

$$4\,Cu + O_2 \longrightarrow 2\,Cu_2O. \tag{3.1}$$

Cu_2O formed by oxidation of Cu in the atmosphere is known to be a p-type semiconductor. Electrical and optical properties of different Cu_2O/metal interfaces have been studied in detail in the literature [94–96]. Cu_2O forms a Schottky barrier when it is in contact with metals such as Cu, but tends to form an Ohmic contact with metals like gold (Au) although, recently, some reports have emerged showing that Au on top of Cu_2O nanowires can form a Schottky contact [97]. Cu_2O/metal interfaces can act as solar cells. However, the practical efficiency of such devices is reported to be $< 2\%$ [98]. Nevertheless, the advantages of Cu_2O for solar energy applications are its low cost and the availability of the base material (Cu), the rather simple material preparation, and a bandgap of 2.1 eV which suitably lies in the visible range.

3.2.2 Cupric oxide

CuO is formed when Cu_2O further interacts with atmospheric oxygen at temperatures above 250°C [99, 100]. It also gets formed by the oxidation of Cu at elevated temperatures. For that reason, the surface layer of Cu_2O can contain traces of CuO if the sample is heated at a temperature above 250°C. CuO has a black appearance, and finds an application in industries as a pigment. CuO also is a p-type semiconductor with a bandgap of 1.35 to 1.5 eV which is lower than that of Cu_2O [101].

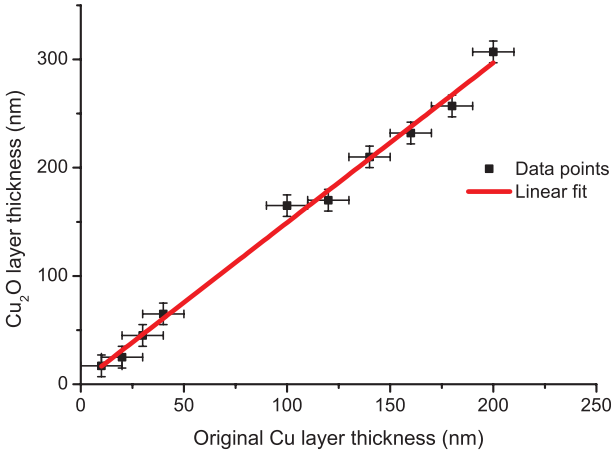

Figure 3.1: Thickness of the Cu_2O film plotted against the thickness of the original Cu layer before oxidation, measured using an α-step profiler. The solid line is a linear fit to the data.

3.3 Preparation of cuprous oxide thin films

3.3.1 Low temperature oxidation of thin films of copper

One easy method to prepare a thin film of Cu_2O is by leaving a clean Cu surface in the atmosphere for a while. Atmospheric oxygen (O_2) reacts with Cu, producing a thin layer of Cu_2O at the surface. Unlike the rusting of iron (Fe), the oxidation of Cu surface slows down further oxidation by forming a somewhat protective layer of oxide on the outside. The oxidation rate of Cu underneath the oxide layer decreases as the oxide layer grows thicker. Thus, an unattended, exposed-to-air Cu piece does not eventually turn completely into a block of Cu_2O or other oxides of Cu, but rather remains as a Cu block covered with a layer of Cu_2O. This method of formation of Cu_2O/Cu interface has one disadvantage from an experimental point of view: it is not easy to limit the thickness of the oxide in a precise manner. The thickness of the oxide layer is an important parameter when it comes to studying the physical mechanism behind the THz emission from it. As we will show later, Cu_2O deposited on the surfaces of other metals like Au and silver (Ag) etc. also emits strong THz pulses, similar to oxidized Cu surfaces (which form a Cu_2O/Cu interface), when excited with femtosecond laser pulses. As mentioned before, the interfaces formed between Cu_2O and Au or Ag are, however, reported to be Ohmic or low-barrier Schottky type in many earlier reports [102–104]. In our experiments, Au is an appropriate choice as it can remain chemically inert during the preparation of the sample. Thin Au films of about 200 nm thickness are prepared by electron-beam (e-beam) evaporation under high vacuum conditions (below a pressure level of 10^{-6} mBar) on suitable substrates like a clean glass slide or a silicon (Si) wafer. For a good adhesion of Au onto the

glass or Si surfaces, a very thin layer (about 10 nm thickness) of chromium (Cr) or titanium (Ti) is deposited as an intermediate layer [105]. Thin films of Cu of suitable thickness, are deposited on top of the Au film, again by e-beam evaporation. An *in situ* quartz crystal thickness monitor is used to measure the thickness of the films. The resonance frequency of vibration of the crystal varies as more and more metal is deposited on it. The thickness of the deposited metal film is calculated from the change in the resonance frequency using the physical parameters of the metal which is being evaporated. Cu_2O films were prepared by heating the Cu layers at 250°C for three hours in the lab atmosphere. During this time, the Cu film gets oxidized completely to produce a thin film of Cu_2O. The thickness of the Cu_2O film is larger than that of the deposited Cu film. The increase in the thickness is because of the inclusion of oxygen in the chemical structure which takes up space. In Figure 3.1 we plot the thickness d_{Cu_2O} of the Cu_2O layer measured using an α-step profiler against the original Cu layer thickness d_{Cu}. Within the thickness range that we use in our experiments, we can find an empirical linear relationship between the thickness of the Cu layer and the Cu_2O layer.

$$d_{Cu_2O} = c d_{Cu} \tag{3.2}$$

The multiplication factor c in Equation 3.2 is found to be ~ 1.5. Confirmation of the presence of Cu_2O in these films is done by X-ray diffraction (XRD) measurements. In Figure 3.2, we show the XRD pattern recorded from an oxidized Cu foil. This foil was partially oxidized by heating in the atmosphere at 250°C for three hours. By comparing the diffraction lines with the ICDD (International Center Diffraction Data) database, it is seen that these thin films of oxidized Cu consist of Cu_2O, polycrystalline in form. No measurable amount of CuO is found in the Cu foils.

3.3.2 Chemical deposition of cuprous oxide

Thin films of Cu_2O can also be prepared by different chemical techniques [106,107]. Ristov *et al.*, in 1985, reported chemical deposition of thin films of Cu_2O on different substrates like glass, metals etc. We used this as an alternative technique to prepare Cu_2O, to check if the THz generation takes place from these Cu_2O/metal interfaces as well. The semiconducting properties of Cu_2O are known to depend on the way the oxide is prepared [108].

The deposition of Cu_2O in the method of Ristov *et al.*, is done by the successive immersion of the substrate in a cold complex solution A, and a hot solution B. Solution A consists of 100 cm^3 of 1 M solution of copper sulphate (Cu_2SO_4) and 400 cm^3 of 1 M solution of sodium thiosulphate ($Na_2S_2O_3$). $Na_2S_2O_3$ is poured into a solution of Cu_2SO_4 until it becomes colorless. Thus, a complex solution of $3\,Cu_2S_2O_3 \cdot 2\,Na_2S_2O_3$ is formed. The complex solution is then diluted with deionized water to 1000 cm^3. Solution A decomposes very easily, so the film deposition should start every time with a freshly prepared solution. Solution B is 2 M solution of sodium hydroxide (NaOH) maintained at a temperature between 60°C and 80°C.

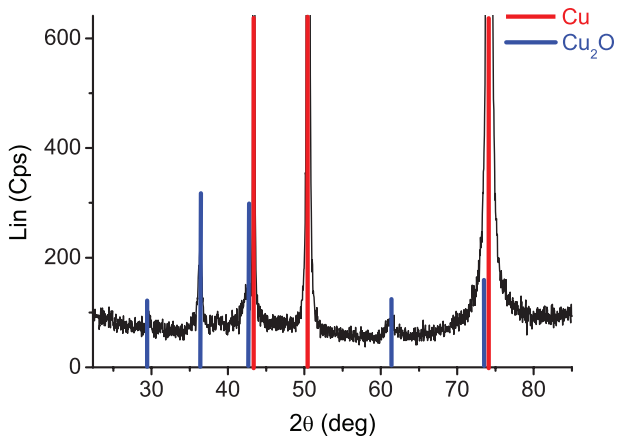

Figure 3.2: Reflected X-ray intensity as a function of the detector angle 2θ, from a partially oxidized Cu foil, oxidized in atmosphere at a temperature of 250°C. The red lines mark the diffraction angles of Cu, and the blue lines mark the diffraction angles of Cu_2O.

A clean substrate is first immersed in solution B, held for about 1-2 seconds and then immersed in the solution A. After three to five immersions, a visible yellow film can be seen on both sides of the substrate. After successive immersions, the Cu_2O film thickens and looks orange and then brown. These colors are the result of the interference and absorption of the white light in the thin films [106]. The chemically prepared Cu_2O films are then characterized using XRD, and are seen to contain only Cu_2O and no other oxide of Cu.

3.4 Experimental setup

The experiments were carried out in a standard THz generation setup as shown in Figure 3.3(a) [20]. We use a Ti: Sapphire oscillator (Scientific XL, Femtolasers) generating p-polarized light pulses of 50 fs duration, centered at a wavelength of 800 nm with a repetition rate of 11 MHz. The average output power from this oscillator is 800 mW which is split into two by an 80/20 beam splitter. The 80% part is used as the pump beam, and the 20% part as the sampling beam. The pump beam is modulated using a mechanical chopper at a frequency of 3 kHz. It is sent to an in-plane retro-reflector delay-stage oscillating at 5 Hz, and is then focused onto the sample surface. The generated THz beam was collected in one of the two different geometries using off-axis paraboloidal mirrors and focused onto an electro-optic detection crystal (ZnTe (110) or GaP (110)) [22]. In one configuration, the pump beam hits the sample at a 45° angle of incidence and the generated THz light is collected in the direction of the specular reflection. In the second case, the generated

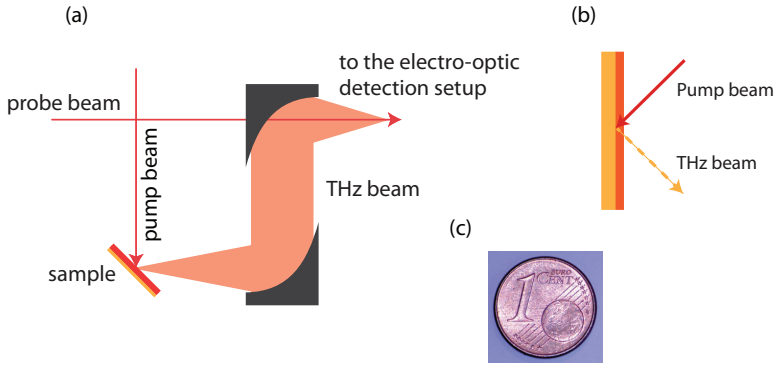

Figure 3.3: (a) Schematic of the experimental setup, (b) Excitation of an oxidized copper surface, (c) A eurocent coin which is capable of emitting strong THz pulses when excited using 800 nm femtosecond laser pulses.

THz beam is collected in the direction of the transmitted pump beam [40]. This requires a transparent (transparent to the pump and/or the THz light) sample. The sample is kept at an oblique angle. The synchronized sampling pulse is also focused onto the detection crystal. The THz electric-field elliptically polarizes the probe beam to an extent proportional to the instantaneous THz electric-field value [22]. The probe beam then propagates toward a differential detection setup consisting of a quarter-wave-plate, a Wollaston prism and a differential detector. Lock-in detection was employed to extract the signal at the chopping frequency of the pump beam. This setup measures the ellipticity of the beam and thus the instantaneous THz electric-field strength [23].

3.5 THz emission from partially oxidized Cu foils

The excitation with 800 nm pulses is done at 45° angle of incidence as shown in Figure 3.3(a) and (b), and the collection of the THz light is done in the specular reflection direction of the pump light. The first set of experiments were performed on partially oxidized copper foils, and even a 1 eurocent coin, as shown in Figure 3.3(c). A typical THz electric field as a function of time, emitted by the sample is shown in Figure 3.4(a). It consists of a nearly single-cycle pulse, followed by a rapidly oscillating tail. The tail is the result of the absorption of THz light by water vapor in the atmosphere and of phase-mismatching effects between the probe and the THz pulses [22]. The emitted THz electric field is mainly p-polarized, irrespective of the polarization of the pump beam. When the angle of incidence of the pump beam is changed to 0°, and the collection of THz light is done in the backward reflected direction, little or no emission could be detected. The THz polarization developed at the sample must therefore be pointed along a direction perpendicular to the Cu_2O/Cu

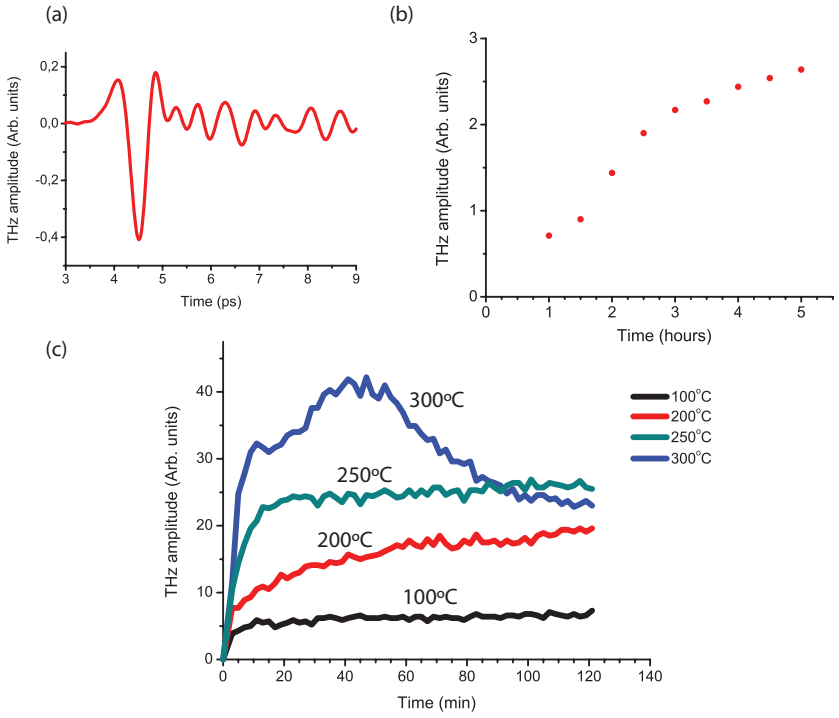

Figure 3.4: (a) THz electric field emitted from an oxidized Cu surface, plotted *vs.* time, (b) THz amplitude from a clean Cu surface kept in air at room temperature, plotted as a function of time, (c) THz amplitude emitted from a clean Cu surface kept at elevated temperatures in air, plotted as a function of time.

interface. An oscillating electric dipole oriented in this direction can not emit along the same direction. No change in the emitted THz pulse is observed when the sample is rotated about its surface normal (azimuthal angle orientation). An azimuthal angle dependence of the emitted THz amplitude is typical for certain crystalline THz emitters showing second-order nonlinear OR [2]. The excitation of Cu_2O films prepared on a glass substrate, does not produce any strong THz emission. On the other hand, freshly cleaned Cu surfaces also produce little or no THz light, confirming that the presence of Cu_2O/Cu interface is necessary for the observation of THz emission.

It is possible to study the oxidation of Cu foils by measuring the THz emission from them over time. A freshly cleaned Cu surface was used for studying the oxidation. Oxides of Cu can be removed from the surface using a weak acid. For our experiments, we use a 1% solution of hydrochloric acid (HCl) which served the purpose well. The foils are dipped inside the acid solution and slowly moved so that the oxide layer is visibly removed and the shiny Cu surface appears. The foils

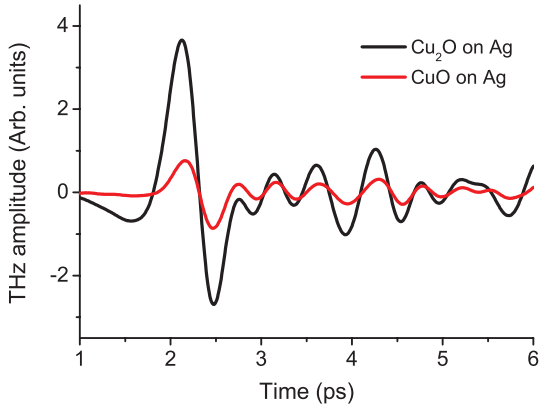

Figure 3.5: THz electric field emitted from a 50 nm thick Cu layer oxidized into Cu_2O (black) and CuO (black) on the surface of an Ag foil, plotted *vs.* time.

are then taken out, cleaned thoroughly with water and dried using compressed dry air. HCl dissolves Cu_2O by forming cupric chloride ($CuCl_2$). In Figure 3.4(b), we show the THz peak amplitude emitted by Cu as a function of time after cleaning the sample with the acid. The figure clearly shows that the THz peak amplitude increases over time, most probably due to the formation of Cu_2O at the surface, which grows thicker as a function of time [109]. It is remarkable that a detectable THz emission is observed just after $\sim$ 60 minutes of exposure to air. The growth of the THz amplitude as a function of time for four different temperatures is shown in Figure 3.4(c). This figure shows that at elevated temperatures the oxidation proceeds much faster. For all temperatures, the emitted THz amplitude increases quickly in the first 10 minutes [110]. At the onset of the oxidation process, Cu_2O is formed by the interaction of the freshly cleaned Cu surface with readily available atmospheric oxygen. As the thickness of the oxide increases, the oxygen has to diffuse through the existing Cu_2O layer in order to interact with the Cu atoms. This slows down the oxidation process [111]. The continued oxidation of the Cu surface leads to changes in the appearance of the sample as a result of the light interference in the film (etalon oscillations). The decrease in the THz emission seen for the sample kept at a temperature of 300°C, after about 50 minutes of oxidation, coincides with visible darkening of the sample surface. This is an indication of the formation of cupric oxide (CuO) by the further oxidation of Cu_2O by atmospheric oxygen at high temperatures. The presence of CuO in this sample is confirmed by XRD analysis. Incidentally, CuO is also a semiconductor material, but with a lower bandgap of $\sim$ 1.35 - 1.5 eV. When CuO gets formed at the surface of the Cu_2O layer, it can prevent the pump light from reaching the Cu_2O/Cu interface, where the actual THz generation takes place. This

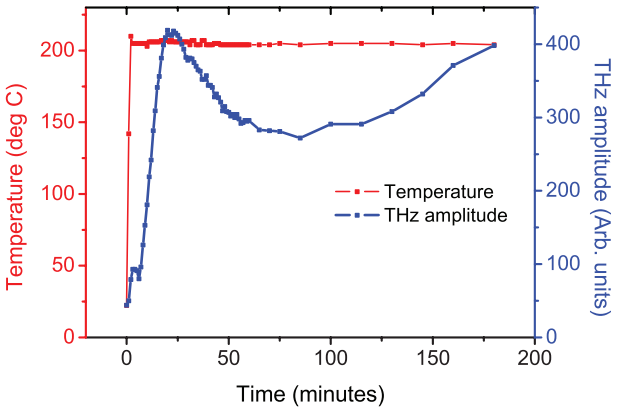

Figure 3.6: THz amplitude from a freshly deposited Cu film of 280 nm thickness on a 200 nm thick Au layer, kept at an elevated temperature of 200°C, plotted as function against time

can result in a decreased THz amplitude.[1] Incidentally, in our experiments, we have observed that CuO/metal interfaces are also capable of generating THz radiation. In Figure 3.5 we plot the THz electric field amplitudes emitted from Cu_2O/Ag and CuO/Ag interfaces prepared from Cu layers of identical thicknesses. The CuO layer was prepared by heating the Cu_2O layer at 450°C for three hours. It is seen that the emitted THz amplitude from the CuO/Ag interface is weaker than that from the Cu_2O/Ag interface. A detailed study of the THz emission from CuO/metal interface is outside the scope of this thesis.

3.6 THz emission from Cu_2O/Au interface

The disadvantage of using oxidized Cu *foils* is that they have an unknown composition and, generally, an optically rough surface which gives rise to optical scattering. In addition, little or no control over the thickness of the oxide layer is attainable. For this reason, we also performed experiments on thin films of Cu deposited on top of 200 nm thick Au on Si substrates. The THz amplitude emitted as a function of time from a 280 nm thick freshly deposited Cu layer on a 200 nm thick Au layer on a Si substrate kept at 200°C, is shown in Figure 3.6. The main difference between this experiment and the previous experiment is that, this time, the layers are prepared on an optically flat substrate. Cu_2O has a refractive index $n \sim 2.7$, and even thin films of it can contribute to interference of the pump light at a wavelength of 800

[1]The decrease in the THz emission can also be because of the diminished absorption of the pump light in the film due to constructive interference of the reflected light. This depends on the thickness of the film. The changes in THz emission due to pump light interference in thin films of semiconductors is the main topic of discussion in Chapter 4.

nm. As a smooth film of oxide is formed on the surface of the Cu layer, the pump light incident on the sample is multiply reflected, and etalon oscillations take place. This results in an oscillating absorption of the pump light as the Cu_2O thickness increases as a function of time. As shown in Figure 3.6, this results also in oscillation of the emitted THz amplitude as a function of time. Absorption of coherent light by thin films depends heavily on the interference of light in them. The first maximum in the THz amplitude is observed after about 5 minutes and the second maximum after about 25 minutes of oxidation. The growth of the oxide layer slows down as the oxidation proceeds. The initially formed oxide layer acts as a barrier for oxygen molecules to pass through to reach the Cu atoms underneath [93]. This process is dominated by diffusion of ions and the oxidation thus eventually slows down. Since the interfaces Cu_2O/Au and Cu_2O/Cu may not be identical in terms of the strength of the Schottky field, the experimental result shown in Figure 3.6 can have two parts. The initial increase in the THz amplitude is from a Cu_2O/Cu interface getting developed at the surface of the Cu film. As the oxide layer grows thicker over time, the Cu layer becomes thinner, and eventually disappears as the Au layer is reached resulting in a Cu_2O/CuAu interface, which possibly gets formed at the interface[2]. It has to be noted that prolonged annealing of Cu_2O could have an effect on its electric and/or optical properties. This is because of possible structural changes [101]. This is not considered in the present work.

In a separate experiment, we have observed that the emitted THz amplitude from Cu_2O on Au shows little variation in the range of temperatures (below 250°C) used in the above experiment (results are not shown here). Thus the contribution of the temperature-induced changes such as thermal excitation of additional free carriers can be ignored for the present case.

It is interesting to note that, although the interfaces of Cu_2O with Au are reported to be mostly Ohmic in nature [112], the depletion field is sufficient to allow THz generation from them. One of the possible reasons for this is the formation of a CuAu alloy at the interface. It has been reported that Cu atoms can diffuse into Au to form a CuAu alloy at the interface when a Cu layer is initially deposited on the Au films [113, 114]. Since the work function of Cu is lower than that of Au, it is very well possible that CuAu has a work function lower than that of pure Au, so that a Schottky contact can be formed between Cu_2O and CuAu.

THz emission from Cu_2O formed on a Cu surface is a sensitive way of detecting very thin films of the oxide. In Figure 3.4(a) we have already seen that a detectable THz emission can be observed after $\sim$ 60 minutes of exposing a clean foil to the atmosphere.

Chemically prepared Cu_2O layers on Au substrates (as described in section 3.3.2) also emit THz pulses when excited using femtosecond laser pulses, similar to the layers produced by the oxidation of Cu layers deposited on Au substrates. The advantage of the chemical method is that a uniform layer can be produced on different substrates, no matter whether they have curved/patterned surfaces or not. In the

[2] CuAu stands for an alloy of Cu and Au.

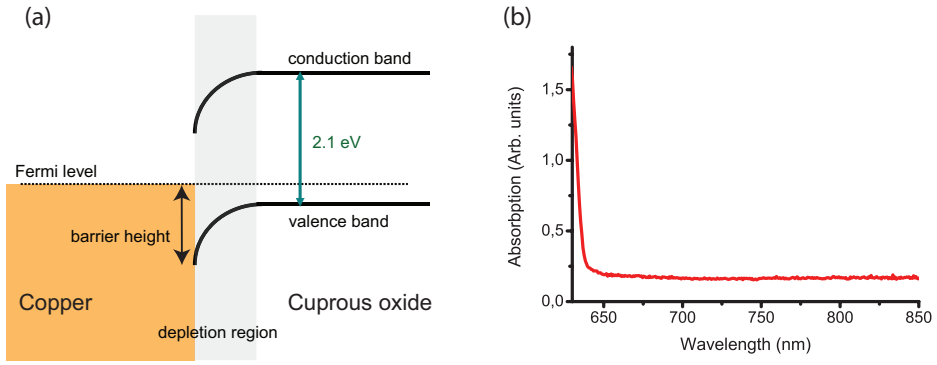

Figure 3.7: a) Band diagram of a Cu_2O/Cu interface, showing the band bending, b) Absorption spectrum of a 500 μm thick Cu_2O crystal, near the bandgap energy.

case of vacuum evaporation of Cu, shadow effects in the deposition can lead to Cu_2O layers of non-uniform thicknesses.

3.7 THz generation mechanism

The topic of THz generation from Cu_2O/metal interfaces becomes interesting considering that Cu_2O alone does not produce any significant amount of THz light when illuminated with the 800 nm laser light. Ideally, Cu_2O does not absorb light at the wavelength of 800 nm. When a semiconductor and a metal are brought together, their Fermi levels match with each other. This results in the bending of valence and conduction bands close to the metal interface. Cu_2O formed by oxidation in the ambient air is reported to be p-type. For p-type Schottky interfaces, the conduction band and the valence band of the semiconductor bend downward when the metal is brought in close contact with the semiconductor [51]. The Fermi level pinning of a typical Cu_2O/Cu interface is schematically shown in Figure 3.7(a). A shrinkage of the bandgap of the semiconductor as a consequence of what is called 'the image potential' at the metal surface has also been suggested [115]. In Figure 3.7(b), the measured absorption spectrum of a 500 μm thick Cu_2O crystal is shown. The increase in absorption below a wavelength of $\sim$ 650 nm is because of the excitation of electron-hole pairs across the bandgap. It is seen that in this crystal, there is little or no absorption at 800 nm. However, for oxidized thin Cu layers, some absorption is possible due to impurities and defect states [116]. The DC offset is the result of the reflection loss of the light at the surface of the crystal, which is not corrected for in the measurement.

In Figure 3.8, we plot the THz amplitude as a function of the incident laser power, emitted from a Cu_2O/Au interface. The THz amplitude increases linearly with the

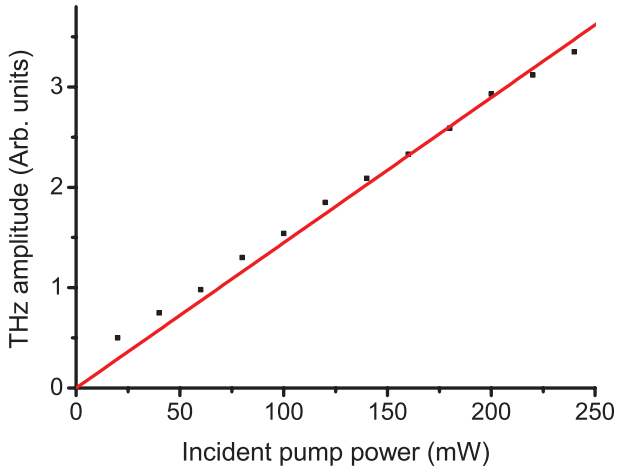

Figure 3.8: The THz amplitude emitted from a 275 nm thick layer of Cu_2O on 10 nm Au on a glass substrate, as a function of the incident laser power. The solid line is a guide to the eye.

laser power, suggesting that a second-order nonlinear optical process is responsible for the THz emission. However, there are different THz emission processes which can show a second-order dependence on the pump electric field. Based on the experimental results, three possible mechanisms can be responsible for the THz emission from Cu_2O/metal interfaces, as described below.

3.7.1 Photocurrent surge in the Schottky field

In an ideal case, Cu_2O crystals do not absorb light at the wavelength of 800 nm, since the bandgap of Cu_2O is 2.1 eV which corresponds to a wavelength of 590 nm. In the samples that are prepared in our laboratory by oxidation of thin films of Cu, we have observed a certain amount of absorption of the laser light at a wavelength of 800 nm. Sub-band excitations by impurities could be responsible for this. As we have already seen in section 1.8, it is possible to generate THz radiation by ultrafast resonant laser excitation of a semiconductor kept under a voltage bias. Cu_2O/metal interfaces can form Schottky barriers. Excitation of electron-hole pairs in the depletion field of a Cu_2O/metal interface by the pump light can lead to the formation of transient currents emitting THz pulses. The emitted THz amplitude from a Cu_2O/Au interface is plotted as a function of the pump beam incident angle in Figure 3.9(a). The Cu_2O/Au interface was prepared by first depositing a 10 nm thick Au layer on a glass slide followed by the complete oxidation of a 150 nm thick Cu layer deposited on top of it. In this experiment, excitation was done in the transmission mode with the pump beam hitting the interface from the glass side. When the pump beam is incident on the sample at normal incidence, no THz emission is detected in the transmission

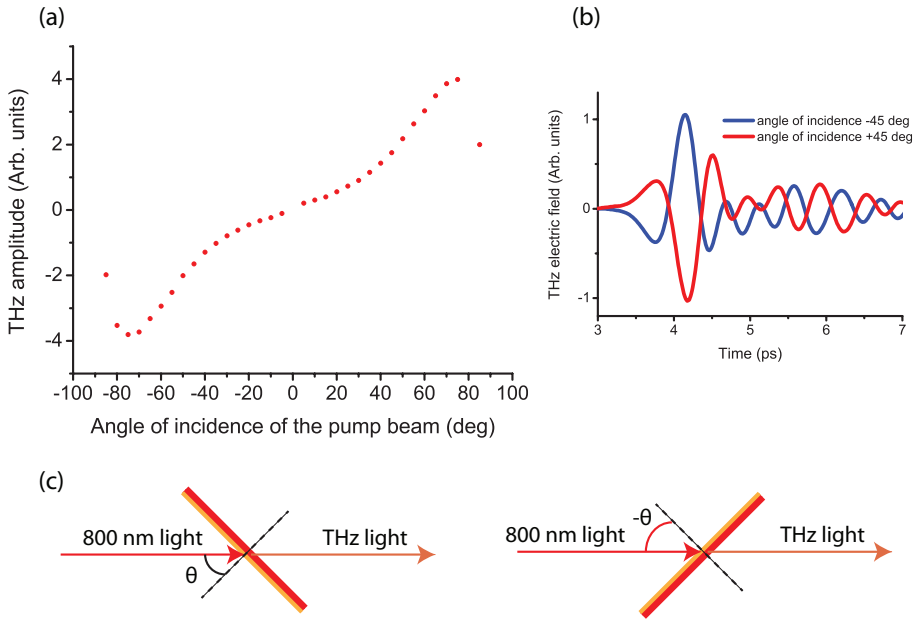

Figure 3.9: a) THz amplitude as a function of the angle of incidence of the pump beam, from a partially transparent Au/Cu_2O sample, b) The reversal of the THz polarity for +45° and -45° angles of incidence of the pump beam, c) A schematic representation of the two alignments

direction. This indicates that the generated THz dipole is in a direction perpendicular to the Cu_2O/Au interface. As the angle of incidence of the pump beam increases, the emitted THz amplitude increases and reaches a maximum for an angle of ± 75°. In Figure 3.9(b) we plot the THz electric field as a function of time, emitted from the sample oriented at angles of +45° and -45° with respect to the incident laser beam (Figure 3.9(c)). The two pulses are opposite in sign, suggesting that the generated THz dipole is along the normal direction to the interface.

As we will see in Chapter 4, the absorption by the Cu_2O films can be surprisingly large when they are interfaced with a metal substrate. This phenomenon is called 'cavity resonance' or 'coherent optical absorption' and is discussed in detail in Chapter 4. Under such conditions, ultrafast photoexcitation of Cu_2O/metal interfaces can lead to the emission of strong THz pulses through a transient current surge in the Schottky field.

3.7.2 Internal photoemission

Another possible mechanism of THz emission from a Cu_2O/metal interface under sub-bandgap excitation is internal photoemission [117]. Internal photoemission

refers to the photoexcitation of electrons from a metal to a semiconductor at an interface. In the case of Cu_2O/metal interfaces this corresponds to excitation of holes from the metal into the p-type Cu_2O. Since the excitation wavelength corresponds to a photon energy which is above the barrier height of Cu_2O/Cu interface (0.75 eV), internal photoemission can in principle take place at the interface [118]. In the presence of the Schottky field, the charge carriers drift along the field direction giving rise to a transient photocurrent. It has been shown in earlier works that internal photoemission takes place at Cu_2O/Cu interfaces with the excitation around the wavelength of 800 nm. When excited using femtosecond laser pulses, this will constitute a picosecond current in the material which results in the emission of pulses of THz radiation into the far-field. The case of ultrafast internal photoemission leading to THz emission has not been reported anywhere in the literature, to our knowledge. However, it was mentioned in a discussion on different carrier dynamics in Au/GaAs interfaces followed by femtosecond laser excitation by Shi *et al.* in 2006 [119].

Internal photoemission is a process which involves real movement of charge carriers. Since the number of holes injected into the Cu_2O is directly proportional to the intensity of the pump light incident on the sample, this process will also be second-order.

3.7.3 Depletion field-induced optical rectification

Second-order nonlinear processes are ideally not possible in materials with a centre of inversion symmetry. Application of an electric field can break the symmetry of the material. When Cu_2O is deposited on metal substrates, certain metals form Schottky type interfaces with it. The depletion field at the interface can be responsible for breaking the symmetry so that a second-order process is possible from Cu_2O. It has been reported that Cu_2O has a large *third-order* nonlinear susceptibility, $\chi^{(3)}$ [120]. In the presence of the depletion field at the interface with the metal, it is possible to have an electric-field-induced OR from Cu_2O. As already discussed in Chapter 1, electric-field induced OR is in fact a $\chi^{(3)}$ process where one of the electric fields is provided by the static depletion field $E^{(depl)}$ at the interface. The emitted THz electric field E_{THz} in the far field can be expressed as [43],

$$E_{THz} \propto \chi^{(2)}_{eff} I_{800} \tag{3.3}$$

where I_{800} is the pump light intensity, and

$$\chi^{(2)}_{eff} \propto \chi^{(3)} E^{(depl)} \tag{3.4}$$

is the effective second-order susceptibility. The emitted THz amplitude in this case varies linearly with the intensity of the pump beam, suggesting a second-order nonlinear optical process. In this, as in the previous explanations, a Schottky field is essential to explain the emission.

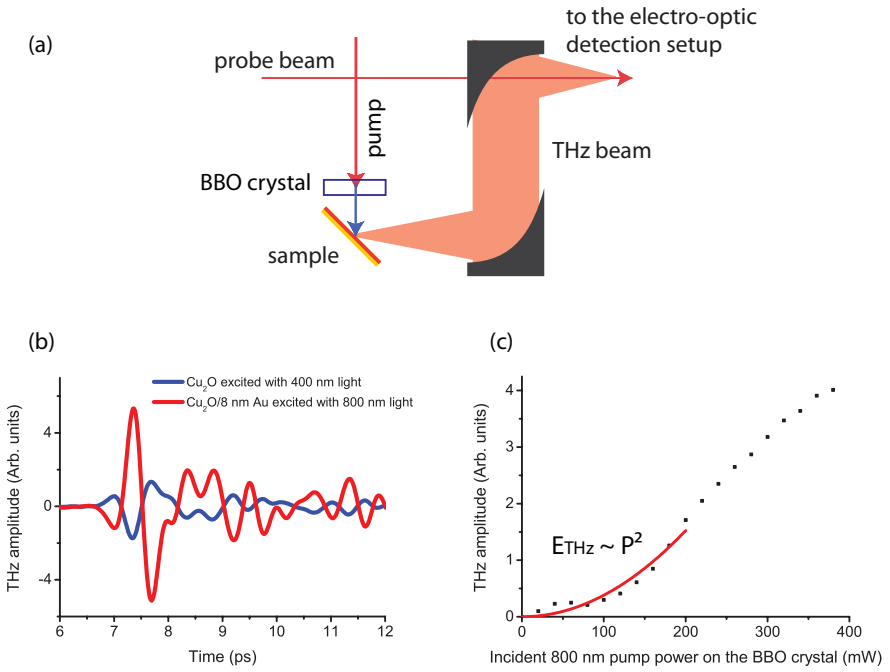

Figure 3.10: (a) Schematic of the experimental setup used for 400 nm light excitation of the sample, (b) The emitted THz electric fields from only-Cu_2O excited with 400 nm light, and Cu_2O/Au (8 nm thick Au layer) excited with 800 nm light, as a function of time, (c) Emitted THz amplitude (E_{THz}) as a function of the incident total 800 nm light power (P). The red curve is a parabolic fit to the data points at low pump powers.

3.8 Above bandgap excitation of Cu_2O with 400 nm light

It is also possible to generate THz pulses by above-bandgap femtosecond laser excitation of Cu_2O. An interface with a metal is not required in this case. Resonant excitation leads to the generation of electron-hole pairs in the material. Cu_2O has a direct bandgap of 2.1 eV. In terms of the light wavelength, this corresponds to 590 nm. When we excite Cu_2O using 800 nm light, the photon energy corresponds to 1.55 eV which is too low to excite electrons from the valence band to the conduction band. In order to see the effect of above-bandgap excitation of Cu_2O, we frequency-doubled the laser light to generate 400 nm light, which corresponds to a photon energy of 3.1 eV. We used a 100 μm thick β-barium borate (BBO) crystal to convert the 800 nm light into 400 nm light [121]. In Figure 3.10(a) we show the setup used for exciting the sample with the 400 nm light. The BBO crystal is inserted

between the pump focusing lens ($f = 150$ mm) and the sample. The orientation of the BBO crystal is adjusted to maximize the second harmonic yield. It has to be noted that the polarization of the 400 nm beam is different from that of the 800 nm beam. By changing the polarization of the incident 800 nm light using a $\lambda/2$ plate, it was made sure that the 400 nm light illuminating the sample is p-polarized. A typical emitted THz electric field as a function of time, from a 150 nm thick film of Cu_2O prepared on a glass slide excited with 400 nm light is shown in Figure 3.10(b). This THz pulse is compared with the THz pulse emitted from Cu_2O on an 8 nm thick Au layer on glass excited with 800 nm light. The THz electric field emitted from only-Cu_2O (excited with 400 nm light) is opposite in sign compared to the THz electric field emitted from Cu_2O/Au (excited with 800 nm light). Cu_2O absorbs 400 nm light considerably. Cu_2O is reported to show the photo-Dember effect [122]. When a concentration gradient of charge carriers is created in a material by ultrafast laser pulses, and if the mobilities of electrons and holes are different, an ultrafast transient dipole gets formed near the surface when the charge carriers diffuse away, electrons moving faster than the holes [2]. Another possible mechanism of THz generation is the transient current surge in the surface depletion field of Cu_2O. Note that the THz generation can occur both at the air/Cu_2O interface and at the Cu_2O/glass interface. Figure 3.10(c) shows the emitted THz amplitude from a Cu_2O thin film, as a function of the total 800 nm light power (measured before the BBO crystal). The quadratic growth of the THz amplitude with the incident 800 nm power suggests that a linear process (linear in the 400 nm light intensity) is responsible for the THz generation.

3.9 THz generation from nonplanar surfaces

Cu_2O and Au layers can be prepared on nonplanar surfaces also. This allows us to fabricate optical components that have a double function, such as a mirror that generates and simultaneously focuses the THz radiation. We prepared a Cu_2O/Au interface on an off-axis paraboloidal mirror surface by first depositing a 200 nm thick Au layer and then a 150 nm thick Cu layer using e-beam evaporation. The Cu layer was then fully oxidized to Cu_2O by heating it in the atmosphere at 250°C. Now, this paraboloidal mirror surface can act as an extended THz source when illuminated with a pump laser beam covering the mirror surface. In Figure 3.11, we show the schematic of the setup used to generate THz radiation from this paraboloidal mirror. A diverging pump beam from the focus of a smaller focal length plano-convex lens is incident on the paraboloidal mirror surface as shown in the figure. The focus of the pump beam is exactly at the focal point of the paraboloidal mirror. At each point at the surface of the paraboloidal mirror, THz light is generated. The phase relationship of all these THz wavelets is such that the emitted THz beam is plane-parallel [123,124]. This THz beam is focused by another off-axis paraboloidal mirror onto the detection crystal. A typically detected THz electric field is shown in the inset of Figure 3.11. This proof-of-principle experiment suggests that nonplanar optical elements in a THz setup can be suitably converted into THz emitters, where the

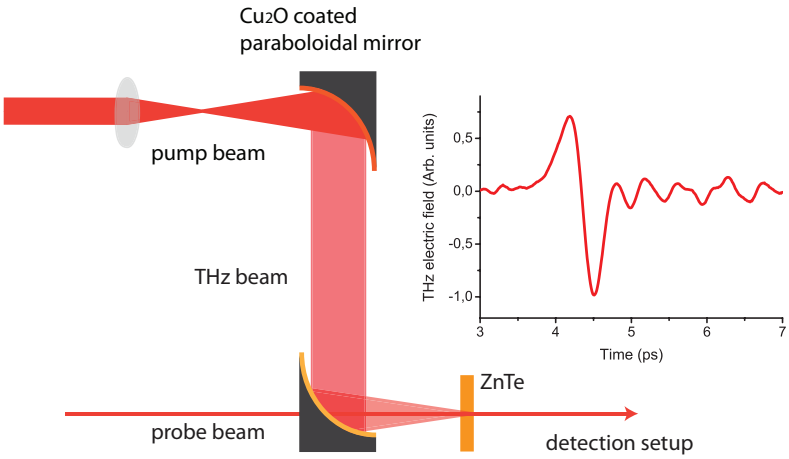

Figure 3.11: Schematic of the setup used for the excitation of a Cu_2O coated paraboloidal mirror. Please note that the single optical element is used as the source of THz light and also the focusing optical element. Inset: A typical THz electric field *vs.* time, detected in the setup.

emitted THz beam automatically follows the functionality of the optical element.

Generating THz radiation from paraboloidal mirrors themselves can help in reducing the number of optical components used in the optical setup to steer and focus the THz light. Paraboloidal mirrors are notoriously difficult to align in an optical setup, also the THz light is not visible. The THz beam path can be considerably reduced by this technique.

3.10 Conclusion

Strong THz emission is observed from Cu_2O/metal interfaces, when they are excited with femtosecond laser pulses. The emission is comparable to that from conventionally used THz generation crystals like GaP (110) or SI-GaAs (100). In Figure 3.12, we show a comparison between the THz electric fields emitted from a 420 nm thick Cu_2O film on Au and that from a 300 μm thick GaP (110) crystal, under the same experimental conditions. The mechanism of THz emission from GaP crystal is non-resonant, second-order OR [38]. It can be seen that the THz amplitude emitted from Cu_2O/Au is about 40% of the THz amplitude emitted from the GaP crystal. Such a large signal strength deserves a careful study because of the possible applications. We have listed some of the mechanisms that could play a role in the THz emission from Cu_2O/metal interfaces, in this chapter. The possible reason for the surprisingly strong emission from thin films of Cu_2O interfaced with Au will be discussed in detail in the next chapter in the context of enhanced THz emission from thin semiconducting films.

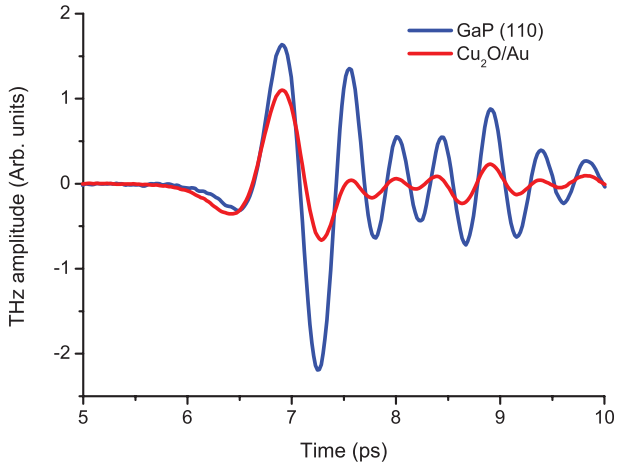

Figure 3.12: THz electric fields emitted from a 420 nm thick Cu_2O layer on a 200 nm thick Au layer (red) and a 300 μm thick GaP(110) crystal (blue), plotted *vs.* time.

Cu_2O/metal interfaces are very easy to fabricate and can be incorporated into various useful designs commonly used in various THz setups, like nonplanar optical elements (paraboloidal, or ellipsoidal mirrors), waveguides etc. Surface plasmon-enhancement of nonlinear optical processes has been discussed in detail in the current literature. Such plasmonic techniques can also be applied to enhance the THz emission from Cu_2O/Au interfaces. This will be discussed in Chapter 5.

Chapter 4

Terahertz emission from semiconductor thin-films

Generation of terahertz radiation in semiconductors is usually done using bulk materials, or in thin layers which are, however, thicker than the absorption depth of the pump light. It therefore seems counter-intuitive to use ultrathin layers of semiconductors with a thickness much less than the absorption depth. In this chapter, we show how ultrathin layers of semiconductors like silicon, germanium, and cuprous oxide on a gold substrate, not only strongly absorb the pump light at a wavelength of 800 nm, but also emit surprisingly strong terahertz pulses when illuminated with femtosecond laser pulses.

4.1 Terahertz emission from semiconductors

4.1.1 Transient photocurrent

One of the most common techniques for generating THz pulses, is the creation of a transient current in a semiconductor by ultrafast laser excitation as reported by Auston and Glass in 1972 [2, 33]. Resonant photo-excitation of the semiconductor leads to the generation of electron-hole pairs. For the generation of THz pulses, these photo-generated charges should move in a defined direction constituting an ultrafast transient current. This is achieved by applying an external bias voltage across the semiconductor. When the excitation is done using a femtosecond laser pulse, the transient photocurrent has a subpicosecond build-up time [123]. This rapid rise in the current results in the emission of a THz electric pulse, E_{THz}, into the far field, according to

$$E_{THz} \propto \frac{\partial J(r,t)}{\partial t}, \tag{4.1}$$

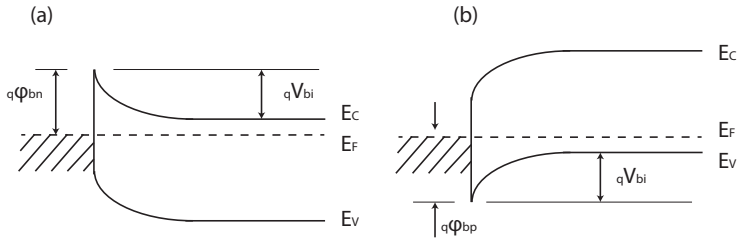

Figure 4.1: Energy band diagram of a metal-semiconductor interface at thermal equilibrium for (a) n-type semiconductor, (b) p-type semiconductor. Shaded part on the left side indicates the metal, and the semiconductor is on the right side. E_F is the Fermi level, E_C and E_V are the bottom of the conduction band and top of the valence band respectively. q is the electronic charge absolute value, ϕ_{bn} and ϕ_{bp} are the barrier potentials for the n-type and p-type respectively, and V_{bi} is the built-in potential.

where $J(r,t)$ is the photocurrent density. The variables r and t represent position and time respectively. When the electrodes which provide the external bias voltage, are antenna-like structures, these emitters are called photoconductive antenna (PCA) emitters, popularly known as Auston switches, named after their inventor. They are widely used in different forms as broadband THz sources for both imaging and spectroscopic applications. Interestingly, it is also possible to generate strong pulses of THz radiation from semiconductors without actually applying an external bias voltage. Transient photocurrents can also be generated by exciting charge carries in the depletion field present at the surfaces and interfaces of semiconductors as described in section 1.9.1. One example of such an interface is a metal-semiconductor Schottky interface which is explained below.

4.1.2 Schottky interface

When a metal is brought into contact with a semiconductor to form an interface, at thermal equilibrium the Fermi levels on both sides of the interface should match. This brings the conduction and valence bands of the semiconductor into a definite energy relation with the Fermi level of the metal [125,126]. In other words, a barrier potential is formed at the interface. Electrons in the n-type semiconductor can lower their energy by traversing the interface. As the electrons leave the semiconductor, a positive charge, due to the ionized donor atoms, stays behind. This charge creates an opposing field and lowers the band edges of the semiconductor. Electrons flow into the metal until an equilibrium is reached between the diffusion of electrons from the semiconductor into the metal and the drift of electrons caused by the field created by the ionized impurity atoms. This equilibrium is characterized by a constant Fermi energy throughout the structure. In thermal equilibrium, i.e. in the absence of a voltage bias, there is a region in the semiconductor close to the interface, which is

depleted of mobile charge carriers.

In Figure 4.1, energy band diagrams of n-type and p-type semiconductor/metal interfaces are shown. For n-type semiconductors, the width W of the depletion region can be expressed as [51],

$$W = \sqrt{\frac{2\epsilon_s}{qN_D}\left(V_{bi} - V - \frac{kT}{q}\right)}, \tag{4.2}$$

considering that the charge density $\rho \simeq qN_D$ for $z < W$ and $\rho \simeq 0$, and $dV/dz \simeq 0$ for $z > W$, where ϵ_s is the semiconductor permittivity, q is the electronic charge absolute value (1.6×10^{19} C), N_D is the donor atom concentration, V_{bi} is the built-in potential, V is the potential across the depletion region, k is the Boltzmann constant (1.38066×10^{-23} J/K), and T is the absolute temperature. The z-axis points across the interface from metal to the semiconductor. The potential $V(z)$ across the depletion region can be expressed as,

$$V(z) = \frac{qN_D}{2\epsilon_s}\left(Wz - \frac{1}{2}z^2\right) - \phi_{Bn}, \tag{4.3}$$

where ϕ_{Bn} is the Schottky barrier height. This position dependent potential gives rise to the Schottky depletion field. It has already been shown that THz pulses can be generated by exciting Schottky interfaces with femtosecond laser pulses [127]. Such studies were usually done by depositing partially transparent thin films of metals such as chromium (Cr)on the surface of the semiconductors [127]. The emission from them, was generally weak, because the thin metal layer blocks both the pump light going into the sample and the THz light emitted from the sample. It is to be noted that a metal/semiconductor interface with the semiconductor layer on top was not much popular in any of these earlier reports. Recently, Bakunov *et al* reported a method to enhance the THz emission from thin film InAs by having a metal layer *below* it [128]. In this experiment, the THz transient dipole formed in the layer emits in both forward direction and backward specular reflection direction. The forward part is reflected by the metal layer and is thus also emitted in the specular reflection direction increasing the total yield. This was also reported earlier in 1995 by Li *et al* [129]. Bakunov *et al* in their report, also went on to further modify the design by incorporating a dielectric lens on top of the semiconductor layer to couple the generated THz light better into the far field, further increasing the yield. In this chapter, we discuss the THz emission from thin films of three different semiconductors deposited on smooth gold (Au) surface. These semiconductors, cuprous oxide (Cu_2O), germanium (Ge) and silicon (Si) are normally poor THz emitters when they are excited with femtosecond laser pulses. In the subsequent sections we see how enhanced pump light absorption, and thereby enhanced THz emission can be achieved in very thin films of these semiconductors when they are interfaced with the metal.

4.1.3 Germanium and silicon

Indirect-bandgap semiconductors like Si and Ge are considered to be bad choices for the optical generation of THz pulses. The main reasons being their relatively long carrier lifetimes, and the fact that the crystals are inversion symmetric which normally forbids second-order nonlinear optical rectification [2]. For crystalline Si, the relatively low absorption leads to absorption depths which are fairly large, larger than the surface depletion depth. This means that most of the light gets absorbed in a region of the material where there is no depletion field present and which therefore does not contribute to the emission of THz pulses, in essence wasting the optical pump photons. Methods to circumvent this problem have been suggested in the literature. In 2008, Hoyer *et al* reported THz emission from black-Si [57]. Black-Si is prepared by surface modification of Si, making the reflectivity low, thus enhancing the light absorption near the surface. The black-Si surface consists of needle shaped structures which are made of single-crystal Si. In this case, the large penetration depth of the near-infrared pump light is reduced significantly. Multiple reflections of the pump light between the nanoscopic needles grown at the surface resulted in the excitation of charge carriers in these wires, leading to the emission of THz pulses. These nanoscopic needles were about 2 μm in height and 300 nm in diameter.

THz generation from nano-crystalline Si in a photo-conductive switch was reported recently in 2011 [130]. In this work, Daghestani *et al* constructed and studied a photoconductive switch based on nano-crystalline Si. THz pulse generation by injection of photocurrents in Si and Ge using a $\chi^{(3)}$ process was reported recently by Spasenovic *et al* [131]. This requires excitation with both fundamental near-infrared light and its second-harmonic. A third-order process can happen irrespective of the symmetry of the material.

Emission of THz pulses from Ge crystal surfaces when excited with femtosecond laser pulses was reported by Urbanowicz *et al* in 2005 [56]. The Photo-Dember effect was suggested as the main THz generation mechanism. The photo-Dember effect occurs when laser light is strongly absorbed in a semiconductor, creating a concentration gradient [122]. Due to the differences in the diffusion coefficients of electrons and holes, a transient dipole field is formed which gives rise to the emission of a THz pulse. The surface depletion field near the surface is relatively weak in these narrow-band semiconductors and the contribution to the drift current can be positive or negative depending on the relative direction. The emitted THz electric field from the transient photo-Dember field shows the same polarity for both n- and p-doped semiconductor surfaces, and can thus be separated from the contribution by the surface depletion field which changes polarity going from n-type to p-type materials [2].

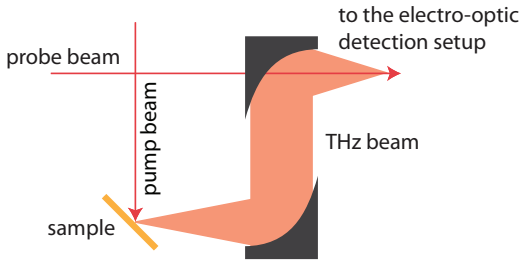

Figure 4.2: Schematic of the experimental setup.

4.2 Experimental

The experiments were carried out in a standard THz generation setup as shown in Figure 4.2 [20]. We use a Ti: Sapphire oscillator (Scientific XL, Femtolasers) generating p-polarized light pulses of 50 fs duration, centered at a wavelength of 800 nm with a repetition rate of 11 MHz. The average output power from this oscillator is 800 mW which is split into two by an 80/20 beam splitter. The 80% part is used as the pump beam, and the 20% part as the sampling beam. The pump part is chopped using a mechanical chopper at a frequency of 3 kHz. It is sent to an in-plane retro-reflector delay-stage oscillating at 5 Hz, and is then focused onto the sample surface. The pump beam is incident on the sample at a 45° angle of incidence and the generated THz light is collected in the direction of the specular reflection using off-axis paraboloidal mirrors and focused onto a (110) oriented zinc telluride (ZnTe) electro-optic detection crystal [22]. The synchronized, co-propagating, sampling pulse is also focused onto the detection crystal. The THz electric field elliptically polarizes the probe beam to an extent proportional to the instantaneous THz electric field value. The probe beam then propagates toward a differential detection setup consisting of a quarter wave plate, a Wollaston prism and a differential detector. Lock-in detection was employed to extract the signal at the chopping frequency of the pump beam. This setup measures the ellipticity of the probe beam and thus the instantaneous THz electric field strength [23].

4.2.1 Sample preparation

Thin films of Au of thickness $>$ 100 nm were prepared on the surfaces of clean glass slides or Si substrates by e-beam evaporation under high vacuum conditions (below a pressure level of 10^{-6} mBar). An inter-layer of chromium (Cr) or titanium (Ti) of thickness 10 - 30 nm was deposited to achieve better adhesion of Au on the substrates. The thickness of the film was monitored *in situ* by a piezo-electric crystal inside the vacuum chamber.

Layers of Cu_2O were prepared by first depositing thin films of Cu using e-beam

evaporation, followed by complete oxidation of them into Cu_2O films by heating at a temperature of 250°C in the ambient atmosphere for three hours. The complete oxidation of Cu into Cu_2O was confirmed by X-ray diffraction (XRD) measurements. We have seen in section 3.3.1 that the resultant oxide layer has a thickness $\sim$ 1.5 times larger than the original Cu layer thickness (Figure 3.1). Ge and Si layers were prepared by radio frequency (RF) sputtering. XRD analysis shows that the sputtered Ge and Si thin films are amorphous in nature.

4.3 Terahertz emission from Cu_2O

In Chapter 3, we discussed the generation of THz pulses by exciting Cu_2O/metal interfaces with femtosecond near-infrared laser pulses. It was seen that the emitted THz amplitude increased as the thickness of the Cu_2O film increased. A systematic analysis of this can be carried out by preparing Cu_2O thin films of different thicknesses on an Au substrate. This was achieved by completely oxidizing thin films of Cu of different thicknesses deposited on Au. In Figure 4.3 we plot the emitted THz amplitude from the sample as a function of the Cu_2O layer thickness. The THz amplitude shows an overall increase with the thickness of the film, and has an oscillatory behavior. In the same figure the absorption of the pump light at each thickness is also plotted. The absorption of the pump beam is obtained from the measurements of the incident and the reflected power from the sample. Normally, Cu_2O is a material which has little absorption at the wavelength of the pump beam, 800 nm. The Cu_2O films that are prepared by the oxidation of Cu layers deposited on glass show a slight amount of absorption, probably because of the impurities introduced during the preparation. For a Cu_2O layer thickness of 60 nm on Au on the other hand, the optical absorption is already $\sim$ 55%, which increases to 75% as the thickness increases to 420 nm. The oscillations in the absorbed power *vs.* layer thickness are due to etalon effects. The absorption is remarkably high considering that the excitation photon energy is 1.5 eV, which is below the 2.1 eV-bandgap of Cu_2O. The surprisingly strong absorption of thin films of semiconductors on top of Au, is a recurring feature in our measurements and will be discussed shortly. In Figure 4.4 we show the measured and calculated absorption at 800 nm wavelength as a function of the Cu_2O layer thickness deposited on Au. The oscillatory peaks seen in the absorbed pump power as a function of the Cu_2O layer thickness are the result of the Fabry-Perot oscillations taking place in the thin film, as we could reproduce them reasonably well based on the calculation of the interference maxima and minima in the reflected light. Considering a three layer system as shown in Figure 4.5, the total reflection coefficient r_p can be calculated using the Fresnel equations as,

$$r_p = \frac{r_{12} + r_{23} e^{2ik_z^2 d}}{1 + r_{12} r_{23} e^{i2k_z^2 d}}, \tag{4.4}$$

where r_{12} and r_{23} are the reflection coefficients corresponding to the interface between the media 1 and 2, and 2 and 3 respectively, d is the thickness of the semiconductor

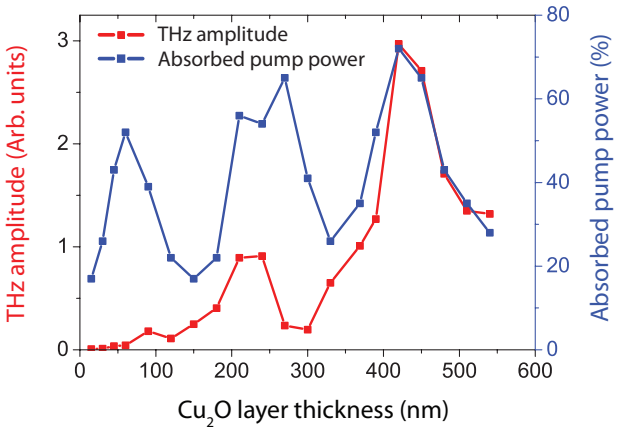

Figure 4.3: Measured emitted THz amplitude (red) and the pump light absorption (blue) plotted against the thickness of Cu_2O thin films prepared on Au.

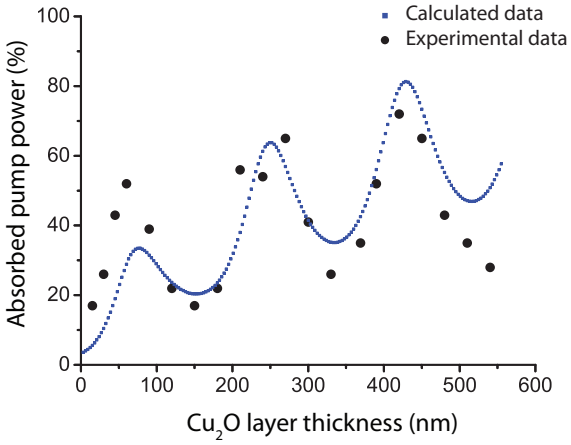

Figure 4.4: Measured (black dots) and calculated (blue) absorption of the pump light, as a function of the Cu_2O layer thickness.

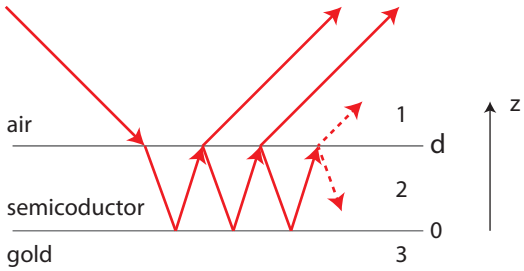

Figure 4.5: Reflection of light from a three layer system of media 1, 2 and 3. d is the thickness of the middle layer.

layer (medium 2), and $k_z^{(2)}$ is the propagation vector in medium 2 along the z axis. The absorbed power in percentage, A, is given by,

$$A = (1 - |r_p|^2) \times 100. \tag{4.5}$$

The refractive index of Cu_2O was adjusted in the calculations to match the peak positions in the calculated curve with those in the experimentally measured curve. This corresponds to a complex refractive index of $\tilde{n} = n + i\kappa = 2.32 + i0.06$. For a single pass, the attenuation of the incident intensity (I_o) of the pump beam as a function of position by bulk Cu_2O is given by the Lambert-Beer law[1],

$$I(z) = I_o e^{-\alpha z}. \tag{4.6}$$

The absorption coefficient α is given by,

$$\alpha = \frac{4\pi\kappa}{\lambda}, \tag{4.7}$$

where κ is the imaginary part of the refractive index, and λ is the wavelength of the light wave. For Cu_2O, the resulting absorption coefficient is 9.42×10^5 m^{-1}. Using Equation 4.6 we can calculate that for 75% of the light to be absorbed in a single pass, a Cu_2O layer of 1.35 μm thick layer is required, which contrasts with the 420 nm seen in the measurements.

In fact, for thicknesses of 60, 240 and 420 nm, the Cu_2O layers act as their own antireflection coating. This happens when the numerator on the right hand side of Equation 4.4, $r_{12}+r_{23}e^{2ik_z^2 d}$, becomes minimum. At these thicknesses, multiple reflections inside the Cu_2O layer, increase the optical path-length inside the Cu_2O which leads to enhanced absorption. Note that this is a subtle effect that depends on the thickness of the layer, and the exact value of the absorption coefficient. For example, if the absorption coefficient is very large, no light reaches the Au layer and the Cu_2O layer acts like a bulk material with the corresponding values for the reflection and

[1]Reflection losses are ignored here.

absorption. If the absorption coefficient is too small, interference between the reflection from the air/Cu_2O interface and from the Cu_2O/Au interface can occur, but most of the light will be reflected anyway. It requires the right absorption coefficient such that, a sufficient number of bounces between the Cu_2O/Au and Cu_2O/air interfaces can occur to allow a sufficient destructive interference in the reflected direction and simultaneously, a significant absorption in the Cu_2O layer. This explains why thin layers of Cu_2O on Au absorb so much light. A more dramatic effect of this will be shown in the next section for the case of thin layers of Ge on Au.

If a perfect metal reflector is in the place of Au, the pump light will experience a phase change of π after the reflection from the Cu_2O/Au interface. For that case, the first maximum in the absorption curve is expected at a Cu_2O thickness of $\sim$ 100 nm. However, Au is not a perfect metal at the pump wavelength, and this therefore introduces a different phase shift, and thus the first maximum in the optical absorption for a thickness of $\sim$ 80 nm. This is taken into account in the calculations.

The increase in the emitted THz amplitude with the thickness of the film can only be expected as long as the film thickness is in the range of the Schottky depletion layer width. Beyond the depletion layer width, the increased absorption by multiple reflections inside Cu_2O may not contribute much to enhanced THz emission, although the pump light absorption still increases. After the 75% absorption achieved at 420 nm thickness, we can assume that more absorption can be achieved at the next peak. However this may not necessarily contribute to higher THz emission from the sample. The exact width of the depletion layer, however, is unknown in this case.

4.4 Terahertz emission from sputtered Ge

In Figure 4.6, we plot the THz electric field as a function of time, emitted from a 25 nm thick Ge layer deposited on glass, and from the same thickness of Ge deposited on Au. The THz amplitude from the Ge/Au sample is about 7 times larger (about 49 times in intensity) than that from the same thickness of Ge deposited on a glass substrate. Interfacing Ge layer with Au increases the THz yield from it.

The emitted THz pulse shown in Figure 4.6 is mainly p-polarized. It consists of a nearly single-cycle pulse with an oscillatory trailing part that is caused mainly by the absorption and re-emission of the THz light by water vapor in the atmosphere.

In Figure 4.7, we plot the emitted THz amplitude as a function of the Ge layer thickness. Also plotted in the same figure is the pump light absorption *vs.* Ge layer thickness. The absorption of the pump light is calculated from the measured reflected and transmitted pump light from the sample. The overall absorption of the pump light increases as the thickness increases, which is expected as the interaction length of the pump light with Ge increases (Lambert-Beer law). It also shows an oscillatory behavior as a function of layer thickness. This arises from the interference of the pump light reflected/transmitted at Ge/air and Ge/glass interfaces, *i.e.* from the Fabry-Perot oscillations inside the thin Ge layer (similar to the case of Cu_2O

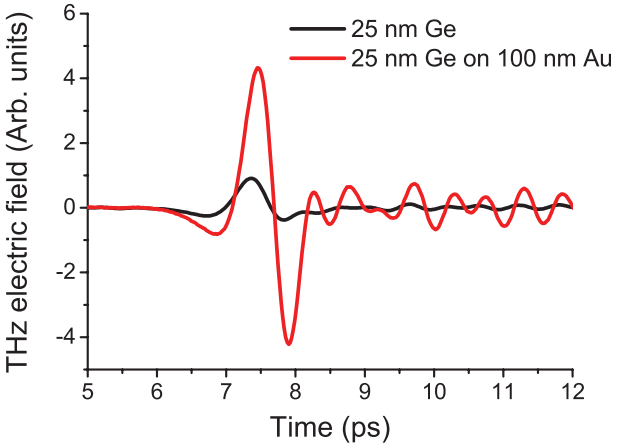

Figure 4.6: Measured THz electric field *vs.* time emitted from a Ge layer of thickness 25 nm deposited on glass (black), and on Au (red).

discussed in the previous section). We see that, as the pump light absorption by Ge layer increases with the thickness, the emitted THz amplitude does not increase accordingly. Two possible THz generation mechanisms in this case are the photo-Dember effect and the transient photocurrent surge in the surface depletion field, which are 'surface-related' phenomena[2]. The portion of the pump light which gets absorbed far away from the surface may thus not contribute to the THz emission, as the charge carriers generated away from the surface do not drift in the surface depletion field, nor they lead to a photo-Dember field. In Figure 4.8, we plot both the measured and the calculated pump light absorption as a function of the layer thickness. The complex refractive index is adjusted in the calculation to obtain the best match with the experimental results, as explained earlier in the case of Cu_2O/Au interfaces. In Figure 4.6 we already saw that the THz emission from Ge thin films is significantly enhanced by interfacing it with Au. In Figure 4.9, the emitted THz amplitude and the percentage absorption of the pump light are plotted as a function of the thickness of the Ge layer on Au. The absorption of the pump power is obtained by measuring the pump power reflected off the samples. In this case, there is no transmitted pump beam from the sample, as the Au layer acts as a good reflector. The pump light gets absorbed by Ge (as well as Au), gets reflected at the Ge/Au interface, and also undergoes multiple reflections inside the Ge layer. This results in Fabry-Perot oscillations in the absorption *vs.* Ge layer thickness as seen in Figure 4.9. For example, at a Ge layer thickness of 25 nm, the reflected pump beams from the top surface of the Ge layer and from the Ge/Au interface, interfere destructively resulting in the smallest reflection and a remarkable absorption of 96%! The emitted

[2]with 'surface', we mean a thin layer of semiconductor close to the interface.

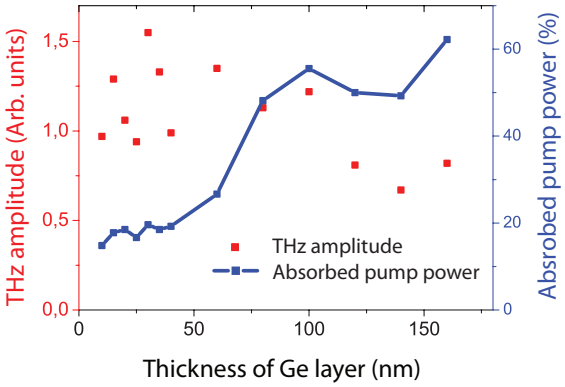

Figure 4.7: Measured, emitted THz amplitude (red) and pump light absorption (blue) as functions of the thickness of Ge thin films sputtered on a glass substrate. THz amplitude is shown in red and the pump beam absorption by the sample is shown in blue.

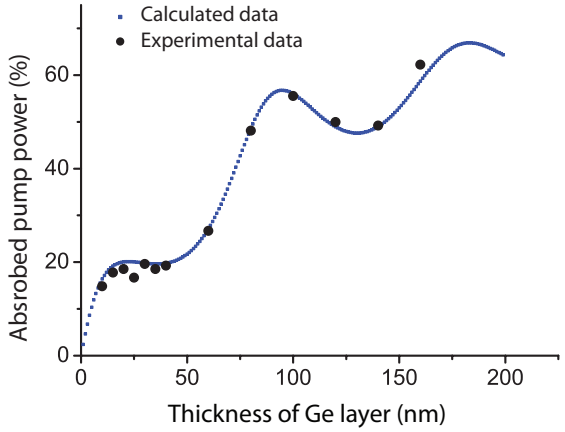

Figure 4.8: Measured (black dots) and calculated (blue) pump light absorption as a function of the Ge layer thickness, prepared on glass.

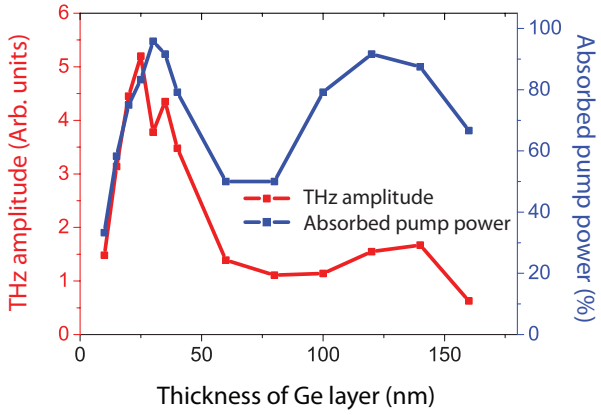

Figure 4.9: Measured emitted THz amplitude (red) and pump light absorption (blue) as a function of the thickness of Ge thin films sputtered on Au substrate.

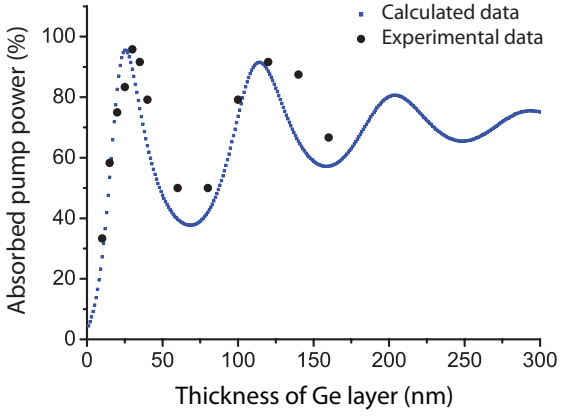

Figure 4.10: Measured (black dots) and calculated (blue) pump light absorption as a function of the Ge layer thickness, prepared on Au.

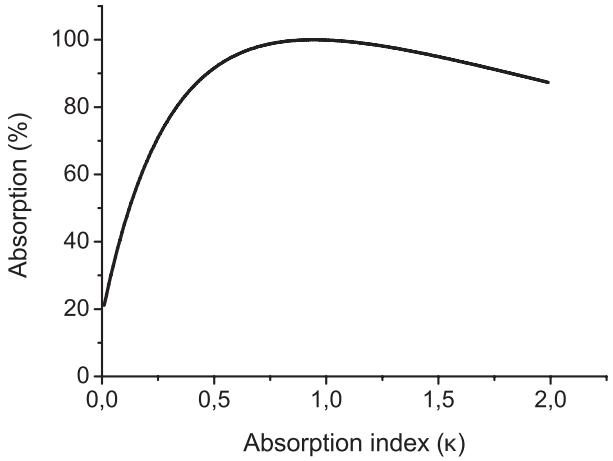

Figure 4.11: Calculated absorption of 800 nm light by 25 nm Ge film on Au, as a function of the absorption index, *i.e,* the imaginary part of the refractive index, κ.

THz amplitude follows a similar behavior as the pump beam absorption in terms of the peak positions; however the maximum emission occurs at a Ge layer thickness of 25 nm where the first pump beam absorption maximum occurs.

In Figure 4.10, we plot the measured and calculated pump power absorption by Ge layers as a function of the layer thickness. Unlike the behavior seen in the case of Cu_2O/Au, the absorption by Ge/Au does not show an overall increase as the thickness of the Ge layer increases. Instead the maximum absorption occurs at a thickness of 25 nm, and the next etalon peak appearing at 140 nm shows a slightly lower absorption. This behavior is also observed in the calculated pump absorption *vs.* Ge layer thickness. For thicker layers the maximum absorption decreases. As in the case of Cu_2O/Au, the explanation of this is to be found in a combination of optical absorption and etalon oscillations. In Figure 4.11 we show the calculated absorption of 800 nm light incident at 45° on a 25 nm thick Ge layer on Au, as a function of the absorption index, which is the imaginary part of the complex refractive index, κ. If κ is very large, the reflection and the absorption by the Ge layer obtain bulk values as no pump light can come out of the Ge layer to interfere with the first reflection from the Ge surface. If κ is very small, most of the light will be reflected. For the complex refractive index used in the calculations shown in Figure 4.10, $\tilde{n} = 4.5 + i0.6$, the absorption is at a maximum for a Ge layer thickness of 25 nm. For this thickness, enough pump light is back-reflected from the Au to give sufficient destructive interference in the reflected direction. At the same time, multiply reflected light inside the Ge layer leads to an increased effective interaction length and thus to more absorption. The absorption coefficient for Ge can be calculated from the imaginary part of the refractive index using Equation 4.7 as 9.42 ×

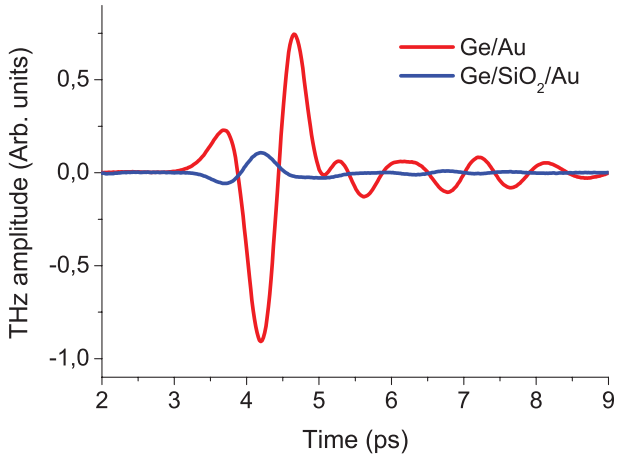

Figure 4.12: Measured THz electric field *vs.* time, emitted from Ge/Au (red) and Ge/SiO_2/Au (blue). The thickness of the SiO_2 layer is $\sim$ 2nm.

10^6 m^{-1}. Assuming the same refractive index for bulk Ge, we can calculate, using Equation 4.6, that for 96% absorption of the pump light to occur in a single pass, a 342 nm thick layer is required. It is remarkable that the same absorption is achieved by a 25 nm thick layer when it is interfaced with an Au layer. This is $\sim$ 14 times thinner. Note that, although firmly based on simple linear optics, Figure 4.11 shows something counter-intuitive: when the absorption index *decreases* from 2 to 0.75, the absorption actually *increases*. Within the context of photodetectors this enhanced coherent absorption is also known as 'cavity enhanced absorption' and is also related to the recently reported anti-laser [61].

4.4.1 Photocurrent in the Schottky field

So far, we have not discussed the origin of the emitted THz pulses. However, in view of the results it seems likely that a Schottky interface, with a corresponding depletion layer and a static electric field is present near the Ge/Au interface. The near infrared pump light centered at the wavelength of 800 nm is absorbed by the Ge layer. This creates electron-hole pairs. The Schottky field at the interface between Au and Ge can act on these charge carriers, resulting in a transient photocurrent. This can emit a THz pulse into the far field as defined by Equation 4.1 [2].

THz emission, although much weaker, is also seen from Ge on glass where no Schottky interface is formed. For crystalline Ge, the photo-Dember effect was reported as the mechanism for the generation of THz pulses. When a concentration gradient is achieved near the surface of a semiconductor by photo-exciting electron-hole pairs, they start diffusing away. If the mobility of the electrons and holes is

different, electrons (in general) move faster than holes and leave the holes behind. This leads to the build-up of a dipole layer near the surface. This is known as the photo-Dember field [54]. When the excitation of the semiconductor is done with a femtosecond laser pulse, this leads to the generation of a time varying dipole which can emit a THz pulse.

Such a gradient can also form, in principle, when a standing wave is formed by the pump light incident on the sample and the light reflected from the Au layer. In order to identify the role of the photo-Dember effect, we included a thin dielectric layer of silicon dioxide (SiO_2) in between Ge and Au to form a metal-insulator-semiconductor (MIS) interface. The purpose of this layer is to strongly reduce the possibility of carrier transport between the Au and the Ge so as to hinder the formation of a depletion field. In Figure 4.12 we plot the THz electric field as a function of time, emitted from the Ge/Au interface and the Ge/SiO_2/Au interface. The thickness of the Ge layer is 25 nm, and that of the SiO_2 layer is $\sim$ 2 nm. The inclusion of a dielectric layer of such a small thickness does not result in any pronounced difference in the standing wave pattern of the pump light inside Ge layer or in the absorption of the pump light. However, the Schottky field is perturbed as the charge carriers now have to tunnel through the dielectric layer. Figure 4.12 shows that the inclusion of the SiO_2 layer reduces the emitted THz amplitude by a factor of about 10. Thus the photo-Dember effect cannot be the main mechanism responsible for the THz emission, since it would largely remain unaffected by the thin SiO_2 layer.

4.5 Terahertz generation from sputtered Si

Sputtered Si layers also show a similar enhancement in THz emission when interfaced with Au, as in the case of Ge. In Figure 4.13, the emitted THz amplitude from thin films of Si on a 200 nm thick Au layer, is plotted as a function of Si layer thickness. Maximum THz emission was observed from a 40 nm thick layer of Si deposited on Au. The absorbed pump power is also plotted as a function of the Si layer thickness in the same figure. The maximum in the THz amplitude at 40 nm thickness corresponds to the first reflection minimum from the thin film on the metal. Unlike in the case of Ge, the emitted THz amplitude from Si layers increases as the thickness of the film increases. In Figure 4.14, we show a comparison of the absorbed pump power measured experimentally with the calculated results. It can be seen that as the thickness of the Si layer increases, the absorbed pump power also increases. We can also see the Fabry-Perot oscillations. The refractive index of Si in this case is extracted to be $\tilde{n} = 3.9 + i0.11$. The absorption coefficient of Si can be calculated from Equation 4.7 and is 1.7×10^6 m^{-1}. Assuming the same values for bulk amorphous Si, using Equation 4.6, we can calculate that a layer of thickness 962 nm is required to achieve 81% of the pump light absorption in a single pass; a value reached here with a layer of 140 nm thickness deposited on Au. Again, the coherent optical absorption, or the cavity resonance effect, increases the effective optical path length, inside the thin Si layer, in this case by a factor of $960/140 = 6.9$.

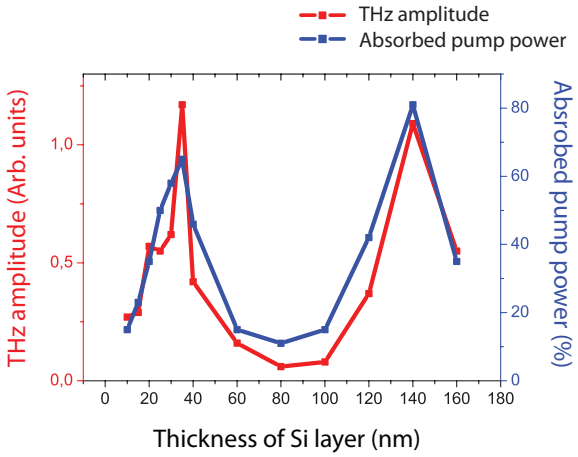

Figure 4.13: Measured emitted THz amplitude (red) and pump light absorption (blue) as a function of the thickness of Si thin films sputtered on Au substrate.

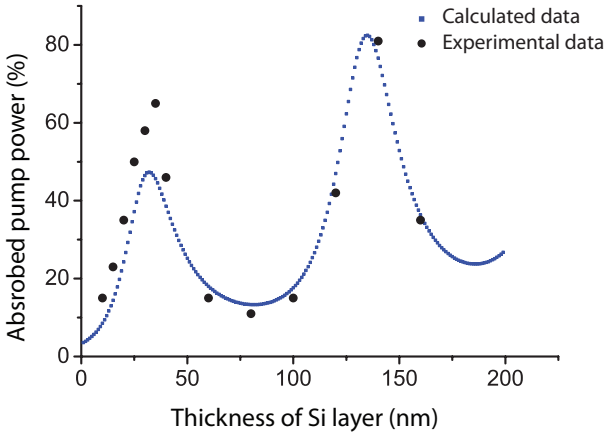

Figure 4.14: Measured (black dots) and calculated (blue) pump light absorption as a function of the Si layer thickness.

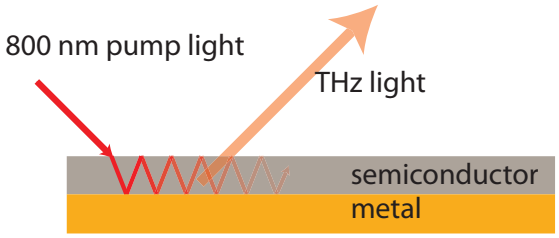

Figure 4.15: Schematic representation of the Fabry-Perot cavity resonance of the pump light inside the semiconductor layer (not to scale), when the semiconductor layer acts as an anti-reflection coating on Au.

Freshly prepared thin films of Si shows a photo-stabilization of the THz emission and the emission reaches a steady level in about 3 minutes [132].

The THz emission from indirect bandgap semiconductors like Si and Ge, is usually small (for Ge) or negligible (for Si). This limits the incorporation of Si and Ge in THz photonic devices. The THz emission from Cu_2O is also very small. However, very thin films of these semiconductors show significant enhancement in THz emission when they are interfaced with Au layers. Various factors can play a role in this process. Based on our experiments, we suggest that the enhancement can happen because of three main factors (a) The Schottky field at the semiconductor/Au interface acts as an accelerating field for the photo-generated charge carriers. This can lead to THz emission [2], (b) The Au layer underneath acts as a reflector for the forward propagating THz light. The generated THz dipole can radiate in both forward and backward directions, but in the end all THz light emerges in the specular reflection direction, (c) As we discussed in detail in this chapter, by choosing the thickness of the semiconductor layer appropriately, the pump light can be confined inside a very thin layer close to Au surface by the Fabry-Perot cavity resonance, leading to increased optical absorption by the film. This is possible because the absorption of coherent light is influenced by the interference pattern it creates in a medium [133]. This leads to enhanced THz emission, because this forces most of the light to be absorbed in a region of the semiconductor, *i.e.* in the Schottky depletion region, where this counts for the THz emission.

4.6 Conclusion

Absorption of light by a thin film is limited by its thickness. If the absorption coefficient of the material is low, light has to travel a large distance inside the material to get absorbed. In most of the cases, the absorption thus does not occur in the region where the absorption *should* take place to maximize the THz emission. In the case of a semiconductor/metal Schottky interface, the depletion layer is of a finite width of micron or submicron dimension depending on the choice of semiconductor and

the metal. The pump light needs to be absorbed inside the depletion region for an efficient THz emission. By varying the thickness and/or the refractive index of the thin film material, destructive and constructive interference can be achieved inside the thin film. When a very thin semiconductor layer is deposited on a metal surface to form a thin film Schottky interface, the film can itself act as an anti-reflection coating on the metal layer. This can confine the optical energy in the semiconductor layer by multiple-reflections, thus enhancing the absorption considerably. This is schematically illustrated in Figure 4.15. When the semiconductor thin film acts as an anti-reflection coating on the metal, the pump light gets trapped inside the semiconductor layer by multiple reflections as shown in the figure.

The idea of Fabry-Perot cavity-enhancement in thin films has been reported in the case of photodetectors or solar cells, as a method to enhance the absorption [133,134]. Since femtosecond laser pulses are used for the generation of THz pulses, this technique can be very useful in enhancing the yield from thin film THz emitters.

In this chapter, we have demonstrated that using this method of coherent optical absorption, the THz emission from three semiconductors Cu_2O, Ge and Si can be significantly enhanced. Our experimental results indicate that the main mechanism responsible for the THz emission in all the three cases is the transient drift of photo-generated charge carriers in the Schottky field. Based on the experiments and calculations we show a remarkable counter-intuitive strong absorption for such thin layers. For Cu_2O, Ge and Si thin films, the effective optical thickness (in terms of the optical absorption) increases by a factor of 3, 14 and 7 respectively, when thin layers of these materials are deposited on Au. Thus, significant THz emission from extremely thin layers becomes possible. Combined with plasmonic enhancements, which will be discussed in detail in Chapter 5, thin film semiconductor/metal interfaces can be of great value in integrated THz photonic devices.

Chapter 5

Plasmonics for enhanced terahertz emission

In this chapter, we discuss the role of surface plasmons in the terahertz emission by optical rectification of femtosecond laser pulses on a metal surface. Unlike other nonlinear optical phenomena, like second harmonic generation, Raman scattering etc., the effect of surface plasmon excitation in the context of optical rectification has not been studied well. Two techniques are used for the present study. A randomly nanostructured ultrathin Au film is studied in the first case. In the second case, surface plasmons are excited on a continuous, plain Au film by using the well-known Kretschmann geometry.

5.1 Terahertz emission from metal surfaces

Ultrafast optical excitation of nonlinear optical materials and semiconductors is widely used as a source for electromagnetic radiation in the terahertz (THz) range [2]. In simple terms, the nonlinear optical process, optical rectification (OR), allows the partial conversion of a femtosecond light pulse into a THz light pulse. Nonlinear materials like zinc telluride (ZnTe), gallium phosphide (GaP), gallium arsenide (GaAs), lithium niobate ($LiNbO_3$) etc. are various media used for the generation of THz radiation in this way [1]. Certain recent works also demonstrated that surfaces of metals like gold (Au) and silver (Ag) can show OR of femtosecond laser pulses. The generation of THz pulses from 'thick' metal films illuminated with femtosecond laser pulses, was reported by Hilton *et al.* [135] on iron (Fe) films, and by Kadlec *et al.* [136] on Au and Ag films, in 2004. Second-order nonlinear optical processes (except for Ag) were suggested as the mechanism responsible for the generation of THz light. Later, Kadlec *et al.* reported further studies of the THz emission from metal films using THz time-domain spectroscopy (THz-TDS), and showed that the THz emission had a non-local characteristic and that no emission was found from Au films of thickness

less than 100 nm. Based on this, they hypothesized that for Au films of thickness less than 100 nm, an ultrafast accumulation of charges at the bottom interface of the Au film cancels out the generated THz dipole [137]. In 2007, Welsh *et al.* were able to generate THz radiation by illuminating metal coated glass gratings with femtosecond laser pulses. A 30 nm thick layer of Au was used in their experiments [138]. They argued that multiphoton excitation can take place at the nanostructured metal surface under the strong evanescent field of surface plasmons. Ponderomotive acceleration of electrons in this strong field close to the metal surface was considered as the major mechanism for the generation of THz radiation [26, 138]. It has to be noted that they observed a *third-* to *fourth- order* pump power dependence in their work, and ruled out the possibility of second-order nonlinear OR taking place [138]. Very recently, in 2011, Polyushkin *et al.* reported the generation of THz pulses from metal nanostructures excited using amplified femtosecond laser pulses. Their results were in accordance with the model suggested by Welsh *et al.* [139]. Another recent report by Garwe *et al.* briefly discussed a new THz generation mechanism based purely on the propagation of surface plasmons on metal coated glass gratings. According to their model, the surface plasmon polaritons propagating perpendicular to the grooves of the gold grating surface constitute a transient current with a lifetime of a few picoseconds. This may emit THz pulses [140].

5.1.1 Percolating gold films

When thin films of metals like Au or Ag are prepared on a substrate like glass, using physical vapor deposition techniques like thermal evaporation or sputtering, initially, randomly placed isolated metal nano-islands are formed. As the deposition progresses, these islands start to coalesce, forming irregularly shaped fractal structures [141–143]. As the average-thickness of the metal layer increases further to about 7 nm, finally an extended metal cluster is formed which spans the whole surface. The thickness where this occurs is known as the percolation threshold. Below the percolation threshold, the discontinuous metal film acts as an electrical insulator, as the different randomly placed nano-islands do not form a complete network. For Au deposited on glass substrates, the percolation threshold is expected at an average thickness of $\sim$ 7 nm [142]. This was also experimentally confirmed by the THz transmission studies reported by Walther *et al.* who found that the average thickness of Au on silicon (Si) where the percolation occurs, is 6.5 nm [143]. Properties of ultrathin Au films near the percolation threshold are known to be very different from that of bulk Au. Various nonlinear optical phenomena have been shown to get enhanced on metal films near the percolation threshold due to disorder-induced localization of plasmons leading to 'hot spots' of locally enhanced fields. Enhanced second-harmonic generation (SHG), higher-harmonic generation, surface-enhanced Raman scattering (SERS), and spectral continuum generation have been reported from such semicontinuous metal films [141, 144, 145].

5.2 Excitation of surface plasmons

Surface plasmons are charge-density oscillations that may exist at the interface between two media, whose real parts of the dielectric constants are of opposite sign [146]. This can be fulfilled at a metal-dielectric interface [147, 148]. The charge density wave is associated with a bound transverse-magnetic (TM) polarized electromagnetic wave at the interface. The electric field of this wave has its maximum at the interface and decays evanescently into both media. The local light intensity near the metal surface will be strongly enhanced when surface plasmons are excited, which leads to the enhancement of nonlinear optical processes at the metal surface as well as that from a material kept very close to it [147].

Surface plasmons are characterized by the dispersion relation,

$$k_{sp} = \frac{\omega}{c}\left(\frac{\epsilon_{r1}(\omega)\epsilon_{r2}(\omega)}{\epsilon_{r1}(\omega)+\epsilon_{r2}(\omega)}\right)^{1/2}, \tag{5.1}$$

where k_{sp} is the wave-number of surface plasmons, ω is the angular frequency of the oscillation, c is the speed of light in vacuum, $\epsilon_{r1}(\omega)$ and $\epsilon_{r2}(\omega)$ are the real parts of the dielectric constants of the dielectric and metal respectively. As $\epsilon_{r1}(\omega)$ and $\epsilon_{r2}(\omega)$ are of opposite sign, from Eqn. 5.1, it directly follows that for real values of k_{sp},

$$\epsilon_{r1}(\omega)\epsilon_{r2}(\omega) < 0 \tag{5.2}$$

and

$$\epsilon_{r1}(\omega)+\epsilon_{r2}(\omega) < 0. \tag{5.3}$$

Assuming that $\epsilon_{r1} > 0$, his is equivalent to

$$\epsilon_{r2}(\omega) < 0 \tag{5.4}$$

and

$$|\epsilon_{r2}(\omega)| > \epsilon_{r1}(\omega), \tag{5.5}$$

It turns out that it is impossible to excite a surface plasmon at a flat metal-air interface by excitation from the air-side. The wave-number of surface plasmons, k_{sp} as defined in Eqn. 5.1 is always larger than the wave-number of the corresponding light waves in air. For that reason, the excitation of surface plasmons requires a special geometry. One of the mandatory conditions for the excitation of surface plasmons using light is that the projection of the wave-vector $\vec{k_x}$ of the light along the interface matches the wave-vector $\vec{k_{sp}}$ of the plasmon. This is the so called surface plasmon resonance (SPR) condition.

There are different ways to meet this condition. One method is by using the so-called Kretschmann geometry [147] as shown in Figure 5.1. In this case, the excitation of surface plasmons at the Au-air interface is achieved by attenuated total internal reflection (ATR) of the light beam inside the glass prism. A matching is

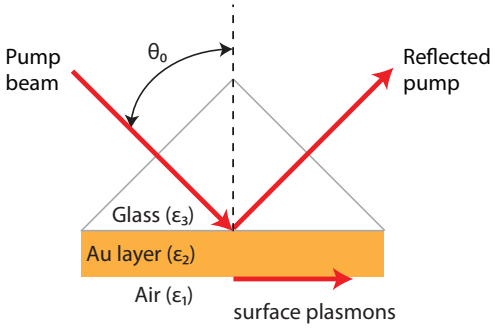

Figure 5.1: Kretschmann geometry for exciting surface plasmons using attenuated total reflection from a glass prism. Surface plasmons are excited at the Au-air interface. ϵ_1, ϵ_2 and ϵ_3 are the dielectric constants of air, Au, and glass respectively.

possible between the horizontal component of the wave-vector of light incident at the glass-Au interface, and the $\vec{k_{sp}}$ of the surface plasmon at the Au-air interface.

$$k_{sp} = \sqrt{\epsilon_3}\frac{w}{c}\sin\theta_0, \tag{5.6}$$

where ϵ_3 is the dielectric constant of glass. Surface plasmons can also be excited at a metal surface by nanostructuring it. Since surface plasmons have a shorter wavelength compared to free propagating light, the extra factor in the propagation constant can be provided by a one-dimensional grating with grating constant a,

$$k_{sp} = \frac{w}{c}\sin\theta_0 \pm \nu g \tag{5.7}$$

where $g = 2\pi/a$, and ν is an integer > 0 [147].

It seems particularly interesting to study the role of surface plasmons in the generation of THz light in view of the recent work by Uzawa *et al.* [62]. They reported OR of nanosecond laser pulses by a self-assembled monolayer (SAM) of hemicyanine terminated alkanethiol molecules on a gold coated glass prism, using surface plasmon excitation in the ATR geometry. The authors suggested that the same geometry could, in principle, be used to generate THz radiation from such a layer if femtosecond laser pulses are used.

In the following sections, the generation of THz light from coated and uncoated percolated and continuous Au films, and the role of surface plasmons therein are discussed.

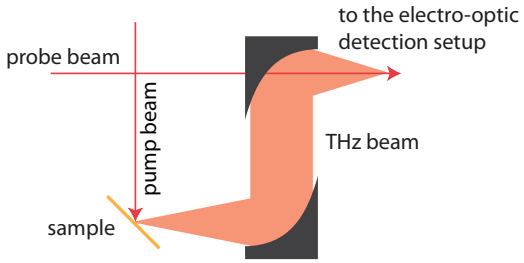

Figure 5.2: Schematic of the experimental setup used for exciting the percolating Au samples at 45°angle of incidence

5.3 Experimental

5.3.1 Setup for exciting the percolating Au film

The experiments were performed using a standard THz generation setup as shown in Figure 5.2 [149]. The laser source used is a Ti:Sapphire oscillator (Scientific XL, Femtolasers) generating pulses of 50 fs duration, centered at a wavelength of 800 nm with a repetition rate of 11 MHz. The average power output from the laser is 800 mW. The 80% part of this is used as the pump beam, and the 20% part as the sampling beam. The pump beam is weakly focused onto the sample surface to a spot-size of about 2 mm, at a 45° angle of incidence, as shown in Figure 5.2. Care is taken to avoid a tighter focus as this was seen to lead to damage and/or restructuring of the metal film. The THz radiation generated from the sample is collected in the specular reflection direction of the pump beam using off-axis paraboloidal mirrors and focused onto a 500 μm thick zinc telluride (ZnTe (110)) detection crystal [22]. The synchronized, co-propagating, sampling pulse is also focused onto the detection crystal. The THz electric-field elliptically polarizes the probe beam to an extent proportional to the instantaneous THz electric-field value. This ellipticity of the beam is measured by a differential detection setup consisting of a quarter wave plate, a Wollaston prism and a differential detector [23].

5.3.2 Excitation using Kretschmann geometry

The experimental setup used for exciting the sample under the ATR geometry (also known as Kretschmann geometry) is shown in Figure 5.3 [150]. The pump beam is focused onto the hypotenuse side of the prism through one of the sides, as shown in the figure. The THz radiation generated from the sample is collected in the direction of the 'pseudo-transmission' of the pump beam from the prism, using off-axis parabolic mirrors and focused onto an electro-optic (EO) detection crystal. We note here that at the prism, the pump beam gets reflected at about 90°and no remaining pump light travels along the THz beam after the prism. This configuration thus serves as

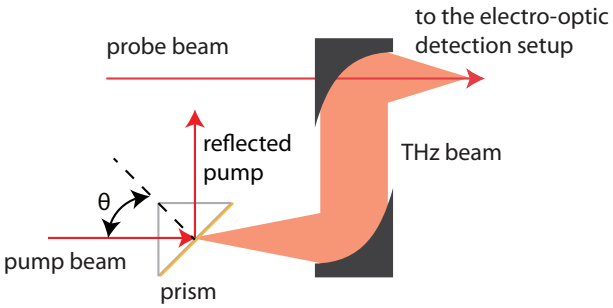

Figure 5.3: Schematic of the experimental setup used for exciting the samples in ATR geometry

an effective method to avoid the pump beam going into the detection crystal along with the THz beam.

5.4 Sample preparation

5.4.1 Ultrathin Au films

The percolating Au layer samples were prepared by e-beam evaporation of Au under high vacuum conditions (below a pressure of 10^{-6} mBar). The glass slides were first treated with 100% fuming nitric acid (HNO_3) in an ultrasonic bath for 5 minutes, followed by cleaning with de-ionized water. After drying with dry nitrogen flux, they were cleaned with acetone and isopropanol and dried again. All Au films were prepared under similar conditions and with a deposition rate of 1 Å/s. A quartz crystal thickness monitor was used to estimate the thickness. Only an average thickness can be defined for Au thin films below the percolation threshold. Figure 5.4 shows a scanning electron microscope (SEM) image of an Au film of 8 nm average thickness deposited on the surface of a glass slide. The random morphology of the percolated film is fractal-like [141]. One of the interesting properties of fractal structures is their scale-invariance. For that reason, percolated Au films are reported to show a broad surface plasmon resonance near the percolation threshold, as a wide range of interaction lengths is available because of all available sizes of the resonating clusters.

5.4.2 Thin films of Au on prisms

Thin films of Au were prepared on the hypotenuse side of clean fused silica right-angled prisms (side a = 10 mm) by e-beam evaporation. A 44 nm thick layer was deposited with a 2 nm chromium (Cr) interlayer for better adhesion of the Au to the prism.

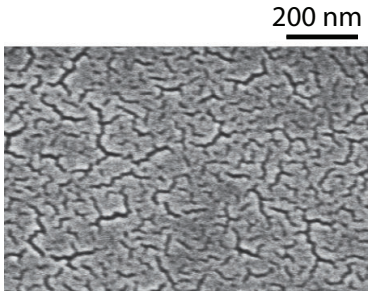

Figure 5.4: SEM image of an Au layer of 8 nm average thickness deposited on a clean glass surface

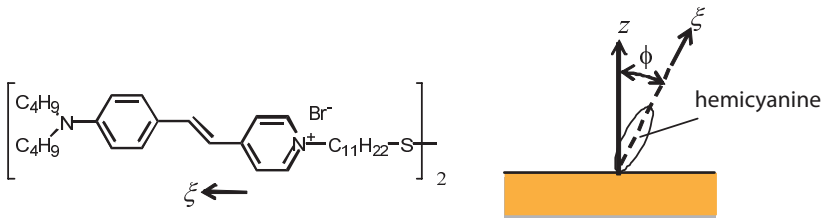

Figure 5.5: Chemical structure of hemicyanine disulfide. ϕ is the angle between the molecular axis ξ and the z-axis which is normal to the sample surface.

5.4.3 Cu_2O thin films

Thin films of Cu_2O were prepared by first depositing thin films of Cu using e-beam evaporation, followed by complete oxidation of the films by heating at 250°C in the laboratory atmosphere for 3 hours. Such a prolonged heating was chosen to make sure that no unoxidized Cu is left in the film. After oxidation, a Cu_2O layer thus remains. It has to be noted that when ultrathin (thickness < 10 nm) Au layers are used as a substrate, their morphology may change as a result of heating at an elevated temperature [151].

5.4.4 Hemicyanine self-assembled monolayer

The hemicyanine is a kind of cyanine dye, which shows a large second-order molecular polarizability along the molecular axis ξ. In order to anchor the hemicyanine on gold, the hemicyanine is designed with an organosulfur group, and the entire molecule hemicyanine disulphide has the chemical structure shown in Figure 5.5. The synthesis, electro-optic, SHG, and OR properties are separately described in detail in the literature [62, 152–154].

Hemicyanine disulfide was dissolved in ethanol and used as a 0.01 mM ethanol

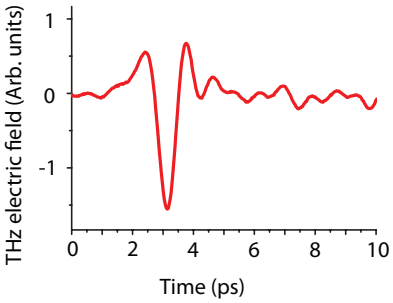

Figure 5.6: A typical THz electric field pulse emitted from a Au layer of 8 nm average thickness, plotted vs. time.

solution. The hemicyanine SAM was formed on the Au film by immersion of the substrate in the solution for one hour[1]. The thickness of the SAM layer thus formed is estimated to be 1.2 nm. Excitation in the ATR geometry at the surface plasmon resonance enables the detection of nonlinear optical phenomena such as SHG, the Pockel's effect and also OR from such thin layers.

5.5 Percolation-enhanced THz emission

Let us first consider the case of the excitation of localized surface plasmons on a percolated Au film. Emission of THz radiation is observed when ultrathin Au films are irradiated with femtosecond laser pulses. A typical example of an emitted THz electric field from an 8 nm thick Au film on glass, is shown in Figure 5.6. It consists of a nearly single-cycle pulse followed by an oscillating tail. These weak oscillations are caused by the absorption and the re-emission of the THz light by the water (vapor) molecules in the atmosphere. The THz electric field emitted from the samples is mainly p-polarized, and does not show any dependence on the azimuthal orientation of the sample (rotation of the sample about its surface normal). No THz emission was detected when the angle of incidence of the pump beam was 0°. This suggests that the generated THz dipole is oriented normal to the sample surface. We note that the emitted THz amplitude from 8 nm Au on glass is relatively weak and is only 0.2% of that emitted from an unbiased semi-insulating gallium arsenide (SI-GaAs (100)) surface emitter.

The emitted THz amplitude is very sensitive to the average thickness of the ultrathin Au layer. The amplitude of the emitted THz electric field as a function of the average Au film thickness, is shown in Figure 5.7. In the same figure, we also

[1]The hemicyanine coated prisms (with Au layer), were provided by Prof. Kotaro Kajikawa of Tokyo Institute of Technology, Japan. The hemicyanine dye was provided by Prof. Haruki Okawa of Kogakuin University, Japan.

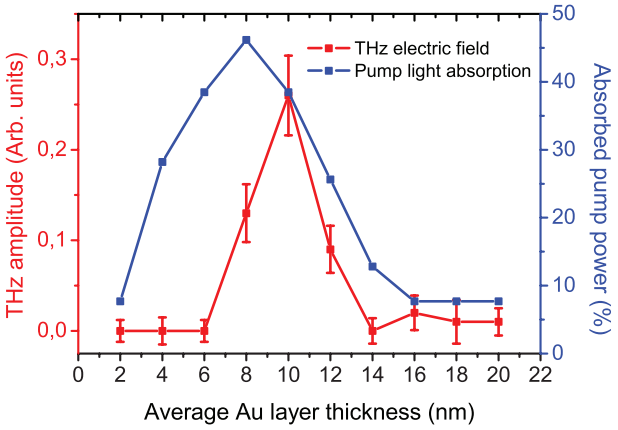

Figure 5.7: Measured emitted THz amplitude (red) and pump light absorption (blue) are shown as a function of the Au layer average thickness

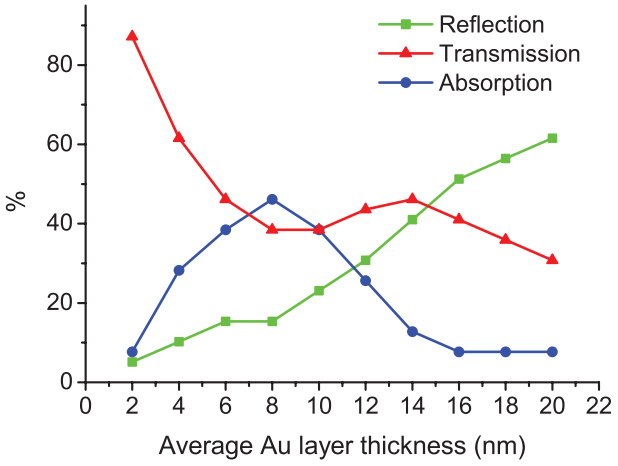

Figure 5.8: Measured reflected (green), transmitted (red) and absorbed (blue) pump light as a function of the Au layer average thickness

plot the 800 nm pump light absorption as a function of the average thickness of the Au film. The figure shows that the THz emission is detected only in the range of thicknesses where the metal layers show enhanced absorption of the pump light. No THz emission from bare glass surfaces could be detected in our experimental setup, thus ruling out the possibility of THz generation from the glass surface. Figure 5.8 shows the transmission, reflection and absorption of the pump light as a function of average Au layer thickness. The broad peak in the absorption near the percolation threshold already shown in Figure 5.7, is attributed to the excitation of 'hot spots' of strong localized surface plasmons [155, 156]. This indicates that the excitation of these 'hot spots' may play a role in the THz emission. For average thicknesses above 14 nm, no THz emission could be detected. We note that our results from the 800 nm reflection and transmission measurements on the samples are nearly identical to those done using 632.8 nm light of He-Ne laser by Gadenne in 1977 [157].

In Figure 5.9, we plot the measured THz amplitude as a function of incident laser power. For an average power density of up to 3.5 W/cm^2, the THz amplitude clearly increases linearly, suggesting that a second-order nonlinear process is responsible for the THz emission. This contradicts the earlier observations by Welsh *et al.* where a higher-order nonlinear process resulted in the THz emission from an Au surface [26, 138]. On the other hand Kadlec *et al.* had reported a second-order process from continuous Au films, but only above a thickness of 100 nm [137]. We add that in our experimental setup we were unable to reproduce the results by Kadlec *et al.* from evaporated thick (200 nm) Au films, perhaps because of the much lower laser power density in our case. A direct comparison of their work with our work is difficult, however, as percolated metal films are known to behave differently from bulk metals [143]. For their work, Kadlec *et al.* used an amplified laser source, whereas we use a Ti:Sapphire oscillator generating pulses with a much lower energy. We note that tighter focusing of the pump beam led to the appearance of a white glow from the percolated sample, accompanied by photo-damage and even removal of the Au layer.

5.5.1 Surface plasmon-enhanced optical rectification

Enhancement of second-order nonlinear processes like SHG has been reported from percolated Au films on glass [141, 145, 158]. Lack of inversion symmetry is essential for a second-order nonlinear optical process [42]. For an ultrathin Au film, the inversion symmetry is broken at the surface in the direction perpendicular to the sample surface. Femtosecond laser excitation can thus lead to the formation of a THz dipole oriented normal to the sample surface. The increased absorption of the pump beam by the Au layers of thickness near the percolation threshold is evidence of the excitation of localized surface plasmon modes. Excitation of 'hot spots' of localized field, leads to the enhancement of second-order OR process resulting in an increased emission of THz light. This increased emission is detectable in our setup. The maximum THz amplitude is observed from an Au film of 10 nm average thickness. We note that this average thickness is slightly higher than the thickness for which the maximum in

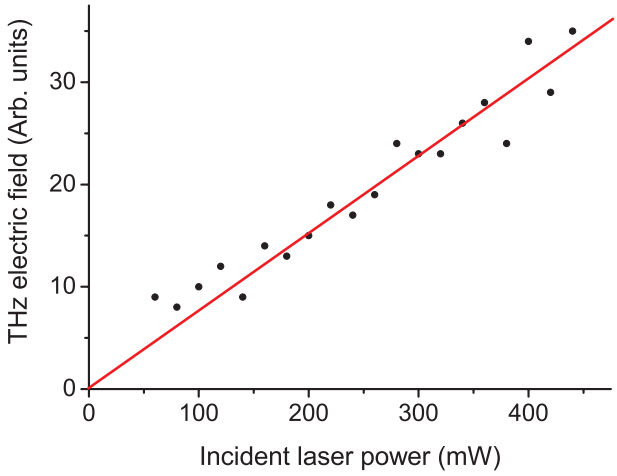

Figure 5.9: THz amplitude emitted from an Au layer with an average thickness of 10 nm on glass, plotted as a function of the incident laser power. The solid line is a guide to the eye

the pump light absorption is observed. This suggests that the degree of percolation plays a role in the THz emission process.

5.6 THz emission from Cu_2O/Au interfaces

In the previous section, we discussed the THz emission from percolating, ultrathin Au films on glass when they were excited using femtosecond laser pulses. A distinct enhancement of the emitted THz amplitude was seen near the percolation threshold of Au on glass. The enhancement was attributed to a high local pump light intensity made possible by the excitation of localized surface plasmon modes. This suggests that if a nonlinear material is deposited on top of the Au layer, an increased nonlinear response can be expected from it. This is similar to the case of surface-enhanced Raman scattering (SERS), where the molecules under study are deposited on a nanostructured metal surface [159]. However, there is one thing that must be taken into account. The surface plasmon resonance on a metal surface is known to be very sensitive to the modifications of the surface [147]. The plasmon resonance on the Au film can in fact be disturbed/destroyed by the deposition of a medium on top of it.

We have already seen that the structure of a percolating Au film on glass is known to be fractal-like. A fractal structure is scale-invariant. In practical cases, we can expect that the scale-invariance of the percolating-Au structure is true over only a finite length range. Still, semi-continuous Au films show a broad surface plasmon resonance ranging from ultra-violet (UV) to near-infrared (IR) wavelengths [141].

Coating the Au layer with a dielectric is similar to scaling the randomly shaped nanostructures, as the refractive index of the dielectric effectively scales the wavelength of the incident pump light. For this reason, it is possible that a Cu_2O layer of suitable thickness on top of the percolating Au structure does not prevent the creation of localized plasmon resonances at a given wavelength.

In Figure 5.10 we plot the emitted THz amplitude and the percentage absorption of the pump power by ultrathin Au films coated with Cu_2O, as a function of the Au layer thickness. The Cu_2O layer is 225 nm thick. This thickness of Cu_2O on Au is the same as the thickness where the second absorption maximum occurs for Cu_2O layers on a *continuous* Au surface, as discussed in Chapter 3 . A distinct peak in the emitted THz amplitude is observed when the average thickness of the Au layer is 8 nm. This is very close to the percolation threshold of Au on glass. We have already seen in the previous section that the THz emission from an Au film is significantly enhanced when the film is percolating [149]. In the same way, surface plasmon excitation and large local enhancements of the pump electric field can be possible at the Cu_2O/Au interface when the Au film is percolating.

The absorption of the pump light by the samples seems to increase monotonously as the average thickness of the Au films increases. From Figure 5.10, we can thus infer that the pump light absorption and the THz emission are not strongly correlated in the case of THz emission from Cu_2O/percolated-Au interfaces, at least for this thickness of the Cu_2O layer. The presence of a thin film of Cu_2O on the nanostructured Au substrate makes the problem non-trivial, as etalon oscillations of the pump light inside the thin film, obscure the plasmonic enhancement occurring around the percolation threshold. In order to understand this better, we prepared a Cu_2O film of 150 nm thickness on top of the ultrathin Au layers. The measured emitted THz amplitude and the percentage absorption of the pump light are plotted as a function of the Au layer average thickness in Figure 5.11. This thickness of Cu_2O on Au corresponds to a minimum in the pump light absorption for Cu_2O on a *continuous* Au layer[2]. We see that the emitted THz amplitude and the absorbed pump power of Cu_2O on percolating Au are more strongly correlated. The increased pump beam absorption seen near the percolation threshold can be attributed to excitation of localized surface plasmon modes in the percolated Au. The THz emission in this case, although it shows enhancement near the Au percolation threshold, is weaker compared to the case of Figure 5.10.

An advantage of the percolated Au layer is that the sample can be excited in both reflection and transmission geometries for THz generation. We also observe that Cu_2O layers deposited on ultrathin Ag films also show enhanced THz emission when the thickness of the Ag layer is about 10 nm (results not shown here). A detailed study of Ag was not, however, carried out. Unlike Au, Ag can more easily oxidize or react with hydrogen sulfide (H_2S) in the atmosphere contaminating the surface.

[2]The optical properties of ultrathin Au films near the percolation threshold are reported to be different from that of continuous Au [141]. For that reason, the thickness of Cu_2O layer on *continuous* Au, corresponding to a minimum absorption of the pump light, may not be the same for the case of *percolated* Au

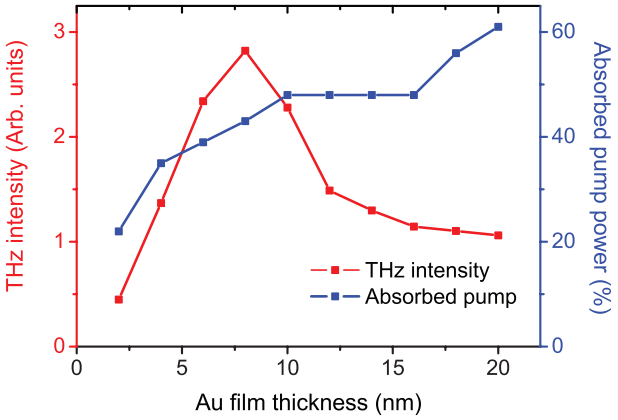

Figure 5.10: Measured emitted THz amplitude (red) and pump light absorption (blue) by Cu_2O/Au samples plotted as a function of the Au layer average thickness. The thickness of Cu_2O in this case corresponds to maximum absorption for a Cu_2O/Au (continuous) interface.

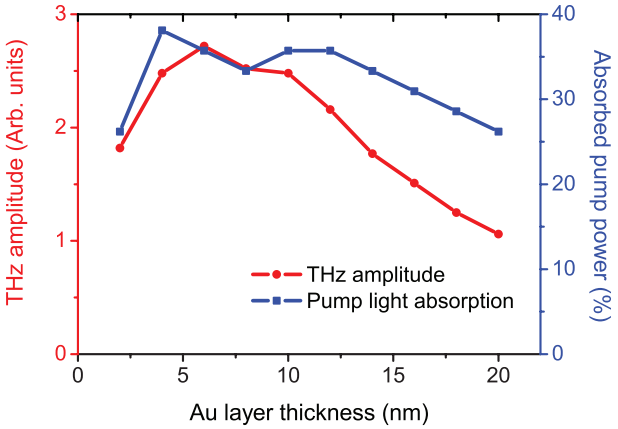

Figure 5.11: Measured emitted THz amplitude (red) and pump light absorption (blue) by Cu_2O/Au samples plotted as a function of the Au layer average thickness. The thickness of Cu_2O in this case corresponds to minimum absorption for a Cu_2O/Au (continuous) interface.

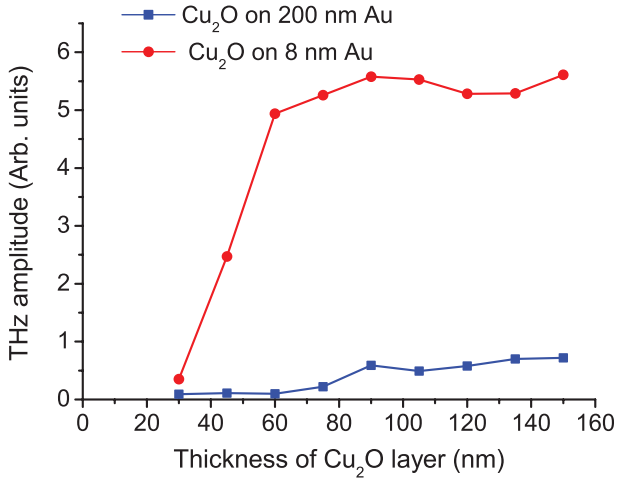

Figure 5.12: Measured THz amplitude emitted from Cu_2O on 8 nm thick Au (red) and 200 nm thick Au (blue), plotted as a function of the thickness of the Cu_2O layer.

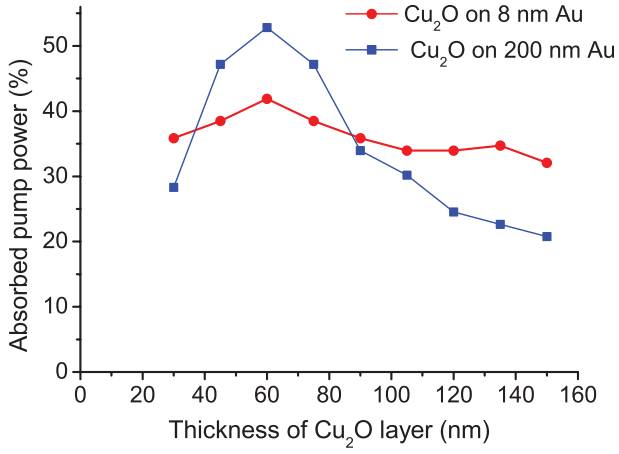

Figure 5.13: Measured Percentage pump light absorption by Cu_2O layers on 8 nm thick Au (blue), and 200 nm thick Au (red), plotted as a function of the thickness of the Cu_2O layer.

Since we prepare Cu_2O films by oxidation of Cu layers on the metal layer, Au layers were more suitable for the above mentioned experiments because of their better stability. However, we can anticipate a similar result from ultrathin bare Ag films as well as from Cu_2O thin films deposited on them.

In Figure 5.12, we plot the measured THz amplitude as a function of the thickness of the Cu_2O layers for two cases: one in which the Au layer has an average thickness of 8 nm, and the other when the Au layer is 200 nm thick. Over the range of Cu_2O thicknesses shown, Cu_2O on percolated Au emits stronger THz pulses. The increase in the emitted THz amplitude as the thickness of Cu_2O increases on the 200 nm thick Au, is superimposed on the Fabry-Perot etalon oscillations of the pump light inside the Cu_2O layer. Such oscillations are weak for Cu_2O on percolated Au. When the pump reflection is minimal, the pump absorption shows a maximum. This coherent optical absorption is discussed in detail in Chapter 4. In the case of percolated Au, there is a sharp increase of THz emission as the Cu_2O layer increases in thickness up to 60 nm. After this, the emitted amplitude stays at an elevated level with a slight oscillatory behavior as the thickness of Cu_2O further increases. This suggests that in the case of Cu_2O on percolated Au, the THz generation takes place in a $\sim$ 40 nm thick Cu_2O layer on top of the Au. On the other hand, in the case of Cu_2O on 200 nm thick Au layer, the THz amplitude increases until the thickness of Cu_2O reaches 420 nm (4.3).

In Figure 5.13, we plot the pump beam absorption for Cu_2O/Au interfaces with an 8 nm thick Au layer, and with a 200 nm thick Au layer. It is interesting to see that for Cu_2O layer thicknesses between 40 nm and 90 nm, the pump beam absorption is higher for Cu_2O on a 200 nm Au layer. However the THz emission from Cu_2O on 8 nm Au is much stronger. This means that the optical absorption is not a good predictor for the strength of the emitted THz electric field. In the case of Cu_2O on percolating Au, because of the surface plasmon excitation at the interface between Au and Cu_2O, the local pump light intensity at the interface becomes enhanced. This can result in enhanced THz emission. In the next section we show that the surface plasmon excitation at the interface between Au and a nonlinear material can lead to enhanced THz emission, also when the Kretschmann geometry is used to excite surface plasmons.

5.7 Excitation using ATR geometry

Excitation of surface plasmons at a metal surface can be achieved using different methods [147]. We have discussed the use of randomly nanostructured, ultrathin semi-continuous Au films near the percolation threshold in the previous section. Surface plasmon excitation can also be achieved by using a metallic grating with the correct periodicity or nanostructured metal surfaces. Another method to excite surface plasmons at a metal surface is by using the Kretschmann geometry [147]. In this case, a thin metal layer is deposited on the hypotenuse side of a right-angled prism and the excitation is done in the ATR geometry as shown in Figure 5.6. This method

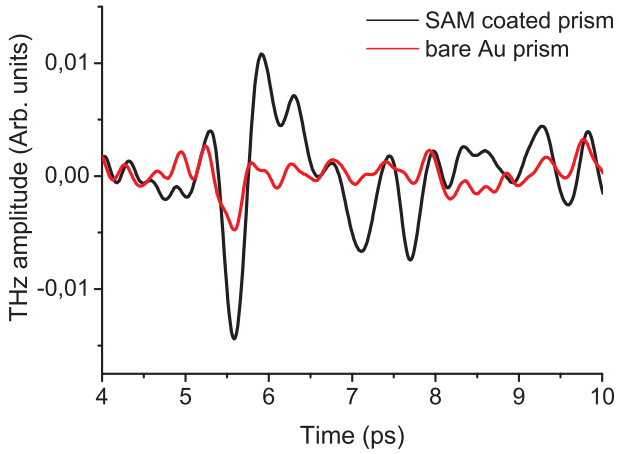

Figure 5.14: The terahertz electric field *vs.* time emitted by bare Au layer at the surface plasmon resonance (black) and by the hemicyanine SAM layer coated on the Au layer (red).

is sometimes used for photo-exciting very thin layers of nonlinear media, as the field enhancement due to surface plasmons is localized very close to the metal surface.

5.8 Results and discussion

5.8.1 THz emission from a thin continuous Au layer

In Figure 5.14, we plot the measured THz electric field as a function of time, emitted by exciting a 44 nm thick Au film using the Kretschmann geometry (Figure 5.3). The signal, although somewhat noisy, consists of a quasi-single cycle oscillation of the electric field, and is only observed when the Au film is illuminated from the glass-side (in the ATR geometry) under the right angle of incidence as discussed below [62]. No measureable THz emission is observed when this film or any other continuous smooth Au surface was illuminated from the air-side. At the surface plasmon resonance condition, the reflected pump power from the prism goes to a minimum and a bright patch of scattered 800 nm light is observed on the Au coated hypotenuse side of the prism. When the incident pump beam is at any other angle, such a patch does not appear. This provides a visual confirmation that surface plasmons are excited around this angle of incidence. In Figure 5.15 we plot the measured THz amplitude from the Au layer at the SPR condition, as a function of the incident laser power. The response is linear, suggesting that a second-order nonlinear optical process is responsible for the THz emission [150].

These experimental results thus point to the fact that the THz emission by second-order OR is possible at thin film Au surfaces when surface plasmons are excited.

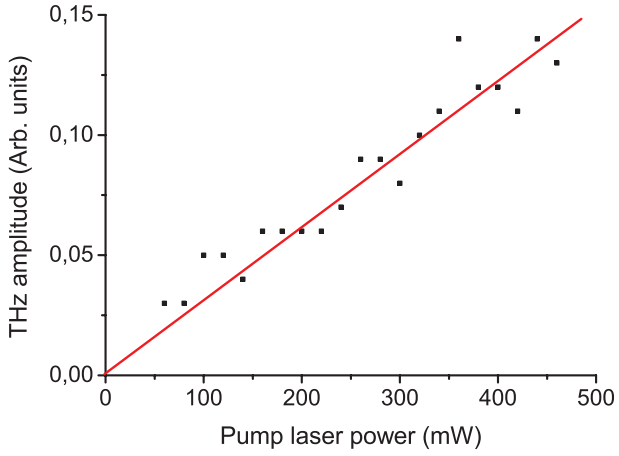

Figure 5.15: THz amplitude emitted by the bare Au surface as a function of the incident laser power. The solid line is a guide to the eye.

When direct excitation of the sample is done from the air-side, the intensity at the sample surface is presumably not strong enough to result in the generation of any detectable THz light. THz emission is facilitated by the excitation of surface plasmons, since they have stronger fields exactly at the surface, where the nonlinear process of converting pump light into THz light takes place [147, 148]. Propagating surface plasmons can also lead to an increased interaction distance at the Au surface, thus enhancing the emission further.

5.8.2 THz emission from a self-assembled monolayer of hemicyanine

In Figure 5.14, we plot the THz electric field emitted from the hemicyanine-SAM coated Au layer when excited in the ATR geometry. The emission is observed only when the angle of incidence of the pump beam fulfills the SPR condition. Remarkably, the emitted THz electric field from the monolayer covered Au surface is a factor of three larger than from the bare surface even though the layer is only 1.2 nm thick. Since a hemicyanine SAM is known to have a large $\chi^{(2)}$, this THz emission can be considered as the sum of the contribution from OR at both the Au surface and the hemicyanine SAM [153]. Due to the presence of this thin monolayer, the resonance angle where plasmons can be excited, is expected to shift a little with respect to that for a bare Au film [152, 153, 160]. The THz signal consists of a quasi-single cycle oscillation followed by rapid oscillations. These oscillations are mainly due to the absorption and re-emission of THz radiation by water vapor in the atmosphere. No detectable THz emission is observed when the SAM layer was directly illuminated by a

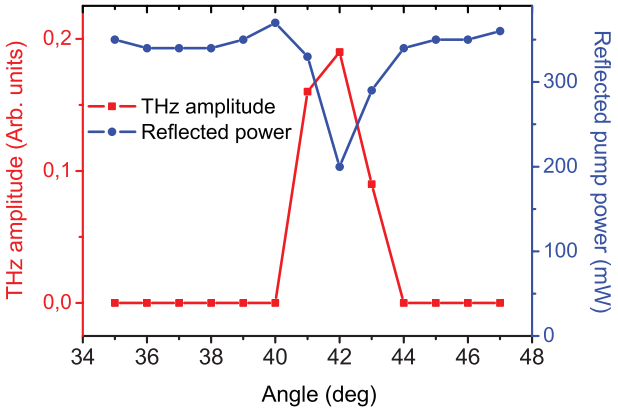

Figure 5.16: Measured THz amplitude (red) and the reflected pump power (blue) as a function of the angle of incidence θ of the pump beam, from a hemicyanine-SAM-coated glass prism excited in the Kretschmann geometry.

focused pump beam from the air-side. Figure 5.16 shows the emitted THz amplitude and the reflected pump power from the prism as a function of the angle of incidence θ. The dip in the reflected pump power observed around $\theta = 42°$corresponds to the angle where surface plasmons are excited at the Au surface. We note that compared to the results reported in the literature [62, 160], a broader resonance is seen in Figure 5.16. In our case, the pump beam is focused onto the sample using a plano-convex lens with $f = 150$ mm. Thus the curve shown in Figure 5.16. is a summation over a small range of incidence angles. Because we use laser pulses, the pump beam has a bandwidth of about 30 nm. This also contributes to a smearing-out of the resonance. The three times larger THz amplitude emitted from the SAM layer compared to the bare Au layer, is consistent with the earlier observation of SHG from similar samples by Naraoka *et al.* [153].

In Figure 5.17, we plot the emitted THz amplitude as a function of the incident laser power. The dependence is, to a good approximation, linear, suggesting that a *second-order* nonlinear optical process is responsible for the THz emission. At the SPR condition, the electric field of the pump light is enhanced close to the metal surface [147, 153]. This provides a localized high intensity at the SAM layer. As a result of this, the THz polarization developed in the SAM layer can be significantly enhanced. This enhancement is very similar to the surface-plasmon mediated enhancement of other nonlinear processes like SHG and Raman scattering reported from metal surfaces [147]. The ATR geometry is very suitable for the excitation of very thin (of a few nanometers thickness) layers of nonlinear materials, because of the strong field localization near the metal surface. In the ATR geometry, the pump beam is focused on the hypotenuse side of the prism to a spot size of diameter ~ 1 mm. As the thickness of the SAM layer is known to be ~ 1.2 nm, we can calculate

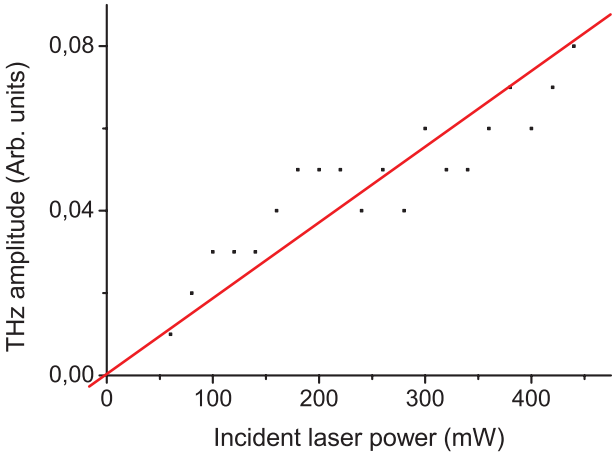

Figure 5.17: THz amplitude as a function of the incident laser power, emitted from an Au layer coated with hemicyanine SAM, excited under the surface plasmon resonance condition. The solid line is a guide to the eye

that the THz light is emitted from a tiny volume of only $\sim 10^{-15}$ m^3.

5.8.3 Cu_2O/Au interface

In Figure 5.18 we show the comparison of the emitted THz amplitude and the reflected pump power from a $\sim$ 15 nm thick layer of Cu_2O excited in the ATR geometry, as a function of the angle θ. The Cu_2O layer is prepared by the complete oxidation of a 10 nm thick Cu layer deposited on a 44 nm thick Au layer. Compared to the result shown in Figure 5.16, we see a significant shift in the plasmon resonance angle to $\sim$ 50°, as seen in the dip in the reflected pump power from the sample. The dip has also smeared out considerably as a consequence of the Cu_2O layer on top of the Au layer [147]. The surface plasmon resonance is not, however, destroyed by the thin Cu_2O film. At the surface plasmon resonance, the THz emission is enhanced. There seems to be a slight shift in the peak position between the dip in the reflected power, and the maximum in the emitted THz amplitude. A similar observation was recently reported in the case of SHG from Ag nanofilms excited under ATR geometry, and was attributed to the different modes of surface plasmons excited in the film [161].

It has to be noted that Cu_2O/Au on the prism emits THz light in the ATR geometry, also for angles far away from the plasmon resonance angle. This is because the evanescent pump light on the hypotenuse side of the prism can excite the Au/Cu_2O interface, even when its wave-vector does not match with the plasmon wave-vector. However, it is clear that the maximum THz emission occurs at the surface plasmon resonance angle.

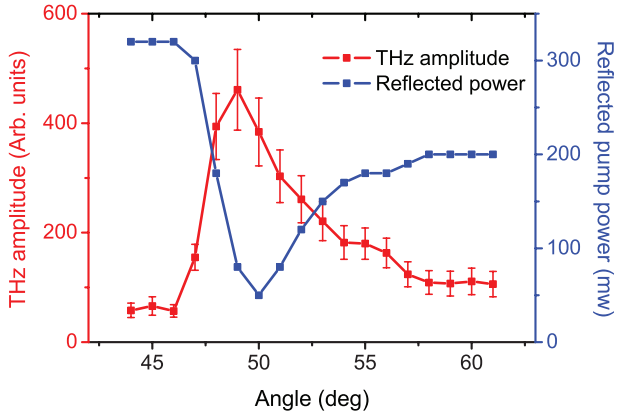

Figure 5.18: Enhanced THz emission from Cu_2O/Au interface at surface plasmon resonance condition. THz amplitude is shown in *red* and the reflected pump power is shown in blue as a function of the angle θ.

5.9 Second-order and higher-order optical rectification

The current literature on THz generation from metal surfaces can be mainly classified in to two parts. In section 5.1 we saw that both second-order and higher order processes were held responsible for THz emission from metal surfaces. Most of these experiments used amplified laser pulses. In contrast with these works, we reported a *second-order* dependence of the emitted THz amplitude on the incident laser power, when a randomly nanostructured gold surface, with an effective thickness of 8 nm, was illuminated with light pulses from a Ti:sapphire laser oscillator, and observed no THz radiation from a plain, flat gold surface under the same conditions [149]. We also show that THz emission through second-order OR is possible from a 44 nm thick planar Au film when surface plasmons are excited on it [150]. Interestingly, either a second-order or a higher-order pump-power dependence of the emitted THz electric field and, consequently, different physical explanations for the emission are reported in all these above mentioned different experiments performed elsewhere and in our laboratory. However, these results do not necessarily contradict each other. The relatively low peak-power of laser pulses emitted by Ti:sapphire laser oscillators makes it less likely that very high nonlinearities can be observed with these lasers. Ti:sapphire laser oscillators have a high repetition rate which facilitates high frequency signal modulation and sensitive lock-in detection and are therefore much better in detecting relatively weak signals from second-order nonlinear optical processes, if present. At the same time, the high peak power of the amplified Ti:sapphire lasers selectively favors higher-order nonlinear generation of THz pulses, but their

low repetition rate makes the detection of weak THz pulse from a second-order nonlinear process, one that might become dominant at low excitation powers, less likely. An interesting question is, whether the excitation of surface plasmons that appears to play an important role in the high-power experiments, also plays a role in low-power experiments in which a second-order nonlinearity seems to be responsible for the THz emission.

5.10 Conclusion

In conclusion, we have shown that the excitation of surface plasmons on a thin film of Au using femtosecond laser pulses, can lead to the emission of THz pulses from it. The excitation of surface plasmons is done in two ways. In the first case, localized surface plasmon modes are excited on a percolating ultrathin Au film deposited on glass [150]. In the second case, surface plasmons are excited on a planar thin film of Au, by using the Kretschmann geometry [149]. In both these cases, THz emission is observed. We attribute the emission to second-order nonlinear OR shown by Au films owing to the asymmetry at the surface. Excitation of intensity 'hot spots' leads to an enhanced nonlinear response in the case of percolating Au film. In the second case, the evanescent wave of the propagating surface plasmons provides a high intensity at the surface, enhancing the nonlinear response. In both cases, the interaction of light with the Au surface is enhanced due to an increased interaction time when surface plasmons are excited.

When surface plasmons are excited on an Au surface, we have shown that it can also act as a substrate for enhancing THz emission from a second material deposited on top of it. This is demonstrated with thin films of Cu_2O prepared on percolated Au films, as well as on planar Au films (in Kretschmann geometry). Cu_2O interfaced with Au emits THz radiation when excited with femtosecond laser pulses. Remarkably, the excitation of surface plasmons can also lead to considerable THz emission from a 1.2 nm thick self-assembled mono-molecular layer of hemicyanine deposited on the Au surface. Hemicyanine is known to have a large second-order susceptibility. Surface plasmon-enhanced THz emission may provide an effective way to probe the local $\chi^{(2)}$ from such thin films. This technique can be very useful for local generation of THz pulses in future compact THz photonic devices.

Chapter 6

Conclusion

6.1 Discussion

Ultrafast laser excitation of semiconductors and nonlinear materials is not only a useful technique to generate broadband electromagnetic radiation in the terahertz (THz) range, but also a tool to understand the properties of the material [2, 4]. In this thesis, we focused on THz emission from certain materials, especially semiconductors, and on the possibility of enhancing the emission using different techniques.

THz emission from graphite was discussed in Chapter 2. Ultrafast laser excitation of graphite surfaces results in the coherent emission of THz pulses. From the analysis of the emitted THz pulses, we could see that photo-excitation and subsequent movement of charge carriers are the possible mechanism behind the emission. The polarization of the emitted THz light with respect to the orientation of the graphite crystal is such that the resultant photocurrent is along the c-axis of graphite. A photocurrent along the c-axis was unexpected, as the electrical conductivity along the c-axis is about three orders of magnitude smaller compared to that along the constituent graphene planes. Such ultrafast charge movements can be effectively detected and studied using the emitted THz pulses.

Relatively strong THz emission was observed from cuprous oxide (Cu_2O). Interfaces of Cu_2O with metals are capable of converting a near-infrared femtosecond laser pulse partly into a THz pulse. In Chapter 3 we discussed in detail the various processes that can result in THz emission in the case of Cu_2O/Au interfaces. We found that the transient photocurrent surge in the Schottky interface formed between Cu_2O and the metal is the most probable THz emission mechanism. This emission is on par in strength with the emission of conventionally used nonlinear crystals like gallium phosphide (GaP), although much lower when compared to photo-conductive antenna (PCA) emitters. However, unlike PCAs, the THz emission from semiconductor interfaces using the in-built potential, does not require any external bias. Cu_2O/metal interfaces are very easy to prepare and can be incorporated into exist-

ing components in a THz optical setup, like in the case of a paraboloidal mirror we discussed in section 3.9.

The work on Cu_2O/Au interfaces opens up a new possibility of using very thin layers of semiconductor/metal interfaces for the THz generation. In the past, experiments on THz emission from semiconductors were done in bulk crystals or in thin films which were much thicker than the absorption depth of the pump light. In contrast with this, we show in Chapter 4 how the coherent optical absorption of the pump light in thin films of semiconductors deposited on Au surfaces can enhance the THz emission from them. Semiconductors like Cu_2O, germanium (Ge) and silicon (Si), which are generally poor THz emitters, turn into good THz emitters by this technique.

The different methods of optical generation of THz radiation can benefit from the different developments in the field of Optics. Plasmonics can be effectively used to enhance THz emission from different nonlinear samples. In Chapter 5, we saw the enhancement of THz emission from a Au surface when surface plasmons were excited. It is also possible to enhance the THz emission from a thin film of a nonlinear material, or from semiconductors deposited on Au, when surface plasmons are excited. One very interesting aspect we observed was that even thin films of Au of thickness $\sim$ 8 nm can result in significant enhancement of THz emission from systems like Cu_2O/Au. Confinement of the pump optical energy into nanometer thick semiconductor layers can lead to enhancement in the emitted THz amplitude as we saw in Chapters 4 and 5. Such techniques have the capability to turn even 'bad' THz emitters into 'strong' THz emitters.

6.2 Future work

The advancement of THz technology in recent years has extended the use of this range of electromagnetic radiation into numerous applications. Both THz-TDS and THz imaging have proven to be very useful in industrial and scientific applications [1]. This thesis presents certain promising results in confining the THz emission process into tiny volumes without losing the emission strength and even increasing the emission.

The techniques for enhancing the THz emission discussed in Chapters 4 and 5 can be of great value in photovoltaic or solar cell applications. Surface-plasmon enhanced THz emission, or surface-enhanced terahertz emission by second-order optical rectification was demonstrated experimentally in both gold (Au) surfaces and in nonlinear materials deposited on Au substrates [149, 150]. This is a powerful technique which can be very useful in future integrated THz photonic devices. Merging of visible light plasmonics and THz plasmonics can be the next step. Local generation of THz surface plasmons and further manipulations using THz plasmonics may lead to miniaturization of THz photonic devices for spectroscopy and imaging.

Bibliography

[1] M. Tonouchi, "Cutting-edge terahertz technology," Nat. Photon. **1**, 97–105 (2007).

[2] K. Sakai, *Terahertz optoelectronics*, Topics in Applied Physics (Springer, 2005).

[3] K. Kawase, Y. Ogawa, Y. Watanabe, and H. Inoue, "Non-destructive terahertz imaging of illicit drugs using spectral fingerprints," Opt. Express **11**, 2549–2554 (2003).

[4] J. B. Baxter and G. W. Guglietta, "Terahertz spectroscopy," Anal. Chem. **83**, 4342–4368 (2011).

[5] P. Planken, "Microscopy: A terahertz nanoscope," Nature **456**, 454–455 (2008).

[6] A. J. Huber, F. Keilmann, J. Wittborn, J. Aizpurua, and R. Hillenbrand, "Terahertz near-field nanoscopy of mobile carriers in single semiconductor nanodevices," Nano Lett. **8**, 3766–3770 (2008).

[7] E. Synge, "A suggested method for extending microscopic resolution into the ultra-microscopic region," Phil. Mag. **6**, 356–362 (1928).

[8] A. Lewis, M. Isaacson, A. Harootunian, and A. Muray, "Development of a 500 Å spatial resolution light microscope: I. light is efficiently transmitted through $\lambda/16$ diameter apertures," Ultramicroscopy **13**, 227–231 (1984).

[9] U. Dürig, D. W. Pohl, and F. Rohner, "Near-field optical-scanning microscopy," J. Appl. Phys. **59**, 3318–3327 (1986).

[10] A. J. L. Adam, J. M. Brok, M. A. Seo, K. J. Ahn, D. S. Kim, J. H. Kang, Q. H. Park, M. Nagel, and P. C. M. Planken, "Advanced terahertz electric near-fieldmeasurements at sub-wavelengthdiameter metallic apertures," Opt. Express **16**, 7407–7417 (2008).

[11] O. Mitrofanov, M. Lee, J. Hsu, I. Brener, R. Harel, J. Federici, J. Wynn, L. Pfeiffer, and K. West, "Collection-mode near-field imaging with 0.5 THz pulses," IEEE J. Sel. Top. Quant. **7**, 600–607 (2001).

[12] S. Hunsche, M. Koch, I. Brener, and M. Nuss, "THz near-field imaging," Opt. Commun. **150**, 22–26 (1998).

[13] N. C. J. van der Valk and P. C. M. Planken, "Electro-optic detection of subwavelength terahertz spot sizes in the near field of a metal tip," Appl. Phys. Lett. **81**, 1558–1560 (2002).

[14] A. Markelz, A. Roitberg, and E. Heilweil, "Pulsed terahertz spectroscopy of DNA, bovine serum albumin and collagen between 0.1 and 2.0 THz," Chem. Phys. Lett. **320**, 42–48 (2000).

[15] K. Cheung and D. Auston, "A novel technique for measuring far-infrared absorption and dispersion," Infrared Phys. **26**, 23–27 (1986).

[16] S. W. Koch, M. Kira, G. Khitrova, and H. M. Gibbs, "Semiconductor excitons in new light," Nat. Mater. **5**, 523–531 (2006).

[17] M. Woerner and T. Elsaesser, *Nonlinear Terahertz Studies of Ultrafast Quasiparticle Dynamics in Semiconductors* (Wiley-VCH Verlag GmbH & Co. KGaA, 2010), pp. 1–32.

[18] G. C. Cho, P. Y. Han, X.-C. Zhang, and H. J. Bakker, "Optical phonon dynamics of GaAs studied with time-resolved terahertz spectroscopy," Opt. Lett. **25**, 1609–1611 (2000).

[19] T. Kiwa, M. Tonouchi, M. Yamashita, and K. Kawase, "Laser terahertz-emission microscope for inspecting electrical faults in integrated circuits," Opt. Lett. **28**, 2058–2060 (2003).

[20] G. Ramakrishnan, R. Chakkittakandy, and P. C. M. Planken, "Terahertz generation from graphite," Opt. Express **17**, 16092–16099 (2009).

[21] G. Gallot and D. Grischkowsky, "Electro-optic detection of terahertz radiation," J. Opt. Soc. Am. B **16**, 1204–1212 (1999).

[22] N. van der Valk, W. T. Wenckebach, and P. Planken, "Full mathematical description of electro-optic detection in optically isotropic crystals," J. Opt. Soc. Am. B **21**, 622–631 (2004).

[23] G. Zhao, R. N. Schouten, N. C. J. van Der Valk, W. T. Wenckebach, and P. Planken, "Design and performance of a THz emission and detection setup based on a semi-insulating GaAs emitter," Rev. Sci. Instrum. **73**, 1715–1719 (2002).

[24] N. C. J. van der Valk, "Towards terahertz microscopy," Ph.D. thesis, Delft University of Technology, The Netherlands (2005).

[25] J. M. Chamberlain, "Where optics meets electronics: recent progress in decreasing the terahertz gap," Philos. T. Roy. Soc. A **362**, 199–213 (2004).

[26] G. H. Welsh and K. Wynne, "Generation of ultrafast terahertz radiation pulses on metallic nanostructured surfaces," Opt. Express **17**, 2470–2480 (2009).

[27] M. Bass, P. A. Franken, J. F. Ward, and G. Weinreich, "Optical rectification," Phys. Rev. Lett. **9**, 446–448 (1962).

[28] M. Bass, P. A. Franken, and J. F. Ward, "Optical rectification," Phys. Rev. **138**, A534–A542 (1965).

[29] F. Zernike and P. R. Berman, "Generation of far infrared as a difference frequency," Phys. Rev. Lett. **15**, 999–1001 (1965).

[30] M. Brienza, A. Demaria, and W. Glenn, "Optical rectification of mode-locked laser pulses," Phys. Lett. A **26**, 390–391 (1968).

[31] A. Rice, Y. Jin, X. F. Ma, X.-C. Zhang, D. Bliss, J. Larkin, and M. Alexander, "Terahertz optical rectification from <110> zinc-blende crystals," Appl. Phys. Lett. **64**, 1324–1326 (1994).

[32] K. H. Yang, P. L. Richards, and Y. R. Shen, "Generation of far-infrared radiation by picosecond light pulses in $LiNbO_3$," Appl. Phys. Lett. **19**, 320–323 (1971).

[33] D. H. Auston and A. M. Glass, "Optical generation of intense picosecond electrical pulses," Appl. Phys. Lett. **20**, 398–399 (1972).

[34] B. B. Hu, X.-C. Zhang, D. H. Auston, and P. R. Smith, "Free-space radiation from electro-optic crystals," Appl. Phys. Lett. **56**, 506–508 (1990).

[35] X.-C. Zhang, X. F. Ma, Y. Jin, T.-M. Lu, E. P. Boden, P. D. Phelps, K. R. Stewart, and C. P. Yakymyshyn, "Terahertz optical rectification from a nonlinear organic crystal," Appl. Phys. Lett. **61**, 3080–3082 (1992).

[36] S. Adachi, *Optical constants of crystalline and amorphous semiconductors: numerical data and graphical information* (Kluwer Academic Publishers, 1999).

[37] Q. Wu and X.-C. Zhang, "7 terahertz broadband GaP electro-optic sensor," Appl. Phys. Lett. **70**, 1784–1786 (1997).

[38] R. Chakkittakandy, "Quasi-near field terahertz spectroscopy," Ph.D. thesis, Delft University of Technology, The Netherlands (2010).

[39] G. Gallot, J. Zhang, R. W. McGowan, T.-I. Jeon, and D. Grischkowsky, "Measurements of the THz absorption and dispersion of ZnTe and their relevance to the electro-optic detection of THz radiation," Appl. Phys. Lett. **74**, 3450–3452 (1999).

[40] R. Chakkittakandy, J. A. Corver, and P. C. Planken, "Quasi-near field terahertz generation and detection," Opt. Express **16**, 12794–12805 (2008).

[41] S. Dexheimer, *Terahertz spectroscopy: principles and applications*, Optical science and engineering (CRC Press, 2007).

[42] R. W. Boyd, *Nonlinear Optics* (Academic Press, San Diego, 2003), 2nd ed.

[43] E. Yablonovitch, J. P. Heritage, D. E. Aspnes, and Y. Yafet, "Virtual photoconductivity," Phys. Rev. Lett. **63**, 976–979 (1989).

[44] D. H. Auston, "Picosecond optoelectronic switching and gating in silicon," Appl. Phys. Lett. **26**, 101–103 (1975).

[45] C. H. Lee, "Picosecond optoelectronic switching in GaAs," Appl. Phys. Lett. **30**, 84–86 (1977).

[46] X.-C. Zhang, J. T. Darrow, B. B. Hu, D. H. Auston, M. T. Schmidt, P. Tham, and E. S. Yang, "Optically induced electromagnetic radiation from semiconductor surfaces," Appl. Phys. Lett. **56**, 2228–2230 (1990).

[47] M. Reid, I. V. Cravetchi, and R. Fedosejevs, "Terahertz radiation and second-harmonic generation from InAs: Bulk versus surface electric-field-induced contributions," Phys. Rev. B **72**, 035201 (2005).

[48] K. Radhanpura, S. Hargreaves, and R. A. Lewis, "Bulk and surface field-induced optical rectification from (11N) zincblende crystals in a quasireflection geometry," Phys. Rev. B **83**, 125322 (2011).

[49] K. Liu, J. Xu, T. Yuan, and X.-C. Zhang, "Terahertz radiation from InAs induced by carrier diffusion and drift," Phys. Rev. B **73**, 155330 (2006).

[50] C. Wolfe, N. Holonyak, and G. Stillman, *Physical properties of semiconductors*, Solid state physical electronics series (Prentice Hall, 1989).

[51] S. Sze and K. Ng, *Physics of semiconductor devices*, Wiley-Interscience publication (Wiley-Interscience, 2007).

[52] Y. K. Yeo, R. L. Hengehold, and D. W. Elsaesser, "Surface-depletion effect correction to nonuniform carrier distributions by Hall measurements," J. Appl. Phys. **61**, 5070–5075 (1987).

[53] T. A. Germer, K. W. Kołasin-acuteski, J. C. Stephenson, and L. J. Richter, "Depletion-electric-field-induced second-harmonic generation near oxidized GaAs(001) surfaces," Phys. Rev. B **55**, 10694–10706 (1997).

[54] H. Dember, "Photoelectromotive force in cuprous oxide crystals," Phys. Z. **32**, 554–556 (1931).

[55] S. Kono, P. Gu, M. Tani, and K. Sakai, "Temperature dependence of terahertz radiation from n-type InSb and n-type InAs surfaces," Appl. Phys. B-Lasers O. **71**, 901–904 (2000).

[56] A. Urbanowicz, R. Adomavičius, and A. Krotkus, "Terahertz emission from photoexcited surfaces of Ge crystals," Physica B **367**, 152 – 157 (2005).

[57] P. Hoyer, M. Theuer, R. Beigang, and E. B. Kley, "Terahertz emission from black silicon," Appl. Phys. Lett. **93**, 091106 (2008).

[58] X. Mu, Y. J. Ding, K. Wang, D. Jena, and Y. B. Zotova, "Resonant terahertz generation from InN thin films," Opt. Lett. **32**, 1423–1425 (2007).

[59] C. T. Que, T. Edamura, M. Nakajima, M. Tani, and M. Hangyo, "Terahertz emission enhancement in InAs thin films using a silicon lens coupler," Jpn. J. Appl. Phys. **50**, 080207 (2011).

[60] E. S. Estacio, C. T. Que, F. C. B. Awitan, J. I. Bugante, F. I. de Vera, J. Azares, J. Afalla, J. de Vero, A. S. Somintac, R. V. Sarmago, A. A. Salvador, K. Yamamoto, and M. Tani, "Terahertz emission from indium oxide films grown on MgO substrates using sub-bandgap photon energy excitation," Opt. Express **20**, 4518–4524 (2012).

[61] W. Wan, Y. Chong, L. Ge, H. Noh, A. D. Stone, and H. Cao, "Time-reversed lasing and interferometric control of absorption," Science **331**, 889–892 (2011).

[62] R. Uzawa, D. Tanaka, H. Okawa, K. Hashimoto, and K. Kajikawa, "Optical rectification in self-assembled monolayers probed at surface plasmon resonance condition," Appl. Phys. Lett. **95**, 021107 (2009).

[63] G. Brumfiel, "Graphene gets ready for the big time," Nature **458**, 390–391 (2009).

[64] K. Krishnan and N. Ganguli, "Large anisotropy of the electrical conductivity of graphite," Nature **144**, 667 (1939).

[65] M. Zanini, D. Grubisic, and J. Fischer, "Optical anisotropy of highly oriented pyrolytic graphite," Phys. Status Solidi B **90**, 151–156 (1978).

[66] B. Kelly, *Physics of graphite* (Applied Science Publishers Ltd., Essex, 1981).

[67] W. Reynolds, *Physical properties of graphite*, Elsevier materials science series (Elsevier Pub. Co., 1968).

[68] M. Breusing, C. Ropers, and T. Elsaesser, "Ultrafast carrier dynamics in graphite," Phys. Rev. Lett. **102**, 086809 (2009).

[69] K. Seibert, G. Cho, W. Kütt, H. Kurz, D. Reitze, J. Dadap, H. Ahn, M. Downer, and A. Malvezzi, "Femtosecond carrier dynamics in graphite," Phys. Rev. B **42**, 2842–2851 (1990).

[70] H. Legall, H. Stiel, A. Antonov, I. Grigorieva, V. Arkadiev, and A. Bjeoumikhov, "A new generation of X-ray optics based on pyrolytic graphite," Proceedings of 28th International Free Electron Laser conference, (BESSY, Berlin, Germany) pp. 798–801 (2006).

[71] G. M. Mikheev, R. G. Zonov, A. N. Obraztsov, and Y. P. Svirko, "Giant optical rectification effect in nanocarbon films," Appl. Phys. Lett. **84**, 4854–4856 (2004).

[72] R. W. Newson, J.-M. Ménard, C. Sames, M. Betz, and H. M. Van Driel, "Coherently controlled ballistic charge currents injected in single-walled carbon nanotubes and graphite," Nano Lett. **8**, 1586–1589 (2008).

[73] N. C. J. van der Valk, P. C. M. Planken, A. N. Buijserd, and H. J. Bakker, "Influence of pump wavelength and crystal length on the phase matching of optical rectification," J. Opt. Soc. Am. B **22**, 1714–1718 (2005).

[74] X.-C. Zhang, Y. Jin, L. E. Kingsley, and M. Weiner, "Influence of electric and magnetic fields on THz radiation," Appl. Phys. Lett. **62**, 2477–2479 (1993).

[75] N. Sarukura, H. Ohtake, S. Izumida, and Z. Liu, "High average-power THz radiation from femtosecond laser-irradiated InAs in a magnetic field and its elliptical polarization characteristics," J. Appl. Phys. **84**, 654–656 (1998).

[76] J. Shan, C. Weiss, R. Wallenstein, R. Beigang, and T. Heinz, "Origin of magnetic field enhancement in the generation of terahertz radiation from semiconductor surfaces," Opt. Lett. **26**, 849–851 (2001).

[77] M. Johnston, D. Whittaker, A. Corchia, A. G. Davies, and E. Linfield, "Theory of magnetic-field enhancement of surface-field terahertz emission," J. Appl. Phys. **91**, 2104–2106 (2002).

[78] E. Abraham, A. Younus, A. E. Fatimy, J. Delagnes, E. Nguéma, and P. Mounaix, "Broadband terahertz imaging of documents written with lead pencils," Opt. Commun. **282**, 3104–3107 (2009).

[79] A. Modestov, J. Gun, and O. Lev, "Graphite photoelectrochemistry: 2. Photoelectrochemical studies of highly oriented pyrolitic graphite," J. Electroanal. Chem. **476**, 118–131 (1999).

[80] J.-P. Randin and E. Yeager, "Differential capacitance study on the basal plane of stress-annealed pyrolytic graphite," J. Electroanal. Chem. **36**, 257–276 (1972).

[81] M. Johnston, D. Whittaker, A. Corchia, A. Davies, and E. Linfield, "Simulation of terahertz generation at semiconductor surfaces," Phys. Rev. B **65**, 1653011–1653018 (2002).

[82] S. Snyden, T. Foecke, H. White, and W. Gerberich, "Imaging of stacking faults in highly oriented pyrolytic graphite using scanning tunneling microscopy," J. Mat. Res. **7**, 341–344 (1992).

[83] Y. Lu, M. Muñoz, C. Steplecaru, C. Hao, M. Bai, N. Garcia, K. Schindler, and P. Esquinazi, "Electrostatic force microscopy on oriented graphite surfaces: Coexistence of insulating and conducting behaviors," Phys. Rev. Lett. **97**, 076805 (2006).

[84] S. Banerjee, M. Sardar, N. Gayathri, A. Tyagi, and B. Raj, "Conductivity landscape of highly oriented pyrolytic graphite surfaces containing ribbons and edges," Phys. Rev. B **72**, 1–7 (2005).

[85] G. D. Metcalfe, H. Shen, M. Wraback, A. Hirai, F. Wu, and J. S. Speck, "Enhanced terahertz radiation from high stacking fault density nonpolar GaN," Appl. Phys. Lett. **92**, 241106 (2008).

[86] F. Carbone, "The interplay between structure and orbitals in the chemical bonding of graphite," Chem. Phys. Lett. **496**, 291–295 (2010).

[87] M. Nagel, A. Michalski, T. Botzem, and H. Kurz, "Near-field investigation of THz surface-wave emission from optically excited graphite flakes," Opt. Express **19**, 4667–4672 (2011).

[88] C. A. Schmuttenmaer, "Exploring dynamics in the far-infrared with terahertz spectroscopy," ChemInform **35**, 1759–1779 (2004).

[89] W. H. Brattain, "The copper oxide rectifier," Rev. Mod. Phys. **23**, 203–212 (1951).

[90] B. Ferguson and X.-C. Zhang, "Materials for terahertz science and technology," Nat. Mater. **1**, 26–33 (2007).

[91] K. Hauffe, *Oxidation of metals* (Plenum Press, 1965).

[92] Y. Zhu, K. Mimura, J.-W. Lim, M. Isshiki, and Q. Jiang, "Brief review of oxidation kinetics of copper at 350°C to 1050°C," Metall. Mater. Trans. A **37**, 1231–1237 (2006).

[93] G. K. P. Ramanandan, G. Ramakrishnan, and P. C. M. Planken, "Oxidation kinetics of nanoscale copper films studied by terahertz transmission spectroscopy," J. Appl. Phys. **111**, 123517 (2012).

[94] A. Parretta, M. K. Jayaraj, A. Di Nocera, S. Loreti, L. Quercia, and A. Agati, "Electrical and optical properties of copper oxide films prepared by reactive RF magnetron sputtering," Phys. Status Solidi A **155**, 399–404 (1996).

[95] M. O'Keeffe and W. J. Moore, "Electrical conductivity of monocrystalline cuprous oxide," J. Chem. Phys. **35**, 1324–1328 (1961).

[96] F. C. Akkari and M. Kanzari, "Optical, structural, and electrical properties of Cu_2O thin films," Phys. Status Solidi A **207**, 1647–1651 (2010).

[97] M. E. Toimil-Molares, "Fabrication and characterisation of copper nanowires electrochemically deposited in etched ion-track membranes," Ph.D. thesis, Ruperto−Carola University of Heidelberg, Germany (2001).

[98] C. Noguet, M. Tapiero, C. Schwab, J. P. Zielinger, D. Trivich, R. J. Komp, E. Y. Wang, and K. Weng, "Cuprous oxide as a photovoltaic converter," in "Photovoltaic Solar Energy Conference," (1978), pp. 1170–1179.

[99] A. Njeh, T. Wieder, and H. Fuess, "Reflectometry studies of the oxidation kinetics of thin copper films," Surf. Interface Anal. **33**, 626–628 (2002).

[100] E. A. Gulbransen, T. P. Copan, and K. F. Andrew, "Oxidation of copper between 250°C and 450°C and the growth of CuO "whiskers"," J. Electrochem. Soc. **108**, 119–123 (1961).

[101] N. Serin, T. Serin, Ş. Horzum, and Y. Çelik, "Annealing effects on the properties of copper oxide thin films prepared by chemical deposition," Semicond. Sci. Tech. **20**, 398 (2005).

[102] M. O'Keeffe and W. J. Moore, "Thermodynamics of the formation and migration of defects in cuprous oxide," J. Chem. Phys. **36**, 3009–3013 (1962).

[103] A. Rakhshani, Y. Makdisi, and X. Mathew, "Deep energy levels and photoelectrical properties of thin cuprous oxide films," Thin Solid Films **288**, 69–75 (1996).

[104] T. Hough, *Trends In Solar Energy Research* (Nova Science Publishers, 2006).

[105] O. Heavens, "Some factors influencing the adhesion of films produced by vacuum evaporation," J. Phys.-Paris **11**, 355–360 (1950).

[106] S. G. G. I. Ristov, M., "Chemical deposition of Cu_2O thin films," Thin Solid Films **123**, 63–67 (1985).

[107] M. Nair, L. Guerrero, O. L. Arenas, and P. Nair, "Chemically deposited copper oxide thin films: structural, optical and electrical characteristics," Appl. Surf. Sci. **150**, 143–151 (1999).

[108] W. Sears and E. Fortin, "Preparation and properties of Cu_2O/Cu photovoltaic cells," Sol. Energ. Mater. **10**, 93–103 (1984).

[109] H. Wieder and A. W. Czanderna, "The oxidation of copper films to $CuO_{0.67}$," J. Phys. Chem. **66**, 816–821 (1962).

[110] N. F. Mott, "Oxidation of metals and the formation of protective films," Nature **145**, 996–1000 (1940).

[111] T. N. Rhodin, "Low temperature oxidation of copper. I. physical mechanism," Journal of the American Chemical Society **72**, 5102–5106 (1950).

[112] X. Mathew, N. Mathews, and P. Sebastian, "Temperature dependence of the optical transitions in electrodeposited Cu_2O thin films," Sol. Energ. Mat. Sol. C. **70**, 277–286 (2001).

[113] H. Mori, M. Komatsu, K. Takeda, and H. Fujita, "Spontaneous alloying of copper into gold atom clusters," Phil. Mag. Lett. **63**, 173–178 (1991).

[114] S. Pucic, "Diffusion of copper into gold plating," in "Instrumentation and Measurement Technology Conference, 1993. IMTC/93. Conference Record., IEEE," (1993), pp. 114–117.

[115] J. C. Inkson, "Schottky barriers and plasmons," J. Vac. Sci. Technol. **11**, 943–946 (1974).

[116] D. Fishman, "Excitions in cuprous oxide," Ph.D. thesis, Rijksuniversiteit Groningen, The Netherlands (2008).

[117] V. V. Afanas'ev, *Internal photoemission spectroscopy: principles and applications* (Elsevier, 2008).

[118] J. A. Assimos and D. Trivich, "Photovoltaic properties and barrier heights of single-crystal and polycrystalline Cu_2O-Cu contacts," J. Appl. Phys. **44**, 1687–1693 (1973).

[119] Y. Shi, Y. Yang, X. Xu, S. Ma, W. Yan, and L. Wang, "Ultrafast carrier dynamics in Au/GaAs interfaces studied by terahertz emission spectroscopy," Appl. Phys. Lett. **88**, 161109 (2006).

[120] S. E. Mani, J. I. Jang, and J. B. Ketterson, "Large third-order susceptibility and third-harmonic generation in centrosymmetric Cu_2O crystal," Opt. Lett. **34**, 2817–2819 (2009).

[121] V. Dmitriev, G. Gurzadyan, and D. Nikogosyan, *Handbook of Nonlinear Optical Crystals*, Springer Series in Optical Sciences Series (Springer, 2010).

[122] H. Dember, "Photoelectromotive force in cuprous oxide crystals," Phys. Z **32**, 554–556 (1931).

[123] B. B. Hu, J. T. Darrow, X.-C. Zhang, D. H. Auston, and P. R. Smith, "Optically steerable photoconducting antennas," Appl. Phys. Lett. **56**, 886–888 (1990).

[124] M. B. Johnston, D. M. Whittaker, A. Dowd, A. G. Davies, E. H. Linfield, X. Li, and D. A. Ritchie, "Generation of high-power terahertz pulses in a prism," Opt. Lett. **27**, 1935–1937 (2002).

[125] W. Mönch, "On the physics of metal-semiconductor interfaces," Rep. Prog. Phys. **53**, 221 (1990).

[126] J. O. McCaldin and T. C. McGill, "The metal-semiconductor interface," Annu. Rev. Mater. Sci. **10**, 65–83 (1980).

[127] Y. Jin, X. F. Ma, G. A. Wagoner, M. Alexander, and X.-C. Zhang, "Anomalous optically generated THz beams from metal/GaAs interfaces," Appl. Phys. Lett. **65**, 682–684 (1994).

[128] M. I. Bakunov, R. V. Mikhaylovskiy, and M. Tani, "Strong interference enhancement of terahertz emission from a photoexcited semiconductor surface," Opt. Express **18**, 22406–22411 (2010).

[129] M. Li, F. G. Sun, G. A. Wagoner, M. Alexander, and X.-C. Zhang, "Measurement and analysis of terahertz radiation from bulk semiconductors," Appl. Phys. Lett. **67**, 25–27 (1995).

[130] N. S. Daghestani, S. Persheyev, M. A. Cataluna, G. Ross, and M. J. Rose, "THz generation from a nanocrystalline silicon-based photoconductive device," Semicond. Sci. Technol. **26**, 075015 (2011).

[131] M. Spasenović, M. Betz, L. Costa, and H. M. van Driel, "All-optical coherent control of electrical currents in centrosymmetric semiconductors," Phys. Rev. B **77**, 085201 (2008).

[132] D. L. Staebler and C. R. Wronski, "Reversible conductivity changes in discharge-produced amorphous Si," Appl. Phys. Lett. **31**, 292–294 (1977).

[133] K. Kishino, M. Unlu, J.-I. Chyi, J. Reed, L. Arsenault, and H. Morkoc, "Resonant cavity-enhanced (RCE) photodetectors," IEEE J. Quantum Elect. **27**, 2025 –2034 (1991).

[134] W. Wang, S. Wu, K. Reinhardt, Y. Lu, and S. Chen, "Broadband light absorption enhancement in thin-film silicon solar cells," Nano Lett. **10**, 2012–2018 (2010).

[135] D. J. Hilton, R. D. Averitt, C. A. Meserole, G. L. Fisher, D. J. Funk, J. D. Thompson, and A. J. Taylor, "Terahertz emission via ultrashort-pulse excitation of magnetic metalfilms," Opt. Lett. **29**, 1805–1807 (2004).

[136] F. Kadlec, P. Kužel, and J.-L. Coutaz, "Optical rectification at metal surfaces," Opt. Lett. **29**, 2674–2676 (2004).

[137] F. Kadlec, P. Kužel, and J.-L. Coutaz, "Study of terahertz radiation generated by optical rectification on thin gold films," Opt. Lett. **30**, 1402–1404 (2005).

[138] G. H. Welsh, N. T. Hunt, and K. Wynne, "Terahertz-pulse emission through laser excitation of surface plasmons in a metal grating," Phys. Rev. Lett. **98**, 026803 (2007).

[139] D. K. Polyushkin, E. Hendry, E. K. Stone, and W. L. Barnes, "THz generation from plasmonic nanoparticle arrays," Nano Lett. **11**, 4718–4724 (2011).

[140] F. Garwe, A. Schmidt, G. Zieger, T. May, K. Wynne, U. Hübner, M. Zeisberger, W. Paa, H. Stafast, and H.-G. Meyer, "Bi-directional terahertz emission from gold-coated nanogratings by excitation via femtosecond laser pulses," Appl. Phys. B **102**, 551–554 (2011).

[141] V. Shalaev, *Nonlinear optics of random media: fractal composites and metal-dielectric films*, Springer tracts in modern physics (Springer, 2000).

[142] V. Shalaev, *Optical properties of nanostructured random media*, Topics in applied physics (Springer, 2002).

[143] M. Walther, D. G. Cooke, C. Sherstan, M. Hajar, M. R. Freeman, and F. A. Hegmann, "Terahertz conductivity of thin gold films at the metal-insulator percolation transition," Phys. Rev. B **76**, 125408 (2007).

[144] V. M. Shalaev and A. K. Sarychev, "Nonlinear optics of random metal-dielectric films," Phys. Rev. B **57**, 13265–13288 (1998).

[145] M. Breit, V. A. Podolskiy, S. Grésillon, G. von Plessen, J. Feldmann, J. C. Rivoal, P. Gadenne, A. K. Sarychev, and V. M. Shalaev, "Experimental observation of percolation-enhanced nonlinear light scattering from semicontinuous metal films," Phys. Rev. B **64**, 125106 (2001).

[146] W. L. Barnes, "Surface plasmon-polariton length scales: a route to sub-wavelength optics," J. Opt. A- Pure Appl. Opt. **8**, S87 (2006).

[147] H. Raether, *Surface plasmons on smooth and rough surfaces and on gratings*, no. v. 111 in Springer tracts in modern physics (Springer, 1988).

[148] S. Maier, *Plasmonics: fundamentals and applications* (Springer, 2007).

[149] G. Ramakrishnan and P. C. M. Planken, "Percolation-enhanced generation of terahertz pulses by optical rectification on ultrathin gold films," Opt. Lett. **36**, 2572–2574 (2011).

[150] G. Ramakrishnan, N. Kumar, P. C. M. Planken, D. Tanaka, and K. Kajikawa, "Surface plasmon-enhanced terahertz emission from a hemicyanine self-assembled monolayer," Opt. Express **20**, 4067–4073 (2012).

[151] A. Serrano, O. R. de la Fuente, and M. A. García, "Extended and localized surface plasmons in annealed Au films on glass substrates," J. of Appl. Phys. **108**, 074303 (2010).

[152] R. Naraoka, G. Kaise, K. Kajikawa, H. Okawa, H. Ikezawa, and K. Hashimoto, "Nonlinear optical property of hemicyanine self-assembled monolayers on gold and its adsorption kinetics probed by optical second-harmonic generation and surface plasmon resonance spectroscopy," Chem. Phys. Lett. **362**, 26–30 (2002).

[153] R. Naraoka, H. Okawa, K. Hashimoto, and K. Kajikawa, "Surface plasmon resonance enhanced second-harmonic generation in Kretschmann configuration," Opt. Commun. **248**, 249–256 (2005).

[154] T. Iiyama, M. Fukuyo, R. Naraoka, H. Okawa, H. Ikezawa, K. Hashimoto, and K. Kajikawa, "Linear electrooptic effect in hemicyanine self-assembled monolayer on gold substrate," Opt. Commun. **279**, 320–323 (2007).

[155] A. K. Sarychev, V. A. Shubin, and V. M. Shalaev, "Anderson localization of surface plasmons and nonlinear optics of metal-dielectric composites," Phys. Rev. B **60**, 16389–16408 (1999).

[156] P. Gadenne, F. Brouers, V. M. Shalaev, and A. K. Sarychev, "Giant Stokes fields on semicontinuous metal films," J. Opt. Soc. Am. B **15**, 68–72 (1998).

[157] P. Gadenne, "Étude de la croissance des couches minces á partir de mesures optiques et èlectriques pendant leur dèpôt," Thin Solid Films **42**, 369–381 (1977).

[158] A. Wokaun, J. G. Bergman, J. P. Heritage, A. M. Glass, P. F. Liao, and D. H. Olson, "Surface second-harmonic generation from metal island films and microlithographic structures," Phys. Rev. B **24**, 849–856 (1981).

[159] P. Gadenne, D. Gagnot, and M. Masson, "Surface enhanced resonant Raman scattering induced by silver thin films close to the percolation threshold," Physica A **241**, 161–165 (1997).

[160] K. Kajikawa, R. Naraoka, H. Okawa, H. Ikezawa, and K. Hashimoto, "Preparation and optical characterization of hemicyanine self-assembled monolayer on Au substrate," Mol. Cryst. and Liq. Cryst. **370**, 277–283 (2001).

[161] N. B. Grosse, J. Heckmann, and U. Woggon, "Nonlinear plasmon-photon interaction resolved by k-space spectroscopy," Phys. Rev. Lett. **108**, 136802 (2012).

[162] A. D. Gladun, V. G. Leiman, and A. V. Arsenin, "On the mechanism of generation of terahertz electromagnetic radiation upon irradiation of a nanostructured metal surface by femtosecond laser pulses," Quantum Electron+ **37**, 1166 (2007).

[163] Y. Gao, M.-K. Chen, C.-E. Yang, Y.-C. Chang, S. Yin, R. Hui, P. Ruffin, C. Brantley, E. Edwards, and C. Luo, "Analysis of terahertz generation via nanostructure enhanced plasmonic excitations," J. Appl. Phys. **106**, 074302 (2009).

[164] R. Ulbricht, E. Hendry, J. Shan, T. F. Heinz, and M. Bonn, "Carrier dynamics in semiconductors studied with time-resolved terahertz spectroscopy," Rev. Mod. Phys. **83**, 543–586 (2011).

[165] P. W. Baumeister, "Optical absorption of cuprous oxide," Phys. Rev. **121**, 359–362 (1961).

[166] M. Tonouchi, N. Wada, S. Shikii, M. Hangyo, M. Tani, and K. Sakai, "Terahertz emission properties from flux-trapped YBCO thin films," Physica C: Superconductivity **293**, 82 – 86 (1997).

[167] B. Kelly, *Physics of graphite*, RES mechanica monographs (Applied Science Publishers, 1981).

[168] R. Ascázubi, I. Wilke, K. Denniston, H. Lu, and W. J. Schaff, "Terahertz emission by InN," Appl. Phys. Lett. **84**, 4810–4812 (2004).

[169] J. A. Schuller, E. S. Barnard, W. Cai, Y. C. Jun, J. S. White, and M. L. Brongersma, "Plasmonics for extreme light concentration and manipulation," Nat. Mater. **9**, 193–204 (2010).

Summary

Terahertz light is electromagnetic radiation, similar to visible light. The photons that the terahertz light is comprised of carry a much smaller amount of energy compared to the visible light photons. Unlike visible light, terahertz light can pass through materials like plastic, cardboards, wood etc.; a very useful property which enables it to replace harmful X-rays in many security applications. However, it is not possible to see the terahertz photons with our naked eyes, and it requires special detectors to observe them.

A lot of attention has been drawn to terahertz radiation recently because of its potential use in various applications in national security (as mentioned before), and in the biomedical and the semiconductor industries. Essential to any terahertz device is a suitable terahertz source. There are different methods to generate this type of radiation. After the advent of ultrafast lasers, an optical technique was developed which became very popular afterwards. In very simple terms, this technique can be considered as producing an extremely quick disturbance in a suitable material using an extremely quick flash of laser light. Here the phrase 'extremely quick' refers to femtosecond time scales where one femtosecond is one millionth of one billionth of a second. The quick electromagnetic disturbance can lead to the emission of a pulse of electromagnetic radiation of a different frequency: terahertz light. Certainly, this process depends on the material in which the disturbance is created, which we will see in a bit more detail below. It is this method of terahertz generation we focus on in this thesis.

Let us now have a closer look at this. Only certain materials have this property of converting a flash of laser light efficiently into a flash of terahertz light, for example, some semiconductors. What type of a disturbance can a flash of laser light, (a laser pulse), create in such a material? In the case of semiconductors, the incident light pulse can lead to the excitation of mobile conduction electrons by providing them with the required energy. The semiconductor becomes momentarily a conductor. If it was initially kept under an external voltage bias, a momentary current is thus induced by the light pulse. A time-varying current can act as a source of electromagnetic waves. The emitted flash of light in this case is a terahertz pulse. Similar momentary disturbances can also be produced in certain nonlinear crystals without really exciting electrons from their bound states, but by causing an ultrafast displacement of the bound charges. In both these cases, the emitted light pulse carries information about

the material's response to the femtosecond flash of light, which in fact is information about the material *per se*. For example, we see that the illumination of graphite with femtosecond laser pulses results in the emission of terahertz light pulses. The properties of the emitted terahertz pulse are suggestive of a transient photocurrent produced in the material. Graphite consists of stacks of atomic planes of carbon which are loosely attached to each other. Electric conductivity along a direction perpendicular to these planes is known to be very low as in this case electrons have to jump from one plane to the other. However, in our experiments the emitted terahertz pulses indicate a resultant photocurrent flowing in that direction.

Oxidized copper surfaces are known to act as a semiconductor-diode. A semiconductor diode is a device which restricts the electric current to flow through it in only one direction. In the case of oxidized copper surfaces, this is possible by a potential barrier formed at the interface between copper and cuprous oxide. When a femtosecond light pulse excites electrons at such an interface, and frees electrons in it, a quick pulse of current flows across the interface. This transient current emits a terahertz pulse.

The same idea can also be applied to different other semiconductor-metal interfaces. We have shown that terahertz pulses can be produced by exciting thin films of germanium and silicon deposited on a gold substrate. If the thin films of these semiconductors prepared on a glass substrate are illuminated with femtosecond light pulses, the emitted terahertz pulses are very feeble. When the thin films of the semiconductors are on a gold substrate, a surprising enhancement of the generated terahertz light from such thin films is observed. The later part of the thesis concentrates on the different possible ways in which the gold substrate can contribute to the enhancement of terahertz radiation from thin films.

When coherent laser light is incident on an extremely thin film of a semiconductor material deposited on a metal surface, light reflected from the top and the bottom of the film can result in a complete or partial reduction of the reflected light. It is equivalent to trapping the light inside the film, which leads to enhanced absorption in the thin film. This is sometimes called 'coherent optical absorption'. Very strong absorption of the pump light can be achieved in thin films as compared to bulk materials, as a result of this. When light is strongly absorbed by the semiconductor, more electrons will be freed and a stronger transient current can be produced which can result in a stronger terahertz emission. This leads to the counter-intuitive result that less material emits more terahertz light.

The concentration of laser light inside the terahertz generation material can also be done by making use of surface plasmon excitation. Surface plasmons are light waves bound to the interface between a metal and a dielectric. In our case, since the terahertz generation takes place at the interface between a metal and a semiconductor, surface plasmons can play a role in the process. As surface plasmons are bound to the interface, they can enhance the local intensity of the pump light at the interface where the generation of terahertz radiation takes place. Using this method, we demonstrate the enhancement of terahertz emission from a layer as thin as a single molecular layer of a nonlinear optical material called hemicyanine. We

also go on to show that enhanced terahertz emission can be achieved from semiconductors deposited on a nanostructured metal surface, where again surface plasmons are excited. Concentration of the laser light intensity using plasmonics also leads to terahertz emission from the metal surfaces itself, *i.e.,* without any semiconductor on top.

In short, this thesis discusses the possibilities of terahertz generation from ultrathin semiconductor layers, metals and their interfaces, and on different optical techniques to enhance the terahertz emission. These techniques not only help in the study of the properties of ultrathin layers of materials, but can also help in miniaturizing terahertz sources for various applications.

Gopakumar Ramakrishnan, 2012.

Samenvatting

Terahertz licht is een vorm van elektromagnetische straling, vergelijkbaar met zichtbaar licht. De fotonen van terahertz licht dragen veel minder energie dan in het geval van zichtbaar licht. In tegenstelling tot zichtbaar licht, kan terahertz licht door materialen als plastic, karton, hout etc. heen schijnen. Een nuttige eigenschap, omdat hiermee schadelijke röntgenstraling, gebruikt voor veiligheidstoepassingen, vervangen zou kunnen worden. Het is echter niet mogelijk om terahertz fotonen te zien met ons blote oog. We hebben speciale detectoren nodig om ze te kunnen waarnemen. Recentelijk is er veel aandacht voor terahertz straling omdat het potentieel toe te passen is in verschillende gebieden, zoals nationale veiligheid en in de biomedische- en de halfgeleiderindustrie. Essentieel voor elk apparaat is een geschikte bron van terahertz licht. Er zijn verschillende methoden om dit type licht te genereren.

Na de ontwikkeling van de femtoseconde laser was er een optische techniek ontwikkeld om dit te doen, die daarna erg populair werd. In simpele termen kan deze techniek beschreven worden als een extreem snelle verstoring in een geschikt materiaal door het gebruik van een extreem korte lichtflits. De term 'extreem kort' refereert aan femtoseconde tijdschalen waarin een femtoseconde gelijk staat aan een miljardste van een miljoenste seconde. De snelle, elektromagnetische verstoring leidt tot de emissie van een puls van elektromagnetische straling in een ander frequentiegebied: het terahertz frequentiegebied. Dit proces is materiaalafhankelijk en we zullen dat hieronder iets gedetailleerder bespreken. Het is deze methode van het genereren van terahertz licht waarop we focusseren in dit proefschrift.

Alleen bepaalde materialen hebben de eigenschap om een flits van zichtbaar licht efficiënt om te zetten in terahertz licht zoals, bijvoorbeeld, halfgeleiders. Wat voor type verstoring kan een flits van licht (een laser puls) in zo'n materiaal creëren? De inkomende laser puls kan, in het geval van halfgeleiders, leiden tot de excitatie van mobiele elektronen, als de fotonen voldoende energie hebben. De halfgeleider wordt tijdelijk geleidend. Als er initieel een spanning aanwezig was over de halfgeleider, induceert de lichtpuls een tijdelijke stroom. Een in de tijd variërende stroom kan als een bron van electromagnetische straling functioneren. De geëmitteerde lichtflits is in dit geval een terahertz puls. Vergelijkbare kortstondige verstoringen kunnen ook optreden in niet-lineare kristallen, zonder elektronen uit hun gebonden toestanden te exciteren maar door een ultrasnelle verplaatsing van de gebonden ladingen. In beide gevallen draagt de geëmitteerde licht puls informatie over het materiaalgedrag

in aanwezigheid van een femtoseconde licht puls, wat in feite informatie over het materiaal per se is. We zien, bijvoorbeeld, dat de belichting van grafiet met femtoseconde laser pulsen resulteert in de emissie van terahertz lichtpulsen. De eigenschappen van de geëmitteerde terahertz puls suggereren een kortstondige fotostroom in het materiaal. Grafiet bestaat uit stapels van atomaire vlakken van koolstof die losjes aan elkaar vast zitten. Het is bekend dat de elektrische geleidbaarheid loodrecht op het vlak erg laag is omdat electronen van het ene naar het andere vlak moeten overspringen. Echter, in onze experimenten geeft de emissie van een terahertz puls aan dat er een resultante fotostroom in die richting ontstaat.

Het is bekend dat geoxideerde koperoppervlakken als een halfgeleiderdiode werken. Een halfgeleiderdiode is een elektronische component die de elektrische stroom alleen in één bepaalde richting doorlaat. In het geval van geoxideerde koperoppervlakken is dat het gevolg van het ontstaan van een potentiaalbarrière op de overgang tussen het koper en koperoxide. Wanneer een femtoseconde lichtpuls elektronen exciteert op zo'n overgang en ze dus vrij (mobiel) maakt, versnellen de elektronen en ontstaat er een snelle stroompuls tussen de twee materialen. Deze tijdelijke stroom genereert terahertz licht.

Hetzelfde idee kan ook toegepast worden op verschillende andere halfgeleidermetaal grensvlakken. We hebben laten zien dat terahertz pulsen ook geproduceerd kunnen worden bij excitatie van extreem dunne lagen van Germanium en Silicium gedeponeerd op een goud substraat. Als deze dunne lagen halfgeleidermateriaal belicht worden met femtoseconde laserpulsen zijn de geëmitteerde terahertz pulsen duidelijk detecteerbaar. Hoewel de lagen extreem dun zijn nemen we verrassende sterke terahertz pulsen waar. Verderop in dit proefschrift behandelen we de mogelijke manieren waarop goudsubstraten bijdragen aan de versterkte hoeveelheid terahertz licht van de dunne lagen.

Wanneer coherent laserlicht op een extreem dunne laag van halfgeleider materiaal, gedeponeerd op een metaaloppervlak, schijnt, kan gereflecteerd licht van de boven -en onderkant voor een gedeeltelijke of, bijna volledige, reductie van gereflecteerd licht zorgen. Het is equivalent met het concentreren van licht in de film, wat leidt tot versterkte absorptie van licht. Dit proces wordt ook wel coherente optische absorptie genoemd. Door dit effect kan heel sterke absorptie van pomplicht al worden bereikt in extreem dunne lagen, in vergelijking tot de absorptie in het bulk materiaal. Wanneer veel licht geabsorbeerd wordt in de halfgeleider komen er meer elektronen vrij en onstaat er een grotere tijdelijke stroom welke leidt tot meer terahertz emissie. Dit leidt tot het contra-intuïtieve resultaat dat minder materiaal resulteert in meer emissie van terahertz licht. De concentratie van laserlicht in het terahertz generende materiaal kan ook gedaan worden door excitatie van oppervlakteplasmonen. Oppervlakteplasmonen zijn lichtgolven gebonden aan het grensvlak tussen een metaal en diëelektricum. In ons geval kunnen oppervlakteplasmonen een rol spelen op het grensvlak tussen het metaal en de halfgeleider, omdat juist daar terahertz licht gegenereerd wordt. Omdat oppervlakteplasmonengebonden zijn aan het oppervlak kunnen ze de lokale intensiteit van de laserbundel vergroten, daar waar de creatie van terahertz straling plaatsvindt. We demonstreren, bij gebruik

van deze methode, de versterking van terahertz emissie van een laag zó dun dat het slechts uit een enkele laag van moleculen van een niet-lineair optisch materiaal, hemicyanine genaamd, bestaat. We vervolgen met het aantonen dat versterkte terahertz emissie bereikt kan worden door halfgeleiders te deponeren op een metaaloppervlak met structuren van nanometer dimensies, waarop oppervlakteplasmonen geëxciteerd worden. Concentratie van laserlicht door het gebruik van plasmonen leidt ook tot terahertz emissie van het metaaloppervlak zelf, zonder dat er een halfgeleidermateriaal aanwezig is.

Samenvattend, bediscussieerd dit proefschrift de mogelijkheden van terahertz generatie van ultradunne halfgeleiderlaagjes, metalen en hun grensvlakken en het gebruik van verschillende optische technieken om terahertz emissie te versterken. Deze technieken helpen niet alleen bij het bestuderen van de eigenschappen van ultradunne lagen, maar helpen mogelijk ook bij de miniaturisatie van terahertz bronnen voor verschillende toepassingen.

Gopakumar Ramakrishnan, 2012.

Acknowledgements

Over the past four years in the Netherlands, it has been my good fortune to meet many wonderful people who have given me a lot of their time, companionship, professional and personal help. With a big "Dankjewel" to all of them, let me briefly mention my gratitude to those who contributed to the development and realization of this thesis.

First of all, I would like to thank my promotor Prof. Paul Planken for all the great support, guidance, knowledge, freedom and beyond all, a lot of patience! I was lucky to learn the basic techniques of terahertz technology from him, which will certainly be something which I will cherish and will be proud of for the rest of my life.

Dr. Aurèle Adam is the person who makes the group lively. He spreads a great deal of energy around (might be terahertz itself!). Thank you for all the support, wonderful discussions and occasional jokes.

A special thanks is paid to Prof. Paul Urbach, the group leader, who is always cheerful and supportive.

There are four fellow researchers whom I would specifically like to thank for being so kind and understanding over these years: Joseph Knab for his help with many experiments in the early stages of the PhD, and for all the wonderful ideas and discussions. Reshmi Chakkittakandy spent a lot of her valuable time training me on the experimental setups in the beginning. Gopika Ramanandan and Nishant Kumar joined the group afterwards. It was a great learning experience, and I always enjoyed working with all of you.

Thank you Omar El Gawhary for all the wonderful long scientific and nonscientific discussions we had, and continue to have, about nearly everything!

In these four years, I was very lucky to have the best office-mates. Thank you Mounir Zeitouny, Moxi Cui, Alessandro Polo, Katsiaryna Ushakova, Young-mi Park, Lei Wei, Alberto Assafrão da Costa and Mark Mahon for being so friendly and kind to me. Young-mi also helped me to spell-check this thesis. "Gamsa hamnida."

A special word of gratitude to Yvonne van Aalst and Lucia Heijenga-Becht. Thanks a lot to Raymond Schouten, Roland Horsten, Thim Zuidwijk, and Rob Pols for all the timely technical support.

Some of the experiments described in Chapter 5 of this thesis are the results of a fruitful collaboration we could establish with the group of Prof. Kotaro Kajikawa of

Tokyo Institute of Technology, Japan. Thanks a lot to Prof. Kajikawa and Dr. Daisuke Tanaka for their valuable time spent on the project.

Some attempts were once made to get more terahertz light from cuprous oxide by using amplified lasers (much higher pulse energy). I would like to thank Prof. Huib J. Bakker and his group at AMOLF, Amsterdam for hosting us.

Thank you Emile van der Drift, Patrick Lew, Marco van der Krogt, Roel Mattern, Marc Zuiddam, Hozanna Miro, Anja van Langen-Suurling, Arnold van Run, Ewan Hendriks and Charles de Boer of the Nanofacility for your timely help with the nanofabrication.

Ruud Hendrikx at the Department of Materials Science and Engineering (TU Delft) is acknowledged for the X-ray analysis of the samples.

I would like to thank all the group members of Optica over these four years for their good company and wonderful presence. Thank you Prof. Joseph Braat, Nandini Bhattacharya, Silvania Pereira, Man Xu, Aura Nugrowati, Florian Bociort, Peter Somers, Julian Spronck, Maatern van Turnhout, Sven van Haver, Olaf Janssen, Pascal van Grol, Sarathi Roy, Thomas Liebig, Andreas Hänsel, Nitish Kumar, Wouter Westerveld, Adonis Reyes Reyes, Mahsa Nemati, Olaf Janssen, Robert Speelpenning, Sjoerd van Luijn, Wioletta Moskaluk, Rik Starmans, Luat Vuong, Luca Cisotto, Jeffrey Meisner, Hui-Shan Chan, Maxim Spreij and Vincent Docter for the wonderful time. Thank you Gerward Weppelman for kindly translating the thesis summary into Dutch.

Beyond words, I am hugely indebted to my wife, my parents and my brother for their monumental, unwavering support and encouragement on all fronts. They have truly always been there for me, and without them none of this would have been even remotely possible.

Delft,
December 2012.

Gopakumar Ramakrishnan.

Biography

Gopakumar Ramakrishnan was born in Nemmara, Kerala, India on May 31, 1981. He completed his bachelors and masters degrees in Physics from University of Calicut (2001) and Cochin University of Science and Technology (2003) respectively. He then specialized in Applied Optics with a masters degree in technology (2005) from Indian Institute of Technology, Delhi. Afterwards, he joined the National Centre for Biological Sciences, Tata Institute of Fundamental Research, Bangalore, India as an interdisciplinary research scholar. In 2008, he joined the Optics Research Group, Delft University of Technology, in The Netherlands, as a PhD candidate. He continues in the same group as a post-doctoral researcher.

Publications

Journals

"Terahertz generation from graphite,"
G. Ramakrishnan, R. Chakkittakandy, and P. C. M. Planken,
Opt. Express 17, 16092–16099 (2009).

"Percolation-enhanced generation of terahertz pulses by optical rectification on ultrathin gold films,"
G. Ramakrishnan and P. C. M. Planken,
Opt. Lett. 36, 2572–2574 (2011).

"Surface plasmon-enhanced terahertz emission from a hemicyanine self-assembled monolayer,"
G. Ramakrishnan, N. Kumar, P. C. M. Planken, D. Tanaka, and K. Kajikawa,
Opt. Express 20, 4067–4073 (2012).

"Oxidation kinetics of nanoscale copper films studied by terahertz transmission spectroscopy,"
G. K. P. Ramanandan, G. Ramakrishnan, and P. C. M. Planken,
J. Appl. Phys. 111, 123517 (2012).

"Terahertz emission from surface-immobilized gold nanospheres,"
K. Kajikawa, Y. Nagai, Y. Uchiho, G. Ramakrishnan, N. Kumar, G. K. P. Ramanandan, and P. C. M. Planken,
Opt. Lett. 37, 4053–4055 (2012).

"Enhanced terahertz emission from semiconductor by coherent optical absorption in ultrathin semiconductor films,"
G. Ramakrishnan, G. K. P. Ramanandan, A. J. L. Adam, M. Xu, R. Hendrikx, and P. C. M. Planken,
(*in preparation*).

"Plasmon-enhanced terahertz emission from Schottky interfaces,"
G. Ramakrishnan, N. Kumar, G. K. P. Ramanandan, A. J. L. Adam, R. Hendrikx, and P. C. M. Planken,
(*in preparation*).

"Surface plasmon-enhanced terahertz emission from single layer graphene,"
Y. -M. Bahk, G. Ramakrishnan. J. H. Choi, H. -R. Park, Y. H. Kim, K. J. Ahn, P. C. M. Planken, and D. -S. Kim,
(*to be published*).

Conference contributions

"Terahertz generation from graphite surfaces,"
G. Ramakrishnan, R. Chakkittakandy, and P. C. M. Planken,
oral presentation, 34th International Conference on Infrared, Millimeter, and Terahertz waves (IRMMW-THz 2009), Busan, Korea, Sept 21–25, 2009.

"Terahertz generation from graphite,"
G. Ramakrishnan, R. Chakkittakandy, and P. C. M. Planken,
oral presentation, 33rd meeting of the section Atomic Molecular and Optical Physics (AMO), Lunteren, The Netherlands, Oct 6–7, 2009.

"Percolation-enhanced terahertz emission from ultrathin gold films,"
G. Ramakrishnan and P. C. M. Planken,
poster presentation, The 5th International Conference on Surface Plasmon Photonics (SPP5), Busan, Korea, May 15–20, 2011.

"Percolation-enhanced terahertz emission from ultrathin gold films,"
G. Ramakrishnan and P. C. M. Planken,
oral presentation, 36th International Conference on Infrared, Millimeter, and Terahertz waves (IRMMW-THz 2011), Houston, United States of America, Oct 2–7, 2011.

"Surface-plasmon enhanced terahertz emission,"
G. Ramakrishnan, N. Kumar, P. C. M. Planken, D. Tanaka, and K. Kajikawa,
poster presentation, 3rd EOS Topical Meeting on Terahertz Science & Technology (TST 2012), Prague, Czech Republic, 17 June 2012 – 20 June, 2012.

“Surface plasmon-enhanced terahertz emission from single layer graphene,”
Y. -M. Bahk, G. Ramakrishnan. J. H. Choi, H. -R. Park, Y. H. Kim, K. J. Ahn, P. C. M. Planken, and D. -S. Kim,
oral presentation, 37th International Conference on Infrared, Milimeter and Terahertz Waves (IRMMW-THz 2013), Wollongong, Australia, September 23–28, 2012.